ENCLOSURE

ROLE OF CHEMICAL PROCESSES, THEIR COUPLING EFFECTS, AND BOUNDING CONDITIONS FOR IN-DRIFT WATER COMPOSITIONS AFFECTING DRIP SHIELD AND WASTE PACKAGE CORROSION (RESPONSE TO ENFE 2.07 AIN-1)

Note Regarding the Status of Supporting Technical Information

This document was prepared using the most current information available at the time of its development. This Technical Basis Document and its appendices providing Key Technical Issue Agreement responses that were prepared using preliminary or draft information reflect the status of the Yucca Mountain Project's scientific and design bases at the time of submittal. In some cases this involved the use of draft Analysis and Model Reports (AMRs) and other draft references whose contents may change with time. Information that evolves through subsequent revisions of the AMRs and other references will be reflected in the License Application (LA) as the approved analyses of record at the time of LA submittal. Consequently, the Project will not routinely update either this Technical Basis Document or its Key Technical Issue Agreement appendices to reflect changes in the supporting references prior to submittal of the LA.

ENCLOSURE

ROLE OF CHEMICAL PROCESSES, THEIR COUPLING EFFECTS, AND BOUNDING CONDITIONS FOR IN-DRIFT WATER COMPOSITIONS AFFECTING DRIP SHIELD AND WASTE PACKAGE CORROSION (RESPONSE TO ENFE 2.07 AIN-1)

This enclosure provides a response for Key Technical Issue (KTI) agreement Evolution of the Near-Field Environment (ENFE) 2.07 Additional Information Needed (AIN)-1. This KTI relates to providing an evaluation of the impact of the range of variation of the local chemistry at the drip shield and waste package.

1. KEY TECHNICAL ISSUE AGREEMENT

1.1 ENFE 2.07 AIN-1

Agreement ENFE 2.07 was reached during the U.S. Nuclear Regulatory Commission (NRC)/U.S. Department of Energy (DOE) technical exchange and management meeting held January 9 to 12, 2001, in Pleasanton, California (Reamer 2001). ENFE KTI subissues 1, 2, 3, and 4 were discussed at that meeting.

The wording of the agreement is as follows:

ENFE 2.07

> Identify specific coupling relationships that are included and excluded from TSPA, including Onsager couples, and give technical bases for their inclusion or exclusion. The DOE will identify specific coupling relationships that are included and excluded from TSPA, including Onsager couples, and give the technical basis for inclusion and exclusion. This information will be documented in a revision to the Engineered Barrier System Degradation, Flow, and Transport PMR (TDR-EBS-MD-000006), expected to be available by September 2001.

The DOE submitted a response to the NRC on ENFE 2.07 on September 27, 2002 (Ziegler 2002). Upon reviewing the submittal, the NRC issued an AIN request for ENFE 2.07 on October 21, 2003 (Schlueter 2003).

The wording of the AIN is as follows:

ENFE 2.07 AIN-1

> The NRC's intent in this agreement was to obtain reasonable assurance that no near-field processes or chemistries omitted from testing or modeling could lead to significantly shorter waste canister lifetimes. DOE's response to ENFE Agreement 2.07 lacks an analysis of the role of chemical reactions in drip shield and waste package corrosion. While it is appropriate for DOE to consider changes in chemical environment due to chemical transport, a variety of solid phase-gas-water interactions might occur in concert with changing thermal-

hydrological conditions and alter the waste package chemical environment. NRC expects DOE to provide technical bases for electrochemical and microbial processes, rates of reactions, mass balance, probability considerations, and temporal and spatial distributions of processes and conditions on scales important to performance. In addition, in addressing chemical couples that were included or excluded from the determination of important near-field chemical environments, DOE should discuss the effects of coupled near-field processes and conditions on waste package and drip shield corrosion.

Additionally, NRC notes that a May 13, 2003, presentation to the Nuclear Waste Technical Review Board by Mark Peters of Los Alamos National Laboratory described the character of the in-drift environment. Among other topics, the presentation covered the three abstracted temperature regions of the drift environment, the chemical evolution of the drift environment, the chemical divide theory, observed water chemistries, in-drift water chemistry modeling and validation, and the investigation of deliquescence during dryout temperature. This presentation provided clarification of DOE's method of characterizing the near-field environment. The environment if modeled using TOUGHREACT and EQ3/6. The modeling produced a range of "bounding" in-drift water compositions, which DOE consolidated into 11 bins. DOE should consider addressing ENFE 2.07 in the context of providing the technical basis for the consolidation or establishment of the 11 bins. This approach would need to address the couples considered, the range of chemistries considered, the rationale for including or excluding couples and chemistries, and the limitations of any codes used to develop the bins.

1.2 Related Key Technical Issues

Other KTI agreements related to ENFE 2.07 are CLST 1.01 (*Technical Basis Document No. 5: In-Drift Chemical Environment*, Appendix A), ENFE 2.05 (*Technical Basis Document No. 5: In-Drift Chemical Environment*, Appendix D), ENFE 2.09 and ENFE 2.15 (*Technical Basis Document No. 5: In-Drift Chemical Environment*, Appendix F), and ENFE 2.10 (*Technical Basis Document No. 5: In-Drift Chemical Environment*, Appendix G).

In addition, as noted by the NRC evaluation of DOE's initial response (Schlueter 2003), this response is indirectly related to the effects of coupled thermal-hydrologic-chemical processes on radionuclide transport properties within the context of the ENFE 4.03 agreement.

ENFE 2.07 AIN-1 is also directly related to TSPAI 3.10 (*Technical Basis Document No. 5: In-Drift Chemical Environment*, Appendix N). TSPAI 3.10 addresses the integrated analyses, including the propagation of uncertainty through the analysis. TSPAI 3.10 primarily focuses on the treatment of parameter uncertainty analysis as it relates predominantly to the in-drift chemical environment, and ENFE 2.07 AIN-1 addresses the integrated coupled analyses.

2. RELEVANCE TO REPOSITORY PERFORMANCE

The physical and chemical processes occurring within the repository drifts affect the degradation characteristics of the titanium drip shield and the Alloy 22 waste package. A number of coupled thermal-hydrologic-chemical processes can affect the likelihood and extent of general corrosion and the initiation of localized corrosion of crevice areas on the drip shield and the waste package. The primary coupling between the major processes identified in this KTI agreement are (1) hydrologic processes affecting the thermal environment in the drift, (2) thermal and hydrologic processes affecting the evolution of temperature, water seepage, and vapor transport in the drift, and (3) thermal and hydrologic processes affecting the evolution of aqueous chemistry and deliquescent mineral deposits in the drift. (Note that the in-drift thermal and hydrologic processes are predicted to be independent of water chemistry. That is, the back couplings to the thermal and hydrologic processes from chemical processes are ignored.) However, secondary couplings that could affect one of the primary state variables (in particular, the aqueous chemistry on the waste package and drip shield surface) caused by, for example, microbial processes, radiolysis processes, and other chemical processes, are also considered in this enclosure.

In addition to the thermal-hydrologic-chemical coupled processes that are the focus of this KTI agreement, other coupled processes related to mechanical degradation of the in-drift environment and the subsequent mechanical degradation of the emplaced engineered materials constituting the engineered barrier system are addressed in Repository Design and Thermal-Mechanical Effects (RDTME) and Structural Deformation and Seismicity (SDS) KTI agreements.

Furthermore, the coupled effects of low-probability disruptive events (e.g., volcanic and seismic events) on the evolution of the in-drift thermal-hydrologic-chemical environment can subsequently affect the corrosion of the drip shield and waste package. This KTI response addresses the effect of changes in the chemical environment due to thermal-hydrologic effects, but the effects of chemistry changes during a volcanic event are discussed in the Igneous Activity (IA) consequence KTI responses.

3. RESPONSE

In the NRC evaluation of the DOE response to ENFE 2.07 (Schlueter 2003), AINs were identified. In this evaluation, it was acknowledged that the presentation to the Nuclear Waste Technical Review Board on May 13, 2003, provided clarification of the DOE method of characterizing the near-field environment. This presentation was based on the information available at that time on (1) the range of abstracted thermal environments in the drift, (2) the models used to evaluate the evolution of in-drift chemical conditions, (3) the data used to support the validation of these models, and (4) the predicted chemical evolution of aqueous and salt brines in the drift based on these models. The evolution of the aqueous solution chemistry was described in terms of mineral precipitation controlling aqueous solution compositions at different temperatures and relative humidity.

The NRC response letter noted that the DOE could consider addressing ENFE 2.07 in the context of better defining and explaining the technical basis for the consolidation or establishment of the 11 bins of potential aqueous chemistry environments mentioned in the above Nuclear Waste

Technical Review Board presentation. If DOE followed this recommendation, the approach would need to consider the range of chemistries considered, the rationale for including or excluding couples and chemistries, and the limitations of any codes used to develop the basis. The basis for the 11 water type bins is discussed in Section 4.4. The consolidation of the 11 bins into brine types (calcium chloride, sulfate, and carbonate) for the purposes of corrosion testing is discussed in Section 4.4.4.3.

The initial response to KTI agreement ENFE 2.07 focused primarily on the coupling of processes, including an evaluation of the potential effects of secondary Onsager-type couplings as they relate to the diffusive transport of radionuclides. Although the initial response was appropriate for the transport aspects relevant to repository performance, it did not address the coupling that could affect the chemical environment on the waste package and drip shield and, therefore, could affect the degradation processes of these engineered features.

The chemical environment on the waste package and drip shield directly depends on the thermal-hydrologic conditions in the drift. Therefore, the response to this KTI agreement AIN request requires defining the temporal evolution of the thermal-hydrologic conditions (Section 4.2) before the evolution of the aqueous chemistry due to salt deliquescence and water seepage is evaluated (Sections 4.3 and 4.4). Other processes that could affect the chemical evolution, such as electrochemical processes on the metal substrate, gamma radiolysis, and microbial interactions, are also considered (Section 4.5). Although the amount and chemistry of the seepage water that could contact the waste package is a function of the degradation characteristics of the drip shield, this coupling is not addressed in this response. Total system performance assessment (TSPA) considers the drip shield degradation with the consequent timing of seepage water contact with the waste package. The subsequent evolution of the water chemistry on the waste packages is considered in this response.

The principal couplings that affect the evolution of the in-drift chemical environment are addressed in this response. The relevant process couplings affecting the in-drift chemical environment and the scientific bases for excluding other coupled processes that do not significantly affect the chemical environment are described. This illustrates that the relevant processes that could affect the degradation of the waste containers have been appropriately included in the models that are abstracted for use in the assessment of system performance.

The in-drift physical and chemical environment affects several aspects of repository performance. Of particular relevance for this enclosure are the effects of these environments on initiation and propagation of crevice corrosion of the waste package. The susceptibility of Alloy 22 to localized corrosion is influenced by several factors that are schematically illustrated in Figure 1. The likelihood of initiation of localized corrosion is dependent on the metallurgical conditions on the waste package surface (including the presence and severity of crevice formers) and the physical and chemical environmental conditions on the metal surface. As indicated in Figure 1, the temperature, acidity (pH), concentration of chloride ions, and the concentration of corrosion inhibitors, such as nitrate and sulfate, are of particular interest.

In the discussion of coupled physical and chemical environments presented in this response, the focus is on the physical conditions (specifically, temperature, humidity, and the presence of liquid water), the chemical conditions (specifically, chloride and nitrate concentrations and the

pH), and the couplings between these and other processes that could affect these environmental conditions. The technical basis for including or excluding coupled processes and chemical conditions from the TSPA model is provided. This also allows the determination of the range of credible near-field processes and chemical conditions to be included in the TSPA.

The information in this enclosure is responsive to AIN request ENFE 2.07 AIN-1. This enclosure contains the information that the DOE considers necessary for NRC review for closure of this agreement.

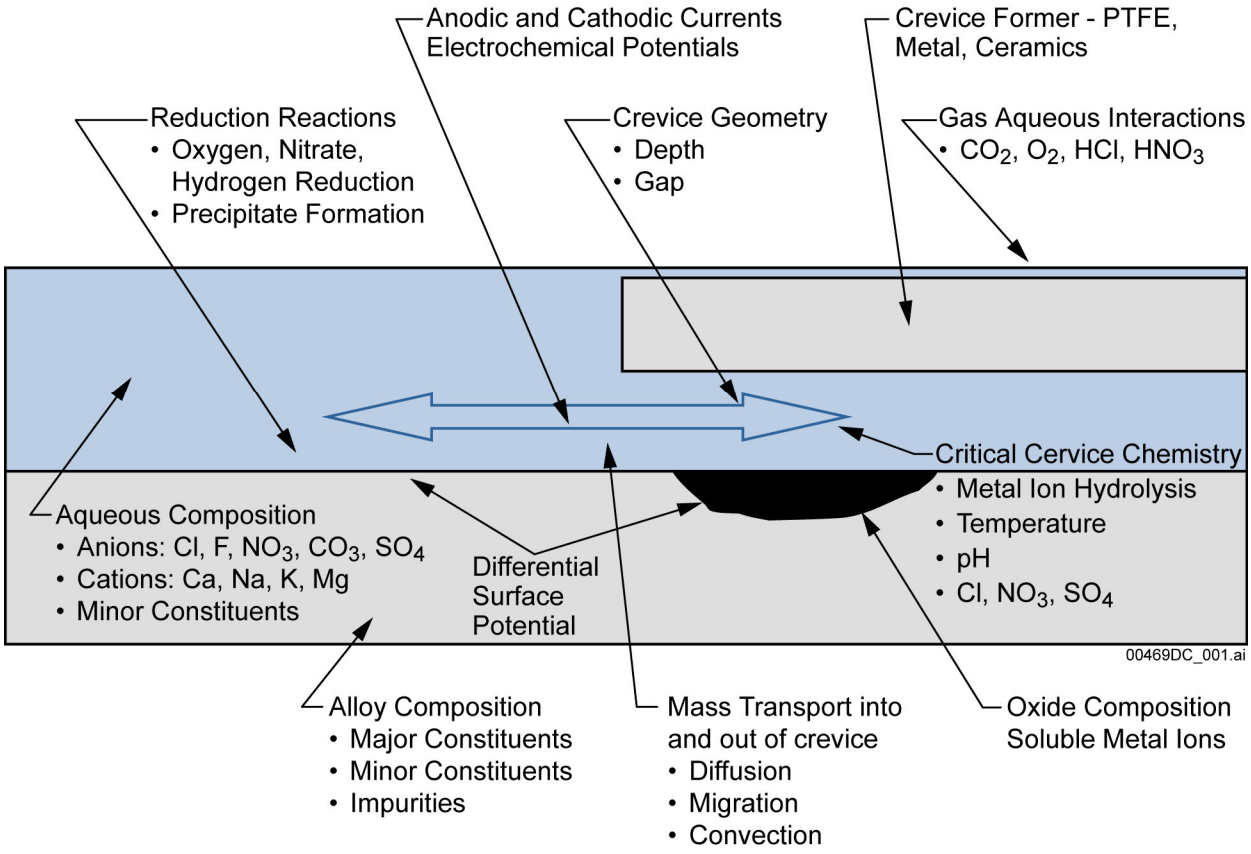

NOTE: PTFE = polytetrafluoroethylene.

Figure 1. Factors Affecting Localized Corrosion Processes

4. BASIS FOR THE RESPONSE

4.1 Introduction

The evolution of the thermal-hydrologic environment in the drift and surrounding rock mass significantly affects the chemical conditions in the drift. In particular, the thermal-hydrologic evolution in the rock mass causes moisture in the fractures and pores to be mobilized in areas of high temperature and to condense in areas of cooler temperature above and around the drift opening. This mobilization of water creates a vaporization barrier effect in the fractures around the drift wall that precludes the aqueous solutions that are evolving in the rock mass from entering the drift until the drift-wall temperature cools to below the boiling point of water,

nominally 96°C at Yucca Mountain. To account for uncertainty in the effects of small-scale drift irregularities, the temperature below which seepage of water into the drift could potentially occur has been set to 100°C in the models used in the TSPA. The thermal-hydrologic evolution of the drift environment that is coupled to and influences the in-drift chemical environment is presented in Section 4.2.

Based on the thermal-hydrologic evolution in the drift, two key time periods have been identified for evaluating the in-drift chemical evolution. The first time period corresponds to the time when aqueous seepage into the drifts is precluded as a result of the combined effects of the vaporization and capillary barrier. This time period varies from location to location in the repository, depending on the rock type, the waste package type, proximity to repository boundaries, and on the uncertainties due to the variability of percolation flux and host-rock thermal conductivity. During this time period, the chemical evolution of the drift environment is controlled by the salt mineral deposits that might be present on the waste package and drip shield surfaces and the temperature and humidity conditions in the drift that control the aqueous solutions that could evolve from these solid salt mixtures. The conditions under which the salt mineral deposits on the waste package surface are expected to deliquesce and the resulting brine solutions evolve in time are presented in Section 4.3. Section 4.3 describes the coupling between the thermal-hydrologic environment (in particular, the temperature and relative humidity of the drift air) and the salts present on the waste package surface in determining the chemical conditions on the waste package. The uncertainty in the prediction of these chemical conditions is also presented in Section 4.3, together with a discussion of other processes that could occur but are unlikely to affect the chemical evolution.

The second time period corresponds to the time when water seepage into the drifts is possible. At these times, the aqueous solutions from seepage water will chemically evolve on the waste packages and drip shields due to evaporation processes. The amount of evaporation that would occur is a function of the thermal-hydrologic conditions (again, temperature and relative humidity) in the drift and the oxygen and carbon dioxide concentration in the drift air. The chemical evolution that a water follows as it evolves in the drift is a function of its composition in the rock.

In general terms, Section 4.4 describes the possible evolution of waters in the drift into three major categories: a calcium chloride-type brine, a sulfate-type brine, or a carbonate–bicarbonate type brine. Due to the heterogeneity of environmental conditions at Yucca Mountain, there is a range of compositions within each of these types of brines. As a result, these three general brine types were divided into 11 separate bins for ease of abstracting the range in the chemical compositions into the TSPA model. The bases for these 11 bins are presented in Section 4.4. Other processes that could occur but are unlikely to affect the chemical composition are presented in Section 4.5. The approach used to evaluate the potential physical separation of salts during evaporation along the seepage flow path when it contacts the drip shield or waste package surface is also addressed in Section 4.5.

4.2 Thermal-Hydrologic Coupled Processes Affecting the In-Drift Environment

4.2.1 Overview of Thermal-Hydrologic Coupled Processes

The coupled thermal-hydrologic processes affecting the in-drift environment can be best understood by breaking down the physical system into two spatial regions of concern: the host rock and the emplacement drift. The first reason for differentiating between these regions is that the primary mechanism of heat transfer is quite different within these two regions, with thermal radiation being the dominant mechanism within the emplacement drifts, whereas thermal conduction is the dominant mechanism within the host rock. Thermal conduction is also the dominant heat-transfer mechanism in the region beyond the near field of the host rock. The second reason is that the mechanism by which relative humidity is reduced below ambient relative humidity is quite different in these two regions. Within the host rock, the relative humidity is reduced as a result of dryout in the host rock, while relative-humidity reduction in the drift, compared to that at the drift wall, depends on the temperature difference between the waste package and the drift wall. Two other aspects important to understanding thermal-hydrologic processes involve the ambient hydrologic system and the distribution of radioactive decay heat across the repository in time and space, which involves the role of ventilation in removing decay heat from the system (BSC 2004a, Section 6.1).

After the emplacement of heat-generating radioactive waste, the thermally driven flow of water vapor away from the heat source causes a redistribution of the pore fluids within the host rock. Water in the matrix pores evaporates, creating zones of rock dryout (with liquid-phase saturation less than ambient values) around the emplacement drifts. This water vapor is driven (primarily in fractures) away from the heat source in the emplacement drifts to where cooler temperatures cause it to condense, forming condensation zones outside of the dryout zones. The reduction in liquid-phase saturation causes a reduction in relative humidity in both the near-field host rock, as well as in the emplacement drifts. As the heating rate declines, the host rock gradually rewets, returning to ambient (humid) preheating conditions (BSC 2004a, Section 6.1.2).

In the host rock, local thermal-hydrologic conditions are dominated by whether a location is inside or outside of the zones where the host rock temperature is above the boiling point of water, which is 96°C at the elevation of the repository horizon at Yucca Mountain (nominally 1,100 m above mean sea level). Although the coupled effects of evaporation, vapor flow (away from the heat source), and condensation occur at below-boiling temperatures, the thermally driven vaporization rates and vapor fluxes in the repository horizon are generally not great enough to result in significant dryout (and relative humidity reduction) in the rock unless temperatures are well above the boiling point (BSC 2004a, Section 6.1.3).

4.2.2 Key Ambient Hydrologic Parameters Affecting In-Drift Thermal-Hydrologic Environment

The key ambient hydrologic parameters affecting the in-drift thermal-hydrologic environment are:

- **Host-Rock Hydrologic Properties**–The host rock consists of welded tuffs, with varying degrees of lithophysal porosity, which are densely fractured, resulting in a permeable,

well-connected network of fractures. Most of the total fluid storage capacity is contained in the matrix pores of the host rock. The permeability in the rock matrix, however, is very low, and, therefore, fractures are the primary conduits for large-scale flow of water, air, and water vapor. Also, the fracture permeability is large enough, and fracture spacing is sufficiently dense to allow boiling and rock dryout to occur in an unthrottled (i.e., unrestricted) fashion. Therefore, the in-drift thermal-hydrologic environment is insensitive to variability and uncertainty in host-rock hydrologic properties (BSC 2004b, Section 6.3.2.4).

- **Percolation Flux Distribution above Repository Drifts**–The percolation flux varies both areally (over the repository area) and as a function of time (as a result of climate change). This distribution depends on the infiltration-flux distribution and lateral redistribution of flux in the PTn unit, which overlies the repository area (BSC 2004b, Section 6.3.1). Rewetting of the dryout zone primarily depends on the percolation flux, except in regions of very low flux (less than 0.1 mm/yr), where it depends on capillary-driven imbibition flux, that is, water sorption by the rock (*Technical Basis Document No. 3: Water Seeping into Drifts*, Appendix I). Thus, the spatial and temporal extent of rock dryout depends on the magnitude of the local percolation flux. Accordingly, the in-drift thermal-hydrologic environment depends strongly on variability and uncertainty in percolation flux (but is insensitive to the variability of host-rock hydrologic properties, as explained above).

Under ambient conditions, the relative humidity in the host rock is very high, generally greater than 99%. Relative humidity is reduced in the host rock as a result of boiling-driven rock dryout in the host rock (BSC 2004a, Section 6.1.2).

4.2.3 Radioactive Decay Heat Distribution

The radioactive decay heat is generated (nominally) by 11,184 waste packages, which are evenly distributed along 96 emplacement drifts (BSC 2004a, Tables 4-1 and 5.8-2). The heat output of the waste packages declines exponentially with time, continuing for tens of thousands of years because of the very long half-life of many of the radionuclides (Figure 2). The heat output also varies from waste package to waste package, with substantially greater heating rates being generated by waste packages that contain spent nuclear fuel than by those that contain high-level radioactive waste. Forced ventilation during the preclosure period removes most of the heat generated by waste packages during the ventilation period, as reported in *Ventilation Model and Analysis Report* (BSC 2004c). Consequently, during the preclosure period, in-drift temperatures are below the boiling point of water.

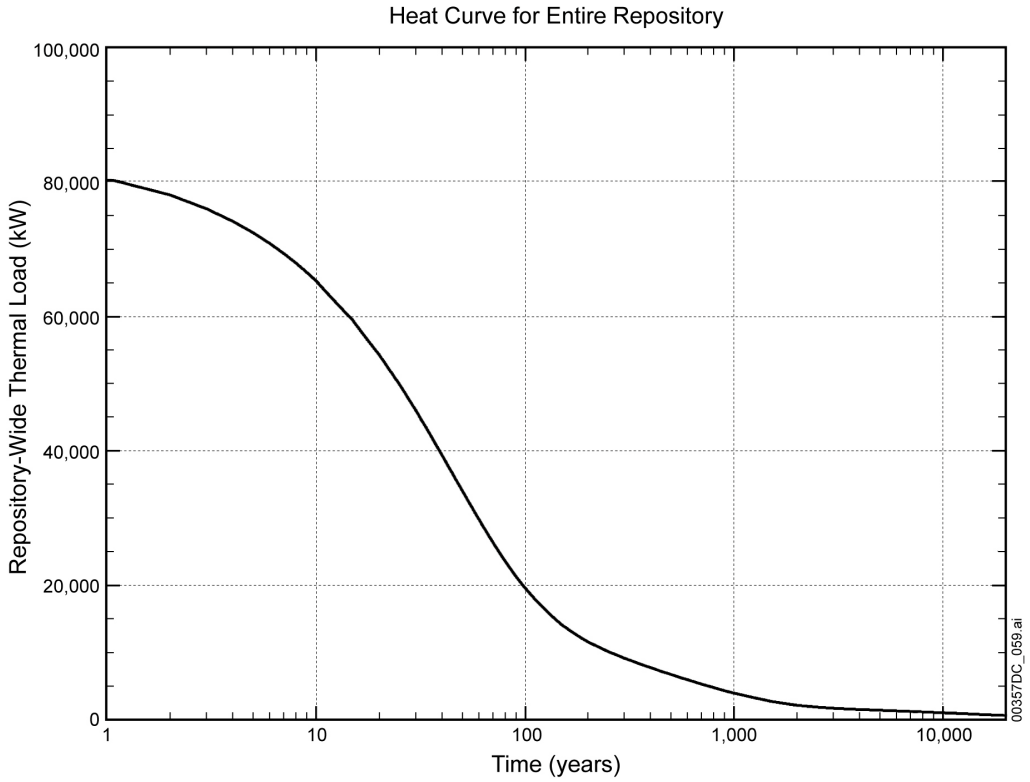

Source: BSC 2004a, Figure 6.1-1.

Figure 2. Repository-Wide Thermal Load as a Function of Time

4.2.4 Thermal-Hydrologic Behavior In and Around Emplacement Drifts

Thermal-hydrologic behavior in and around emplacement drifts can be simply broken down to three fundamental processes:

1. **Heat Flow**–Occurs in emplacement drifts, primarily by thermal radiation, and in the adjoining host rock, primarily by thermal conduction. Consequently, host-rock thermal conductivity is the key natural-system parameter that determines the magnitude of temperature increase in the host rock (BSC 2004a, Section 6.3.4). The thermal conductivity of the host rock depends on liquid-phase saturation in the rock, on heat flow, and on the rock temperature.

2. **Host-Rock Dryout**–Occurs as a result of evaporation (boiling) of water, which lowers the liquid-phase saturation in the host rock, thereby lowering the relative humidity in the host rock and in the emplacement drifts. Dryout depends on the extent and duration of boiling in the host rock, which depends on the magnitude of temperature increase. Because the effective permeability of the fractured rock mass is sufficiently large, only a small gas-phase pressure is built up, allowing boiling to progress in an unthrottled (i.e., unrestricted) fashion (*Technical Basis Document No. 3: Water Seeping into Drifts*, Appendix I).

3. **Host-Rock Rewetting**–Primarily occurs as a result of gravity-driven percolation in fractures, with capillary-driven imbibition into the adjoining matrix. The rate of

rewetting is controlled by the local percolation flux, except in regions of very low percolation flux (less than approximately 0.1 mm/yr), where it is controlled by capillary-driven imbibition in the matrix (*Technical Basis Document No. 3: Water Seeping into Drifts*, Appendix I).

The coupled processes of dryout and rewetting act in opposition. The net host-rock dryout, which is the difference between dryout and rewetting, is greatest in regions with a combination of low host-rock thermal conductivity (which facilitates greater temperature rise) and low local percolation flux (which facilitates slower rewetting). The net host-rock dryout is the least in regions with a combination of high host-rock thermal conductivity (which facilitates smaller temperature rise) and high local percolation flux (which facilitates faster rewetting).

Two important factors that influence the physical conditions in the emplacement drifts are (1) the temperature and relative humidity at the drift wall and (2) the temperature difference between the waste package and drift wall, which depends on heat transfer between the engineered components (waste package and drip shield) and the drift wall (BSC 2004a, Section 6.1.4). The temperature at the drift wall is controlled by the temperature rise in the host rock, which is influenced by the local heating conditions and the host-rock thermal conductivity. The relative humidity at the drift wall is controlled by the reduction in liquid-phase saturation within the rock that results from boiling and rock dryout.

The local relative humidity at the drift wall controls the maximum local relative humidity within the drift; relative humidity in the drift can be no greater than it is at the drift wall. The temperature at the drift wall also determines whether liquid water seeps into the drift, with above-boiling temperatures creating a vaporization barrier. Heat transfer between engineered components, such as the waste package and drip shield, and the drift wall determines the temperature difference between the waste package and drift wall. This temperature difference controls the reduction in relative humidity on the waste package and the drift wall. Thus, a large temperature difference between the waste package and drift wall results in a large reduction in relative humidity on the waste package compared to that on the drift wall. The drip shield, which lies between the waste package and drift wall, functions as a thermal-radiation shield, which increases the temperature difference. The temperature difference between the waste package and drift (and resulting reduction in relative humidity) is greatest immediately after closure. This temperature difference slowly decreases with time (BSC 2004b, Section 6.1.3).

During the preclosure period (nominally 50 years), waste package heat output will be at a maximum, but the emplacement drifts will be ventilated to remove most of the heat generated during this period (BSC 2004c, Section 6). Waste package temperatures will be elevated, and some packages may approach 100°C immediately after emplacement (subject to control by ventilation). However, the warming of ventilation air ensures that preclosure conditions are dry (e.g., less than 20% relative humidity), especially where in-drift temperatures are the greatest (BSC 2004c, Section 6.9).

At permanent closure, ventilation ceases and the drift-wall rock temperatures will increase sharply from below boiling, with the temperature peaking within about 20 years after closure (BSC 2004b, Section 6.3.1). Waste package temperatures follow the evolution of the local drift-wall temperature but are as much as 10°C to 20°C (18°F to 36°F) warmer at the time when

waste package temperatures peak, because of thermal resistance across the drip shield and the in-drift air spaces (BSC 2004a, Section 6.3.1.2, Figure 6.3-11 to 6.3-15). This temperature difference will eventually approach zero, with the continued decline in the heat output. The maximum postclosure temperature of a waste package at any location is determined by the combined effects of (1) the heat-generation-rate-versus-time relationship for that waste package, (2) the resistance to dissipation of heat in the host rock (which is controlled by the host-rock thermal conductivity), (3) heat transfer from the waste package to the drift wall (which is controlled by thermal radiation), (4) the proximity to adjacent heat sources (and their respective heat-generation-rate-versus-time relationships), and (5) the proximity of that location to the external boundary of the repository.

4.2.5 Range of In-Drift Thermal-Hydrologic Conditions across the Repository

The multiscale thermal-hydrologic model captures the influence of the key engineering-design variables and natural system parameters that affect the thermal-hydrologic conditions in the emplacement drifts and in the adjoining host rock (BSC 2004a, Section 1). While the list of design variables and natural system parameters is rather long, a relatively small number of these are responsible for the majority of variability and uncertainty in thermal-hydrologic conditions across the repository. In order of importance, these are:

1. Edge-cooling effect, which increases with proximity to the edges of the repository
2. Variability and uncertainty in host-rock thermal conductivity
3. Variability and uncertainty in percolation flux above the repository
4. Variability in heat output among waste packages.

This ranking is obtained from an evaluation of the primary contributors to thermal-hydrologic variability across the repository, which is discussed in *Multiscale Thermohydrologic Model* (BSC 2004a, Section 6.3). The multiscale thermal-hydrologic model simulations supporting TSPA-LA fully address the influence of these four items by incorporating five infiltration flux–host rock thermal conductivity cases and their associated probabilities (Table 1). The rationale for these five selected cases and their associated probabilities is given in *Multiscale Thermohydrologic Model* (BSC 2004a, Section 6.3.4). A sensitivity study of the influence of hydrologic-property uncertainty (BSC 2004b, Section 6.3.2.4) supports the conclusion (BSC 2004b, Section 8.2) that hydrologic-property uncertainty does not need to be propagated in the multiscale thermal-hydrologic model calculations of in-drift temperature and relative humidity.

Table 1. Probabilities of the Combinations of the Three Infiltration Flux Cases and the Three Host-Rock Thermal Conductivity Cases

Infiltration Flux Case	Probability			
	Host-Rock Thermal-Conductivity Case			
	All	Low (Mean −1σ)	Mean	High (Mean +1σ)
All	1.0000	0.33333	0.33333	0.33333
Lower	0.2400	0.08000	0.21667	—
Mean	0.4100	—	0.33333	—
Upper	0.3500	—	0.25334	0.11666

Source: BSC 2004a, Table 6.3-35.

NOTE: σ = standard deviation. As discussed in *Multiscale Thermohydrologic Model* (BSC 2004a, Section 6.3.4), the four cases without listed probabilities are addressed by grouping them into equivalent cases. Thus, the mean-infiltration flux low-thermal-conductivity case is grouped into the lower-infiltration flux mean-thermal-conductivity case, while the mean-infiltration-flux high-thermal-conductivity case is grouped into the upper-infiltration-flux mean-thermal-conductivity case. Both the lower-infiltration-flux high-thermal-conductivity case and the upper-infiltration-flux low-thermal-conductivity case are grouped into the mean-infiltration flux mean-thermal-conductivity case.

Figure 3 is a plot of the range of temperature histories for all waste packages across the repository, accounting for the influence of parametric uncertainty of host-rock thermal conductivity and percolation flux above the repository. Figure 4 shows the corresponding range of waste package relative humidity histories across the repository. Figure 5 gives the corresponding range of temperature versus relative humidity trajectories, during cool down (i.e., after the waste-package temperature has peaked). Also plotted on these three figures are predicted trajectories for three distinct waste packages, including (1) a cool U.S. Department of Energy (DOE) high-level radioactive waste waste package close to the edge of the repository, (2) an average boiling water reactor (BWR) waste package at the center of the repository, and (3) a hot pressurized water reactor (PWR) waste package at the edge of the repository.

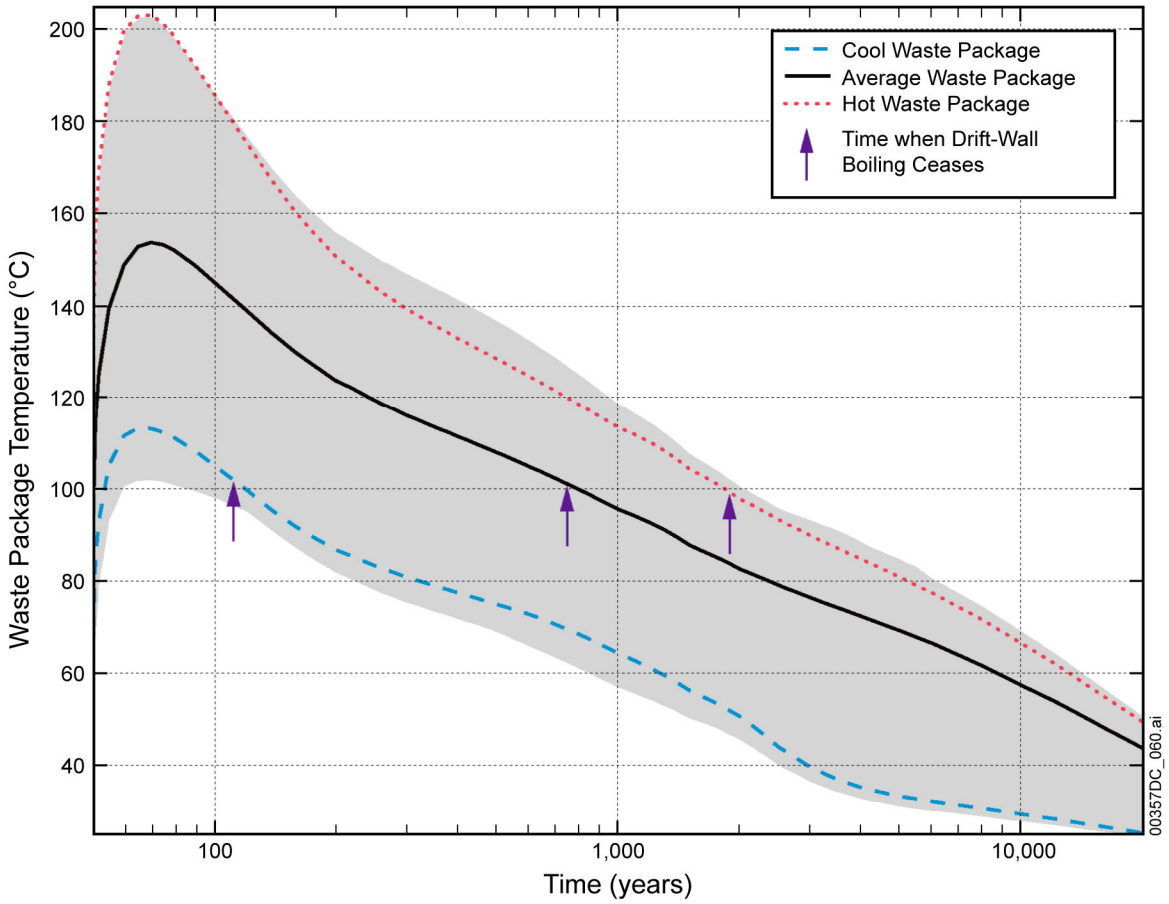

Source: DTNs: LL030906131032.002; LL031206723122.041; LL030906531032.005; LL030905931032.001; LL030906331032.004.

NOTE: The upward arrows indicate the time when boiling ceases at the drift wall.

Figure 3. Range of Temperature Histories for All Waste Packages, Accounting for Uncertainty of Host-Rock Thermal Conductivity and Percolation Flux

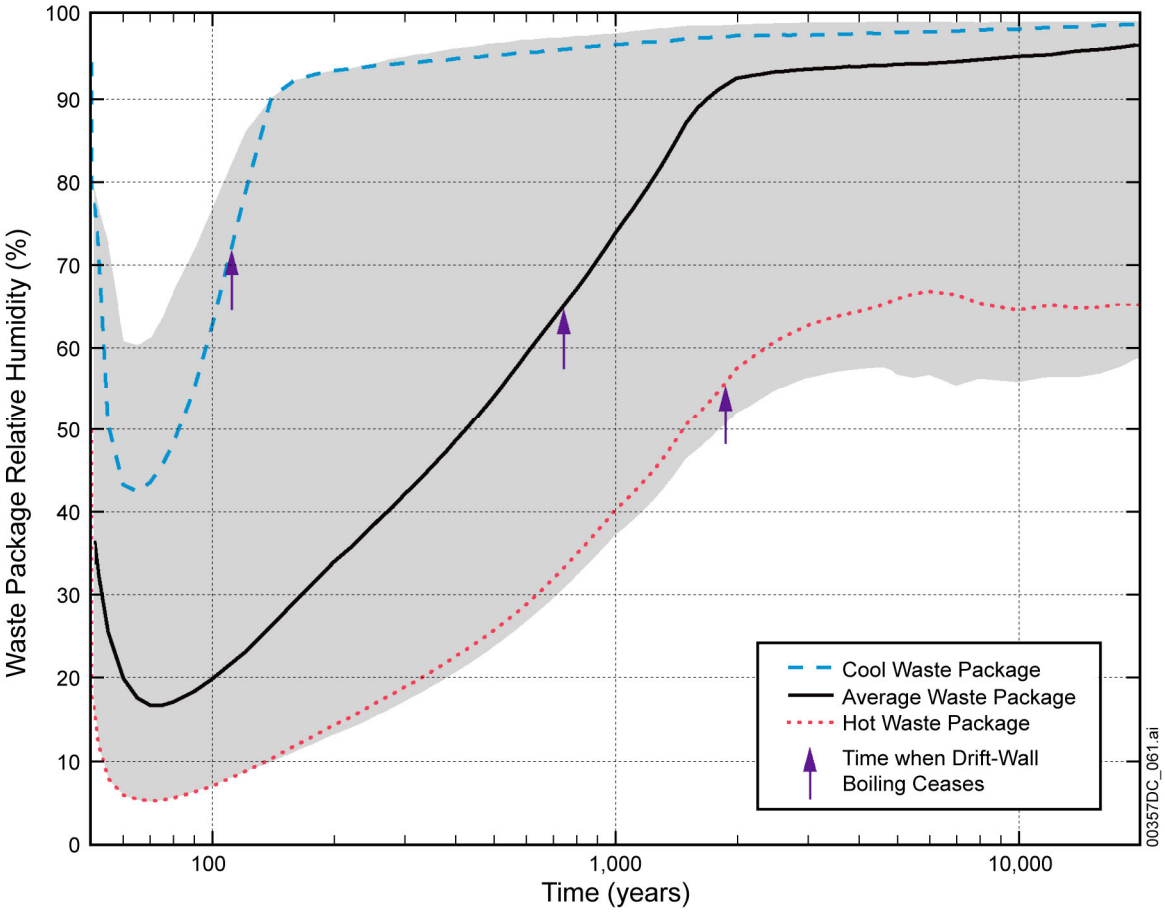

Source: DTNs: LL030906131032.002; LL031206723122.041; LL030906531032.005; LL030905931032.001; LL030906331032.004.

NOTE: The upward arrows indicate the time when boiling ceases at the drift wall.

Figure 4. Range of Relative Humidity Histories for All Waste Packages, Accounting for Uncertainty of Host-Rock Thermal Conductivity and Percolation Flux

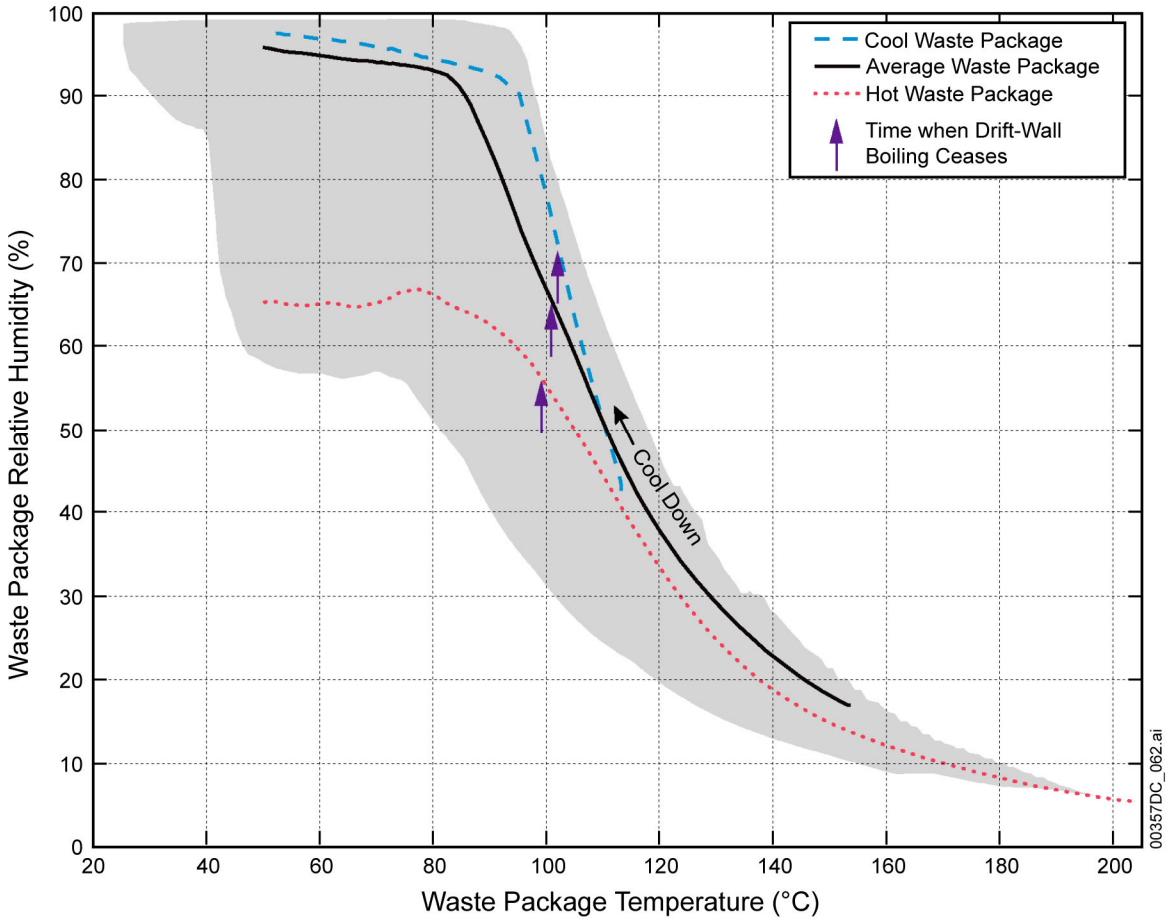

Source: DTNs: LL030906131032.002; LL031206723122.041; LL030906531032.005; LL030905931032.001; LL030906331032.004.

NOTE: The upward arrows indicate the time when boiling ceases at the drift wall.

Figure 5. Range of Temperature versus Relative Humidity Trajectories for All Waste Packages during Cooldown Accounting for Uncertainty in Host-Rock Thermal Conductivity and Percolation Flux

4.3 In-Drift Chemical Environment with Above-Boiling Conditions at Drift Wall

Seepage of liquid water into the drifts is not expected as long as the drift wall temperatures remain above the boiling point for dilute water (greater than 96°C at the repository elevation). For TSPA purposes, the more conservative, sea-level boiling point temperature of 100°C at the drift wall is used for the seepage threshold. In the absence of seepage, deliquescence of salts is the only expected mechanism for the formation of liquid water. Prior to the beginning of water seepage into the drift, the only source of salts is likely to be dust deposited in the drifts (on the metal barriers and elsewhere). This dust is expected to consist primarily of atmospheric dust brought into the repository during the ventilation period, though other sources, such as rock dust, are possible. Nearly all waste packages are expected to be affected by the presence of dust. Even after seepage is initiated, most waste packages will not be contacted by water, either because of the low probability of seepage or the presence of the drip shield. Therefore, the deliquescence process is likely to continue to determine the chemical environment for the majority of waste packages even in the subsequent period at below-boiling temperatures.

4.3.1 Coupled Processes Affecting the Above-Boiling In-Drift Chemical Environment

In the above-boiling period, the temperature at the drift wall will be in excess of 96°C and the temperatures on the metal barriers will be even higher (higher on the waste package outer barrier than on the drip shield). The anticipated temperature and relative humidity conditions are derived from the thermal-hydrologic conditions described in Section 4.2. The air mass in the drift is expected to be well mixed due to the in-drift temperature gradients. Any projected temperature–relative humidity history (as represented by the thermal-hydrologic modeling) will show an increase in relative humidity as temperature decreases during the above-boiling period. The total pressure in the drift is not expected to deviate significantly from the ambient pressure for the repository elevation (i.e., nominally 90 kPa or 0.90 bar pressure).

If only pure liquid water could form in the drift, the above-boiling period would be characterized by the absence of liquid water. Liquid water could form from vapor only after the relative humidity has risen to 100% (normal condensation). The presence of salts in dust allows the formation of liquid water at relative humidity values less than 100% (actual relative humidity depends on the composition of the salt mixture). In that sense, deliquescence can be viewed as salt-assisted condensation. The presence of liquid water at relative humidity notably lower than 100% requires the liquid to be a concentrated brine, as will be discussed in the following section. Depending on the brine composition, this liquid may, therefore, be more corrosive to the metal barriers than pure water. The brine composition is a function of the salts present, the temperature, and the relative humidity, and as the relative humidity rises through time, the brine will become progressively more dilute.

To describe the process of deliquescence, it is necessary to review the coupled relationships between the vapor pressure of water, the relative humidity, and the thermodynamic activity of water. The vapor pressure of water is the partial pressure of water vapor–air mixture. The relative humidity is defined by relative humidity equal to $100 p_w / p_w^o$, where p_w is the vapor pressure of water in equilibrium with the aqueous solution, and p_w^o is the vapor pressure of pure water at the same temperature. The activity of water, a_w, is related to the vapor pressure of water (in equilibrated vapor) by $a_w \equiv p_w / p_w^o$. It has a value of unity for pure water, values close to unity (e.g., 0.98) for dilute salt solutions, and can have much lower values (e.g., 0.5, 0.2) for concentrated salt solutions. In effect, the percent relative humidity is related to water activity by relative humidity equal to $100 a_w$.

Figure 6 shows the vapor pressure of water as a function of temperature for some fixed values of the activity of water. The case of pure water corresponds to unit water activity. Each vapor pressure curve shows a rapid increase with increasing temperature. The horizontal blue line in the figure represents standard atmospheric pressure, 101.325 kPa (1.01325 bar), and the horizontal red line represents the maximum sustained pressure expected in the drifts, 90 kPa (0.90 bar). An aqueous solution boils when the associated water vapor pressure exceeds the total confining pressure. Thus, pure water boils at 100°C at 1 atm and at 96°C at the expected (maximum) repository pressure. The effect of boiling point elevation is apparent for lower water activities. The case of water activity fixed at 0.75 closely represents the behavior of a system saturated with NaCl. Here, the boiling point is about 106°C at repository pressure. The boiling

point of an aqueous $CaC1_2$ solution is about 161°C (Kracek 1928), so water activity is between 0.2 and 0.1.

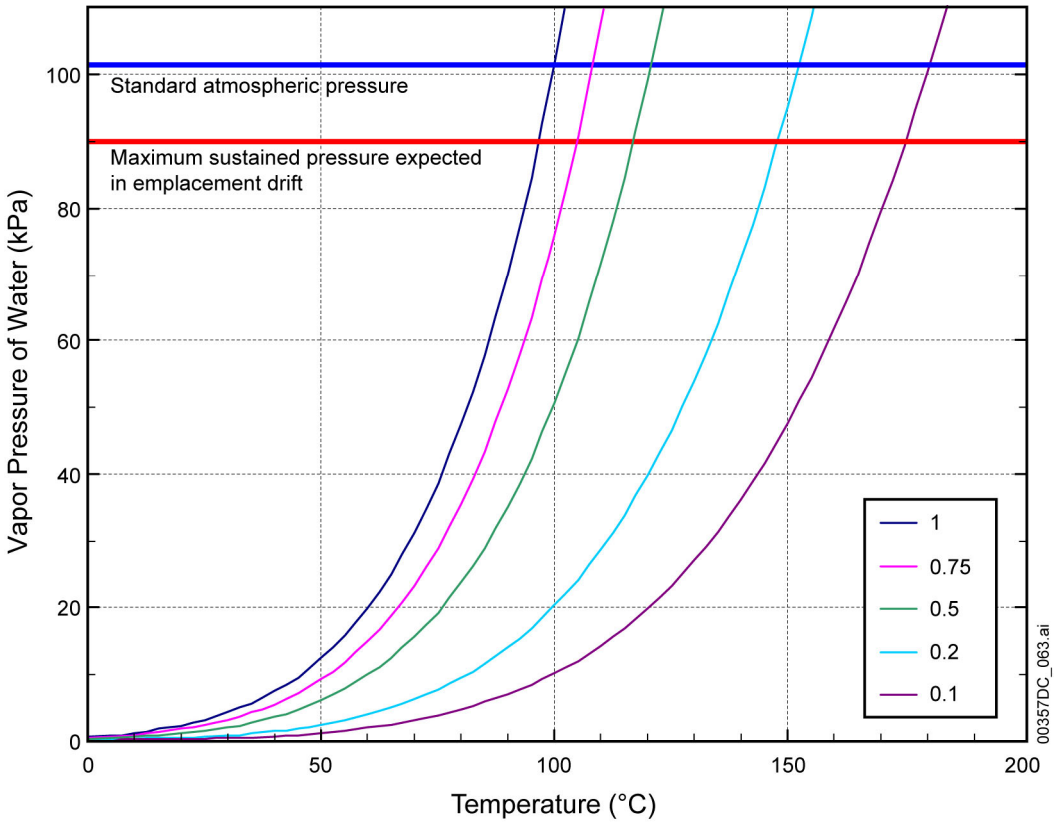

Source: BSC 2003a, Section 6.7.2.3, Figure 2: spreadsheet WaterPressureTable.xls; DTN: LL030500712251.060.

NOTE: The condition of constant water activity with changing temperature is not, in general, a characteristic of real saturated salts.

Figure 6. Vapor Pressure of Water as a Function of Temperature and Water Activity (Water Activity Values are Shown in the Legend)

When the partial pressure of water vapor is constrained (e.g., by standard atmospheric pressure or the expected maximum pressure at the repository horizon), the attainable values of relative humidity are constrained. The relative humidity cannot attain a value for which the partial pressure of water is greater than the constraining total pressure. This constraint is illustrated in Figure 7, which shows two curves, the left one for the expected mean repository pressure (slightly less than the expected maximum of 90 kPa or 0.90 bar) and the right one for standard atmospheric pressure. For the given pressure, the relative humidity curve is equal to the maximum relative humidity allowed. The region above the curve is, therefore, not attainable.

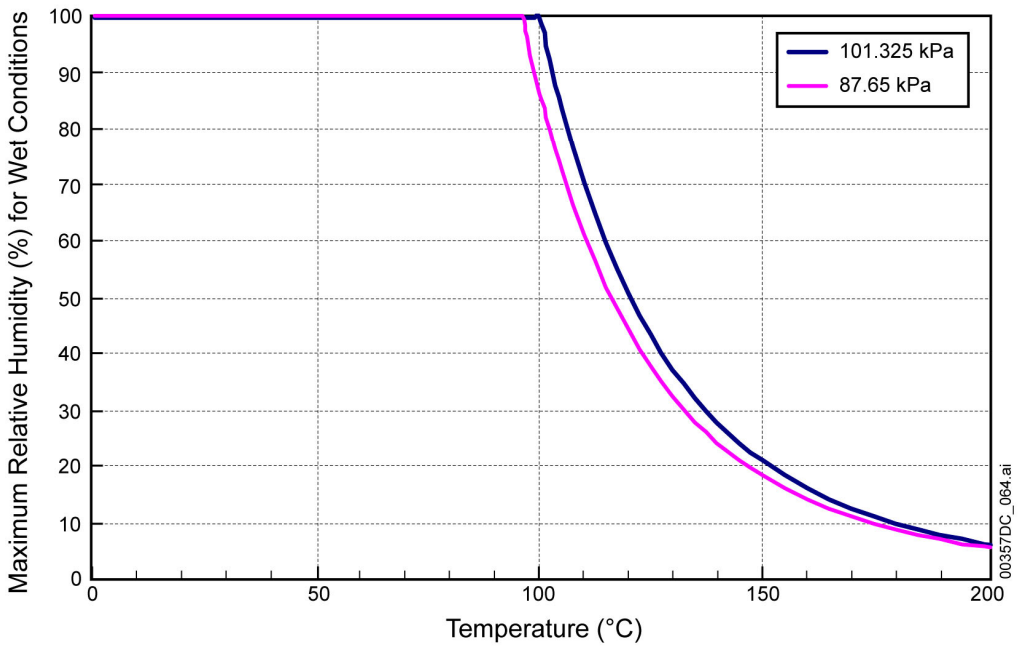

Source: BSC 2003a, Section 6.7.2.3, Figure 3: spreadsheet WaterPressureTable.xls; DTN: LL030500712251.060.

Figure 7. Maximum Relative Humidity for Wet Conditions as a Function of Temperature, for Repository Ambient Pressure (Left) and Standard Atmospheric Pressure (Right)

In addition to the interpretation of deliquescence as salt-assisted condensation, deliquescence can be considered as the inverse of the evaporation process, as indicated in Figure 8. Water in the liquid phase is lost to the vapor phase until the relative humidity of the vapor phase is equilibrated with the activity of water in solution. This process will continue until either the vapor and liquid phases reach equilibrium (with the relative humidity equal to $100a_w$%) or the liquid phase disappears due to complete evaporation (i.e., dryout). Often, the relative humidity in the vapor phase is effectively fixed due to the presence of an open system in which the vapor phase is unrestricted in communication with an external reservoir of water that is large in comparison to the amount of liquid water in the system. The loss of liquid water increases the concentrations of the solute components in the residual water. The activity of water, initially close to unity (relative humidity near 100%), would slowly decrease and saturation is reached with any relatively insoluble solids, such as calcite ($CaCO_3$) or amorphous silica (SiO_2). If thermodynamic equilibrium holds, these phases will then begin to precipitate from the solution.

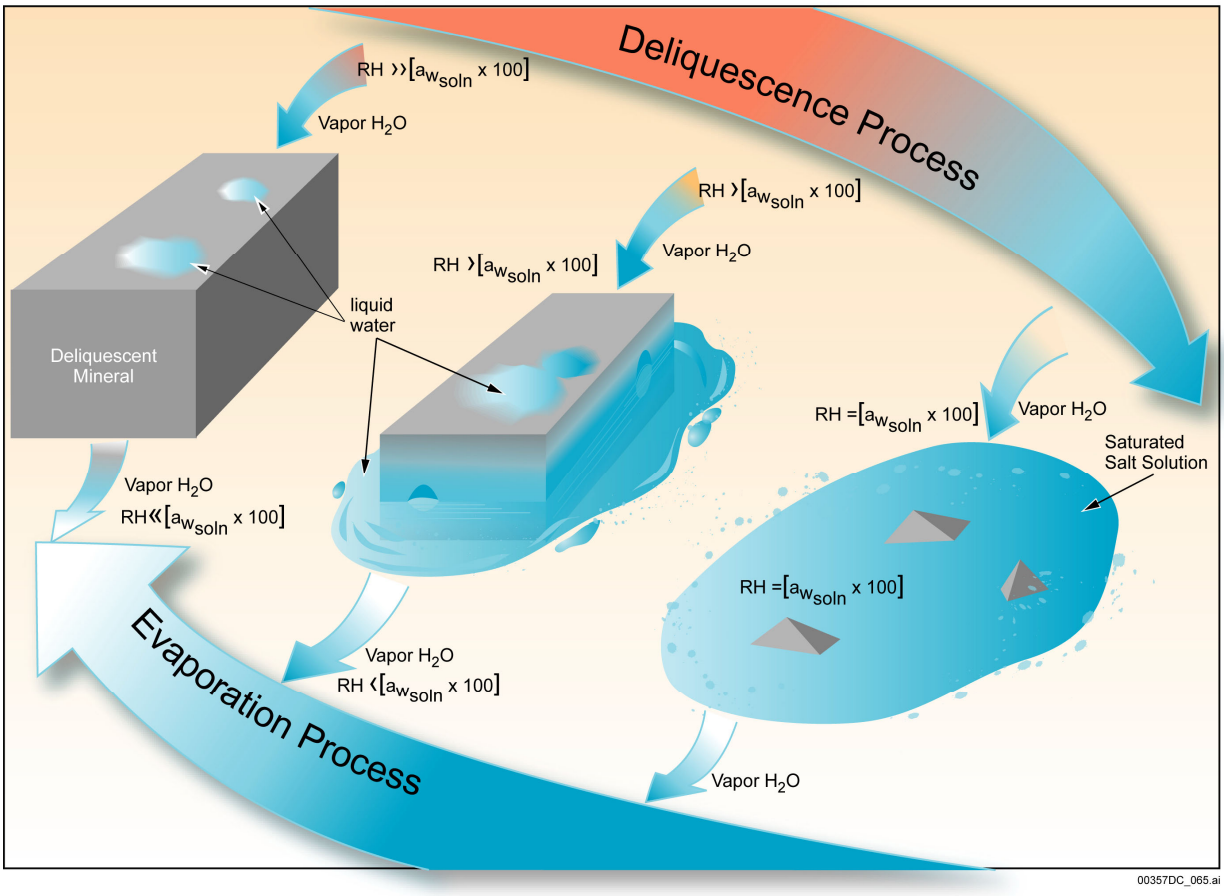

Figure 8. Schematic Illustration of Deliquescence and Evaporation

As the evaporation process continues, the activity of water in the solution and relative humidity of the vapor phase will decrease further, and the concentrations of the more soluble dissolved components in the solution will continue to increase and, at some point, the solution will become saturated with respect to mineral phases that will then precipitate. Typically, an evaporating solution reaches a eutectic state in which the solute compositions and the activity of water remains constant up to the point of dryout. The set of solids corresponding to this eutectic state is referred to as the eutectic assemblage. The number of such solids is fixed by the mineralogical phase rule (Wolery 1979, pp. 22 and 23), which relates the number of minerals (including any gases, such as CO_2, for which fixed fugacity constraints are employed) to the number of chemical components. The relative humidity that corresponds to the eutectic state can be referred to as the dryout relative humidity. During the process of evaporation, some minerals may form as transient precipitates, only to redissolve at some later point as other more thermodynamically stable minerals that compete for common components begin to form. Thus, not all minerals formed during evaporation are part of the final eutectic assemblage.

The process of deliquescence starts with a dry assemblage of solids. For the present discussion, the assumption will be made that this is the same as the eutectic assemblage produced in the above discussion of evaporation of solutions accompanied by precipitation of minerals. If the relative humidity in the vapor phase is raised to a value above the dryout relative humidity of the

assemblage, deliquescence will occur. An aqueous solution will then form, initially at the composition of the eutectic mineral assemblage. The mass of this solution will grow at constant relative humidity until one or more of the solids present (generally the most soluble) dissolves completely; the solution then moves out of the eutectic state. With the increase in water content, the solution becomes progressively more dilute until the other remaining solids dissolve completely, accompanied by increasing water activity until vapor pressure equilibrium is eventually achieved. During this process, some minerals not present in the original dry mineral assemblage may precipitate and appear as new solid phases. In essence, deliquescence is the inverse of the process of evaporation, in that the same processes occur in both but in opposite directions along the reaction path.

If the deliquescence and evaporation processes occur sufficiently slowly, then the process should be fairly well described by equilibrium thermodynamics. In the repository drifts, the assumption of thermodynamic equilibrium is appropriate because deliquescence will be driven by slowly decreasing temperature and slowly increasing relative humidity. Although the initial mixture of dry minerals in the dust may not be a mechanical mixture equivalent to a eutectic assemblage, once liquid water is present, such a mixture would be expected to equilibrate relatively quickly. From that point onward, the process would be similar to that described above for the evolution of a eutectic mixture. However, evaporation processes may not occur under equilibrium conditions if, for example, seepage water dripping onto a hotter metal barrier surface evaporates quickly. In that case, some metastable solids may form in place of the more thermodynamically stable solids that would be expected to form under conditions near thermodynamic equilibrium.

The methodology used in TSPA for determining the aqueous chemistry of the chemical environments on the metal barrier surfaces is shown in Figure 9. The top of this figure depicts the procedure used in the case of the seepage water evaporation, and the bottom depicts the procedure used for dust deliquescence. The basic notion underlying these procedures is that a characteristic set of discrete water or dust chemistries with each composition referred to as a bin can be used to satisfactorily contain and represent the actual evolution of the chemistries over the expected range of their variation. Lookup tables contain the corresponding water compositions for each bin as a function of temperature and relative humidity. The temperature and relative humidity in the drift at any point in time are those obtained from a calculated thermal-hydrologic evolution of the drift environment.

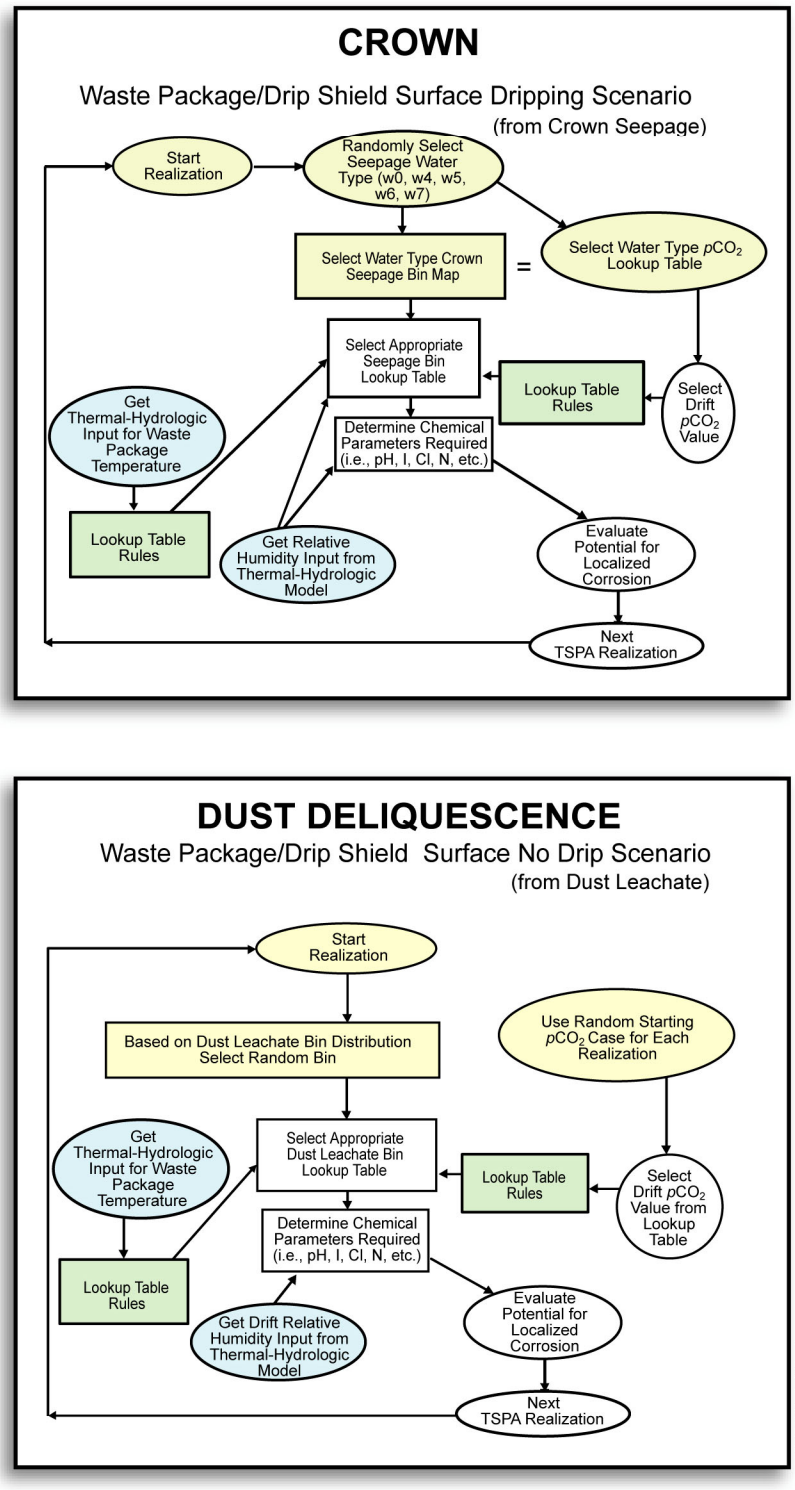

Source: BSC 2004d, Section 8.2.2, Figure 8.2-1.

Figure 9. Schematic Treatment in Total System Performance Assessment for Derivation of Engineered Barrier System Water Chemistries by Source and Location

Implicit in this methodology is the assumption that feedback effects from seepage or deliquescence on the thermal-hydrologic evolution of the drift environment can be ignored. That is, the back coupling of these processes is assumed to not perturb the temperature or relative humidity in any significant way. This is a reasonable assumption because the vapor phase movement into and through the repository is large compared with the mass influx of expected dust salts, and the contributions to the water mass and heat source terms in the thermal-hydrologic calculations by these sources of dust will be correspondingly small. The vapor phase is highly mobile within the drifts and through the rock. Any water vapor consumed by dust deliquescence and any associated increase in temperature by deliquescence is insignificant compared to the magnitudes of water mass and heat transported by gas phase convection and dispersion. The amount of dust deposited is discussed in *Engineered Barrier System Physical and Chemical Environment Model* (BSC 2004d). Similar arguments apply to the evaporation of seepage water. The water chemistries calculated using the predicted thermal-hydrologic states without these feedback effects are then used to evaluate the effect of the water chemistry on corrosion of the metal waste package surfaces. Evaporation of seepage water is further described in Section 4.4. Several factors, in addition to those described above, may influence the solution chemistry arising from dust deliquescence. These factors include differences in the solubility of the salts, their interactions in solution, and their interactions with the gas phase. An example is the formation of KCl (sylvite) from NaCl (halite) and KNO_3 (niter) at temperatures above 100°C, the residual Na^+ and NO_3^- entering the aqueous solution.

In a hydrologically unsaturated environment, some salts can also react with liquid water to form other usually less soluble and less deliquescent salts while emitting an acid gas species. In general, it is expected that in such a case the salt would dissolve before such a reaction could proceed, although it is possible that reaction of the dry salt with water vapor may be sufficient to produce such a reaction. In any event, dissolved salts would participate in such a process, as discussed in Section 4.5 and is exemplified by the reaction $MgCl_2 + H_2O = MgOHCl(s) + HCl(g)$.

In the drifts, acid gas generated in this way could be quickly transported elsewhere (e.g., the drift wall, which is cooler and relatively alkaline due to the presence of the tuff) and be removed from the chemical system. The implication of such a reaction is that certain types of brine are unstable under hydrologically unsaturated conditions. Such acid gas species could be neutralized all or in part in the dust layer itself by reaction with certain insoluble components of the dust, such as calcite (only a small fraction of which appears in the soluble fraction, owing to its limited solubility).

4.3.2 General Description and Theory of Deliquescence Processes

Deliquescence is a topic of study in several fields. The most extensive literature is in the field of atmospheric science (e.g., Tang and Munkelwitz 1993; Tang and Munkelwitz 1994; Ge et al. 1998; Ansari and Pandis 1999; Pilinis 1999). In atmospheric science, the interest is focused on the generation of aqueous aerosols from salt aerosols, various reactions important to the budgets of chemical species in the atmosphere, coupling to mechanisms of climate and climatic change, and the fate and consequences of anthropogenic inputs. Deliquescence is also a topic of interest in chemical engineering (e.g., Greenspan 1977), cave science (e.g., Hill and Forti 1997), and the preservation of museum artifacts (e.g., Creahan 1991).

The atmospheric chemistry literature, in particular, differentiates between deliquescence relative humidity and efflorescence relative humidity. Efflorescence is equivalent in meaning to evaporative dryout. Deliquescence is, as noted earlier, closely governed by equilibrium thermodynamics. On the relatively short timescales (e.g., minutes, hours) appropriate to atmospheric phenomena of interest, the drying out process may be associated with supersaturation of certain salts that allow the efflorescence relative humidity to be less than the deliquescence relative humidity. This concept is not pertinent to the much longer timescales applicable to a geologic repository system.

Thermodynamic calculations to illustrate the deliquescence and solubility characteristics of mixed salts were performed with the computer code EQ3/6. The calculations shown below were made using EQ3/6 version 8.0 (BSC 2003b; SNL 2003) and its supporting high-temperature Pitzer-based thermodynamic database data0.ypf.R1 (DTN: SN0302T0510102.002). EQ3/6 is a software package for modeling aqueous geochemical systems. The database used here is based on the phenomenology of Pitzer (1991), which addresses the thermodynamic behavior of aqueous salt solutions to high concentration.

The phenomenon of deliquescence follows certain broad rules. The first rule is that every mineral has a characteristic deliquescence relative humidity, which in general is a function of temperature. Figure 10 shows EQ3/6 computer code calculations of the deliquescence relative humidity versus temperature for six salt minerals spanning much of the relative humidity range of interest. In this figure, NaCl (halite) exhibits a nearly constant deliquescence relative humidity. Some minerals have decreasing deliquescence relative humidity (becoming more deliquescent with increasing temperature, while others have increasing deliquescence relative humidity (becoming less deliquescent with increasing temperature). The curves shown here are truncated at water vapor pressures near or slightly above 105 kPa (1.05 bar), thus extending farther than for the expected maximum repository pressure of 90 kPa (0.90 bar).

Actual data for simple single salts, such as those presented in Figure 10, can be found in handbooks (e.g., Weast and Astle 1981) and other published sources (e.g., Greenspan 1977).

The second rule of deliquescence is that every assemblage of salt minerals has a characteristic deliquescence relative humidity that is lower than the characteristic deliquescence relative humidity for any individual salt mineral in the assemblage or subassemblage of these minerals (Ge et al. 1998). This rule is illustrated in the case of the salt pair NaCl-$NaNO_3$ in Figure 11, where the curves shown are results of EQ3/6 code calculations. At 25°C, the two-salt mixture is more deliquescent than either mineral by itself. At higher temperature, however, the pair is not significantly more deliquescent than the more deliquescent mineral of the pair (i.e., $NaNO_3$). For complex salt mineral assemblages, such computer modeling results are important because direct experimental data for salt mixtures becomes increasingly scarce as the number of salts in the mixture increases. This is especially true for temperatures above 25°C, which are not of much interest in atmospheric chemistry.

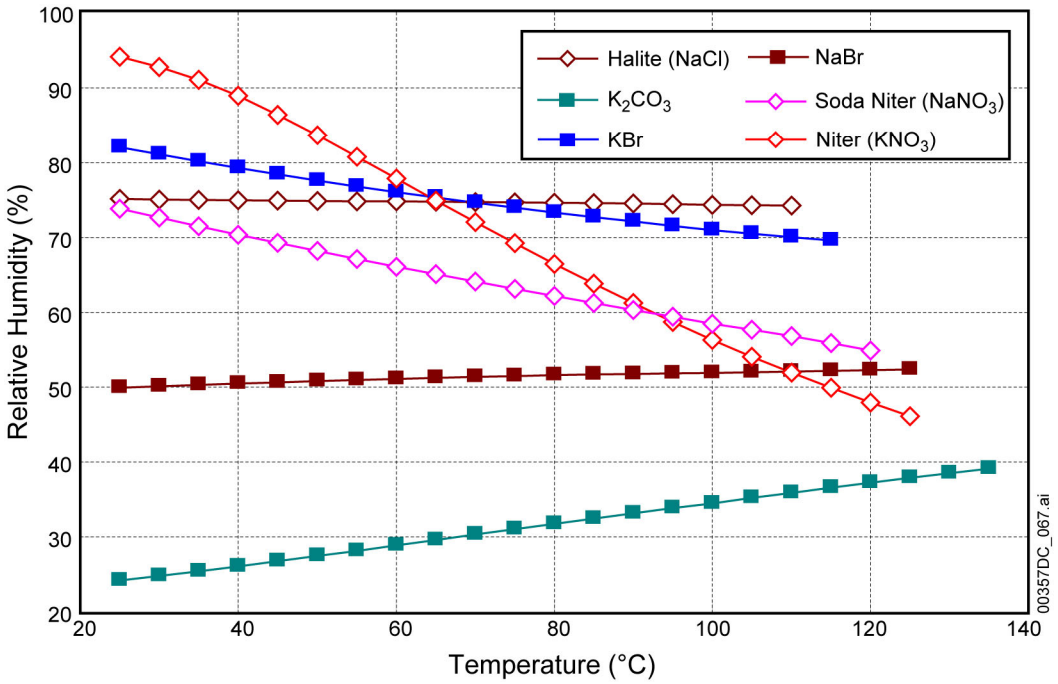

Source: BSC 2003a, Section 6.7.2.9, Figure 4: spreadsheet RH_Temp_Minerals_EQ3_6_Calcs.xls; DTN: LL030409012251.048.

Figure 10. Deliquescence Relative Humidity as a Function of Temperature for Some Deliquescent Salts (EQ3/6 calculations).

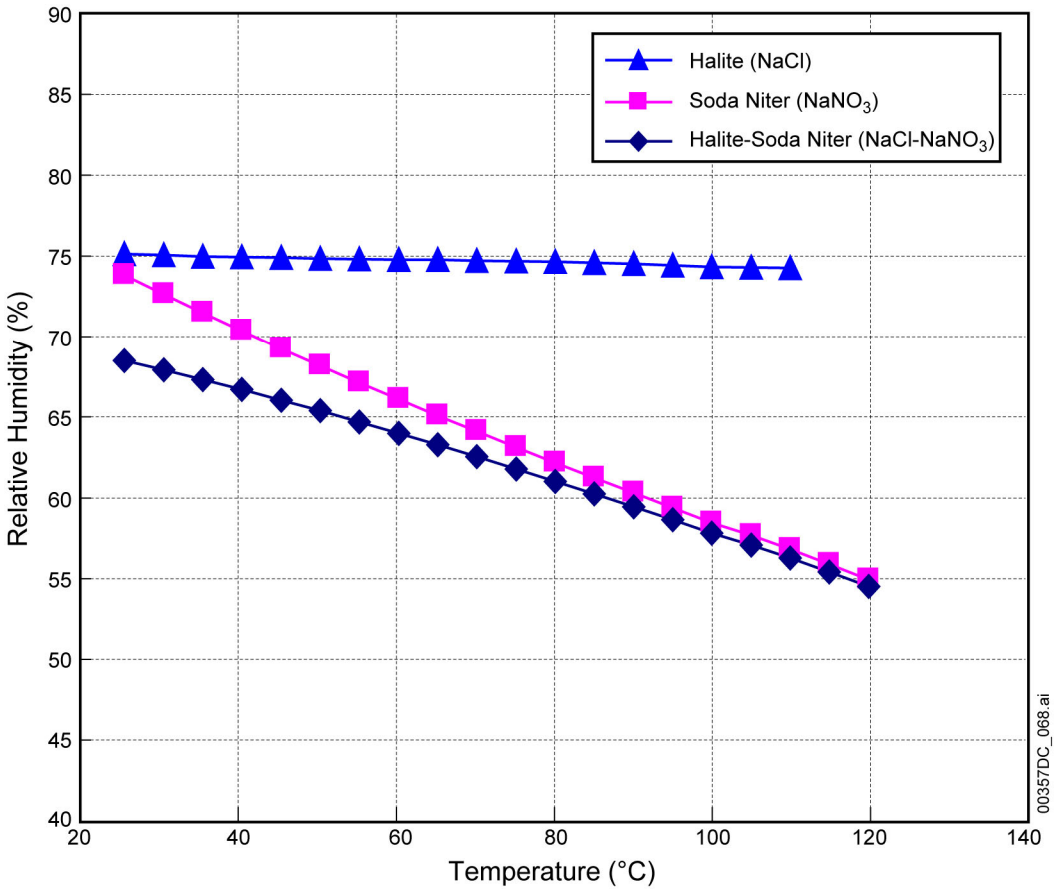

Source: BSC 2003a, Section 6.7.2.9, Figure 10: spreadsheet RH_Temp_Minerals_EQ3_6_Calcs.xls; DTN: LL030409012251.048.

Figure 11. Deliquescence Relative Humidity as a Function of Temperature for the Single Minerals Halite (NaCl) and Soda Niter ($NaNO_3$) and the Two-Mineral Assemblage Halite and Soda Niter (NaCl-$NaNO_3$) (EQ3/6 Calculations).

Figure 11 shows only the effect of the onset of deliquescence in a typical two-salt mixture composed of halite and soda niter. A method of showing the full deliquescence of a two-salt system is exemplified by Figure 12, which shows relative humidity as a function of the mole fraction of aqueous nitrate defined by the molality ratio $NO_3/(Cl + NO_3)$ for the system NaCl-$NaNO_3$-H_2O at 25°C. Point A on the left side of the figure (the 100% NaCl side) defines the state in which the relative humidity becomes equal to the deliquescence relative humidity of halite (i.e., NaCl) in the system NaCl-H_2O. Point B on the right side (the $NaNO_3$ side) marks where the relative humidity is equal to the deliquescence relative humidity of soda niter (i.e., $NaNO_3$) in the system $NaNO_3$-H_2O. Point C (near the middle of the plot) represents the deliquescence relative humidity of the halite–soda niter two-mineral assemblage. This diagram is consistent with the rule that the deliquescence relative humidity of a mineral assemblage must be lower than that of any mineral in the assemblage or mineral subassemblage. The two-salt deliquescence relative humidity is also the lowest point on the composite curve. The curve between point C and point A corresponds to saturation with halite (i.e., NaCl) with soda niter below saturation concentration; the curve between point C and point B corresponds to saturation with soda niter (i.e., $NaNO_3$) with halite below saturation concentration.

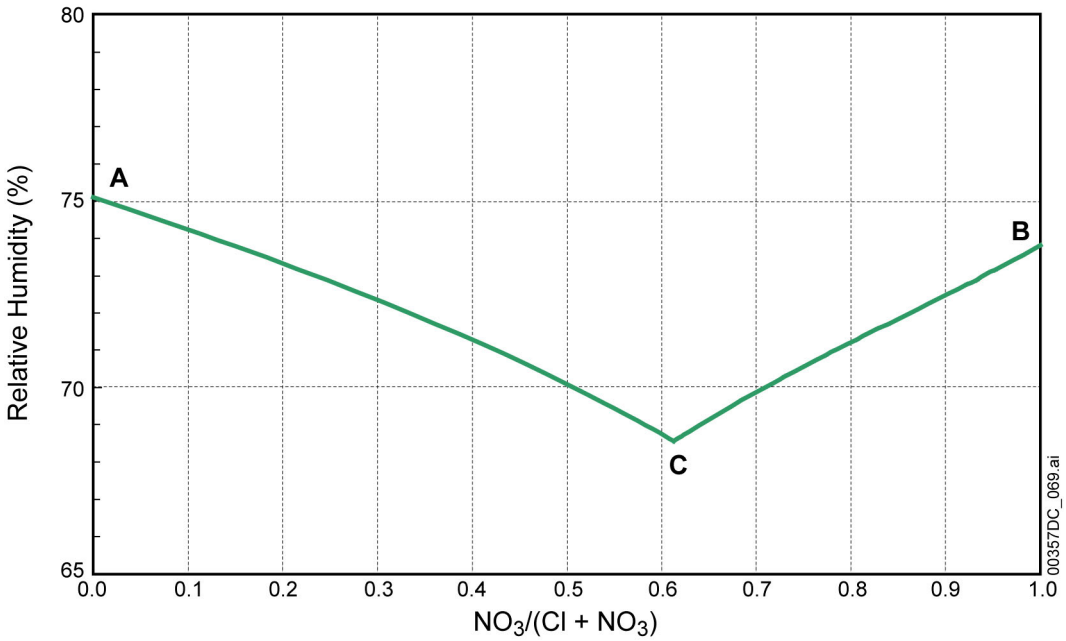

Source: BSC 2003a, Section 6.7.2.9, Figure 16: spreadsheet RH_Temp_Minerals_EQ3_6_Calcs.xls; DTN: LL030409012251.048.

NOTE: Point A marks the deliquescence relative humidity of halite in the system NaCl-H_2O; point B marks the deliquescence relative humidity of soda niter in the system ($NaNO_3$-H_2O); and point C marks the deliquescence relative humidity of halite and soda niter in the system NaCl-$NaNO_3$-H_2O.

Figure 12. Relative Humidity Versus Nitrate Mole Fraction [NO_3/(Cl + NO_3)] in Aqueous Solution in the Halite-Soda Niter (NaCl-$NaNO_3$) System at 25°C (EQ3/6 Calculations)

In a deliquescence experiment performed at 25°C using a mixture of halite and soda niter, in which the relative humidity is gradually increased by externally controlling the relative humidity of a gas mixture, and starting at a relative humidity below the deliquescence relative humidity for the two-salt assemblage, an aqueous solution would form at the two-salt deliquescence relative humidity corresponding to point C in Figure 12. The formation of this solution would maintain the local relative humidity defined by point C (resisting the external driving force exerted by higher relative humidity in the introduced gas mixture) until one or both of the two solid salts is completely dissolved. If the initial composition of the salt mixture was such that both salts disappear simultaneously at point C, the relative humidity would increase as the aqueous solution mass continues to grow. In this instance, the nitrate mole fraction would remain constant as the solution becomes more dilute. If the halite (i.e., NaCl) disappears first (i.e., nitrate mole fraction greater than point C), the relative humidity and composition will evolve along the curve leading from point C to point B, with the final aqueous solution having a mole fraction equal to the dry salt mole fraction. A similar scenario develops if the nitrate mole fraction is less than at point C in Figure 12.

The corresponding molalities of nitrate and chloride are shown in Figure 13. The maximum for the nitrate curve is substantially greater than that for the chloride curve, reflecting the fact that soda niter is much more soluble than halite. There is a slight break in the slope of the two curves at the mole fraction of nitrate corresponding to the deliquescence relative humidity for the two-salt assemblage (the ordinate for which is marked in Figure 13 as point C).

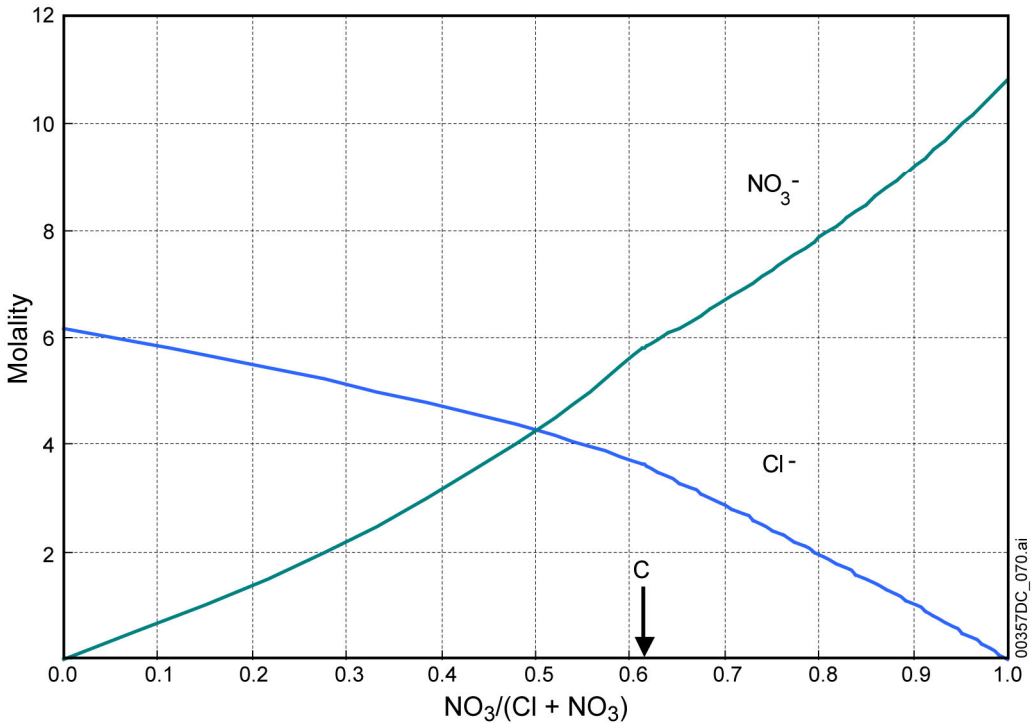

Source: BSC 2003a, Section 6.7.2.9, Figure 17: spreadsheet RH_Temp_Minerals_EQ3_6_Calcs.xls; DTN: LL030409012251.048.

NOTE: The ordinate for point C (the deliquescence relative humidity for the two-salt assemblage) is marked by "C" and an arrow.

Figure 13. Nitrate and Chloride Molalities Versus Nitrate Mole Fraction [NO_3/(Cl + NO_3)] in Aqueous Solution in the Halite-Soda Niter (NaCl-$NaNO_3$) System at 25°C (EQ3/6 Calculations).

The NO_3/Cl ratio is a potential factor in localized corrosion modeling (i.e., NO_3 acting as a corrosion inhibitor and Cl^- as a corrosion promoter (e.g., Farmer et al. 2000)). At the two-salt deliquescence relative humidity in the NaCl-$NaNO_3$-H_2O system, the aqueous solution contains more nitrate than chloride; hence, the NO_3/Cl ratio is greater than unity at this point. A lower nitrate to chloride ratio can only be achieved if the soda niter can be completely dissolved away before the halite (so that the system then evolves to the left in Figures 12 and 13). To lower the NO_3/Cl ratio to 0.25, for example, the mole fraction of nitrate must be reduced to 0.2 (at which point, the mole fraction of chloride is 0.8). Figure 12 indicates that, although the two-salt assemblages deliquesce at about 68% relative humidity, the minimum relative humidity required to achieve a NO_3/Cl ratio of 0.25 is about 74%. If halite disappears before soda niter, the system evolves to the right in Figures 12 and 13, and the NO_3/Cl ratio only increases with increasing relative humidity.

Relative humidity and aqueous solution composition relationships of the type shown above depend on temperature. Figure 14 shows how the relative humidity versus the nitrate mole fraction [NO_3/(Cl + NO_3)] curves for the system NaCl-$NaNO_3$-H_2O vary over the range 25°C to 120°C. The relative humidity curves for the various temperatures considered do not change significantly with temperature on the NaCl side, but they change quite markedly with temperature on the $NaNO_3$ side beyond the minimum deliquescence point for the assemblage at

each temperature. This is a consequence of the near-constancy with increasing temperature of the deliquescence relative humidity of halite in the system NaCl-H_2O and the notable decrease with increasing temperature of the deliquescence relative humidity of soda niter in the system $NaNO_3$-H_2O. A related factor is that the solubility of halite increases slowly with temperature whereas that of soda niter increases markedly. The solubility changes are evident in Figure 15, which shows the molality of nitrate and chloride as functions of the nitrate mole fraction [NO_3/(Cl + NO_3)] for the same temperatures considered in Figure 14.

The behavior in more complex systems is basically an extension of that shown in the above example.

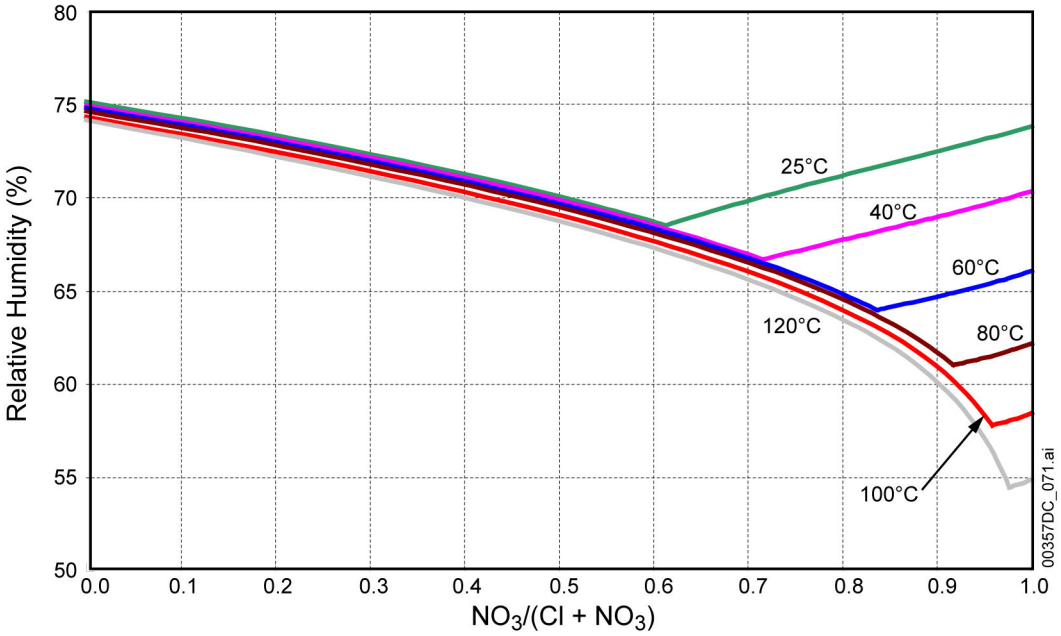

Source: BSC 2003a, Section 6.7.2.9, Figure 18: spreadsheet RH_Temp_Minerals_EQ3_6_Calcs.xls; DTN: LL030409012251.048.

Figure 14. Relative Humidity versus Nitrate Mole Fraction [NO_3/(Cl + NO_3)] in Aqueous Solution in the Halite-Soda Niter (NaCl-$NaNO_3$) System at Temperatures of 25°C, 40°C, 60°C, 80°C, 100°C, and 120°C

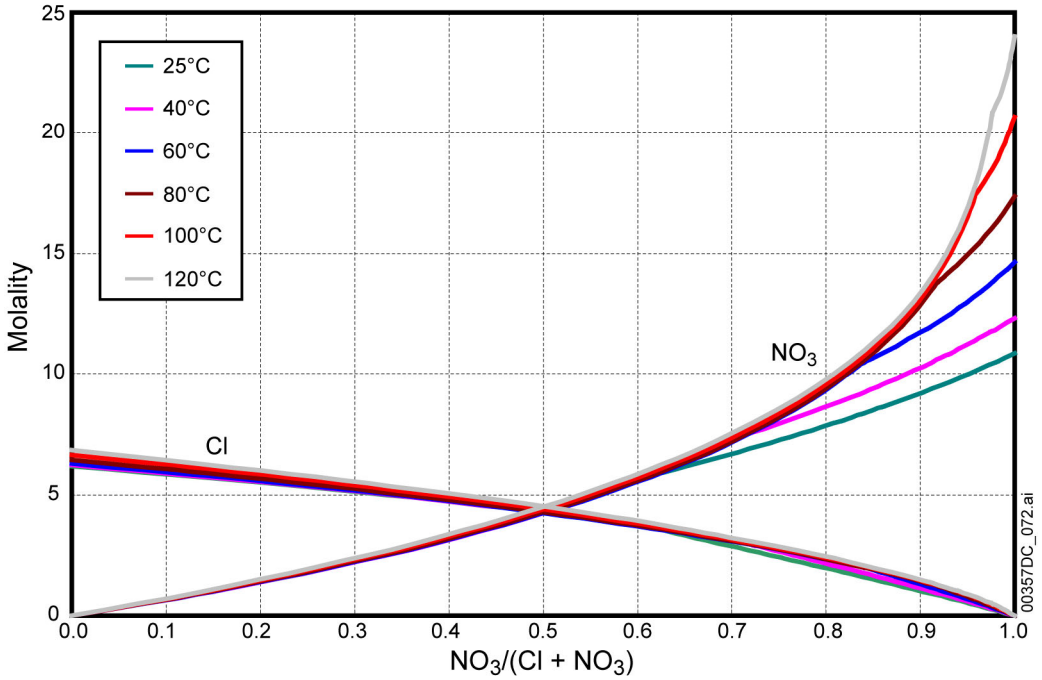

Source: BSC 2003a, Section 6.7.2.9, Figure 19: spreadsheet RH_Temp_Minerals_EQ3_6_Calcs.xls; DTN: LL030409012251.048.

Figure 15. Nitrate and Chloride Molality Versus Nitrate Mole Fraction [NO_3/(Cl + NO_3)] in Aqueous Solution in the Halite-Soda Niter (NaCl-$NaNO_3$) System at Temperatures of 25°C, 40°C, 60°C, 80°C, 100°C, and 120°C

4.3.3 Expected Dusts and Salt Mineralogy

The capability to define (or, at least, constrain) the chemical environment expected on the drip shield and waste package outer barrier depends on which salt mineral assemblages are likely to be present in the dust. The source of the dust is likely to be varied, with some component being generated in situ from tunneling, boring, and other operations. This dust component will consist mainly of rock dust (rock flour) generated during tunneling, but other constituents may also be present, generated by construction-related processes, such as combustion and welding. Dust will also be brought into the tunnels from the outside air in the course of repository ventilation. Such outside dust may include material from local, regional, and global sources (e.g., Arimoto 2001; Blank et al. 1999; Reheis and Kihl 1995) and may differ from tunnel dusts generated during construction activities. The approach taken here is to first examine the tunnel dusts, and then outside dusts. In both cases, interest is focused on the soluble salt fraction, as the insoluble fraction is nondeliquescent.

4.3.3.1 Tunnel Dusts

The data for Yucca Mountain tunnel dusts were taken from DTNs: MO0207EBSDUSTS.020 and MO0209EBSDUST2.030. The variation in the compositions of dust samples collected and the related leachates analyzed by the USGS (total of 59 leachate analyses) is used to represent their compositional variability within the repository (BSC 2004d, Section 6.10.1). Of the 59 measurements, two analyses (00574984B and 00574984C) were excluded from the dust

deliquescence calculations because they were incomplete. Three more were excluded (00574979A, 00574979B, and 00574979C) because they were not collected inside the ESF but at the surface near the North Portal. Simulation of the evaporation of 54 dust leachates at 25°C (BSC 2004d) was used to determine the corresponding salt assemblages. Those calculations were made using the same EQ3/6 Version 8.0 software and the high-temperature Pitzer thermodynamic property database data0.ypf.R1 used for the deliquescence process calculations presented previously.

The results of the salt mineral reconstitution calculations are given in Table 2. Three of the 54 samples were excluded from further analysis because the EQ3/6 runs failed to reach the actual terminal eutectic or dryout point. From the remaining 51 samples, 16 unique mineral assemblages, in which 20 minerals appeared, were identified. Each such assemblage is identified by the tag (e.g., "p07") of the first sample exhibiting this assemblage. Each eutectic assemblage contains 10 minerals. The number of minerals in a eutectic assemblage is fixed by the mineralogical phase rule (Wolery 1979, pp. 22 to 23), which relates the number of minerals (including gases, such as CO_2, for which fixed fugacities are specified) to the number of chemical components (which is the same for all samples).

The occurrence of each unique assemblage was identified in Table 2 by grouping those samples sharing a common mineral assemblage. Weighted occurrences were obtained by assigning each Phase I or "P" sample a weighting factor of three, while each Phase II or "S" sample was given a weighting factor of unity. The Phase I samples were treated in chemical analysis as unit samples. However, the original Phase II samples were split into three size fractions that were then analyzed and reported separately. Because each sample is actually a size fraction split of an original sample, the weighting is adjusted accordingly. The total weighting for the three size fractions of a Phase II sample is three, matching the weighting for a Phase I sample.

Examining the assemblages reveals several salient features. Table 3 summarizes the occurrences of minerals in the assemblages. Calcite ($CaCO_3$), halite (NaCl), niter (KNO_3), potassium bromide (KBr), and sepiolite ($Mg_4Si_6O_{15}(OH)_2 \cdot 6H_2O$) are present in all 16 assemblages. Fluorite (CaF_2) and glauberite [$Na_2Ca(SO_4)_2$] are each present in 10, amorphous silica (SiO_2(am)) in 8, and thenardite (Na_2SO_4) and sellaite (MgF_2) each in 8 assemblages. Others are present in fewer assemblages. Soda niter ($NaNO_3$; also known as nitratine) appears in only four assemblages, and sylvite (KCl) appears in only one.

Table 2. EQ3/6 Calculations of Reconstituted Salt Minerals in Dust Samples (with Weighted Occurrences)

Mineral	Formula	P07	P10	P12	P14	P18	P22	P24	P27	P30	S80a	S82c	S90b	S91a	S91b	S92a	S92b
Anhydrite	$CaSO_4$	X			X		X						X		X		
Calcite	$CaCO_3$	X	X	X	X	X	X	X	X	X	X	X	X	X	X	X	X
Nitrocalcite	$Ca(NO_3)_2{\cdot}4H_2O$	X															
Fluorite	CaF_2	X	X	X	X	X			X		X		X	X		X	
Halite	NaCl	X	X	X	X	X	X	X	X	X	X	X	X	X	X	X	X
KBr	KBr	X	X	X	X	X	X	X	X	X	X	X	X	X	X	X	X
Niter	KNO_3	X	X	X	X	X	X	X	X	X	X	X	X	X	X	X	X
Sepiolite	$Mg_4Si_6O_{15}(OH)_2{\cdot}6H_2O$	X	X	X	X	X	X	X	X	X	X	X	X	X	X	X	X
SiO_2(am)	SiO_2(am)	X	X	X	X	X					X			X		X	
Soda Niter	$NaNO_3$	X			X		X					X					
Glauberite	$Na_2Ca(SO_4)_2$		X	X	X		X		X	X		X	X	X	X		
Syngenite	$K_2Ca(SO_4)_2{\cdot}H_2O$		X								X			X			
Thenardite	Na_2SO_4		X	X		X		X	X	X	X						X
Darapskite	$Na_3NO_3SO_4{\cdot}H_2O$			X				X	X	X		X					
Arcanite	K_2SO_4					X					X					X	X
Pirssonite	$Na_2Ca(CO_3)_2{\cdot}2H_2O$					X		X								X	X
Huntite	$CaMg_3(CO_3)_4$						X	X		X		X			X		X
Sellaite	MgF_2						X	X	X	X		X	X		X		X
Sylvite	KCl															X	
Pentasalt	$K_2Ca_5(SO_4)_6{\cdot}H_2O$												X	X	X		
P-series (Phase I) Samples		P07	P10 P11 P32 P33	P12 P15 P19 P26 P32	P14 P16 P17 P28	P18 P20	P22 P23 P25	P24 P29	P27	P30							

Table 2. EQ3/6 Calculations of Reconstituted Salt Minerals in Dust Samples (with Weighted Occurrences) (Continued)

S-series (Phase II) Samples		S80c	S81b S85a S85b S86b S90a S90c S91c	S85c	S86c S87b S87c	S82a S83a S84a S86a	S80b S83c			S82b S83b	S80a S92c	S82c	S90b	S91a	S91b	S92a	S92b
P-series Occurrences		1	4	5	4	2	3	2	1	1							
S-series Occurrences		1	7	1	3	4	2	0	0	2	2	1	1	1	1	1	1
Weighted Occurrences		4	19	16	15	10	11	6	3	5	2	1	1	1	1	1	1
Percentage Weighted Occurrences		4.1	19.6	16.5	15.5	10.3	11.3	6.2	3.1	5.2	2.1	1.0	1.0	1.0	1.0	1.0	1.0

Source: BSC 2003a, Section 6.7.2.10, Table 36.

NOTE: Samples s79a, s79b, and s79c were excluded from the EQ3/6 evaporation runs because the dust samples were collected outside the tunnel in a zone of likely contamination. Three other samples (s81a, s81c, and s87a) were excluded from further analysis because the runs did not converge to the eutectic (dryout) state. The number of successful runs was 51. In subsequent analysis, each sample from the Phase I (P) series was given a weighting factor of three. Each sample from the Phase II (S) series was assigned a weighting factor of 1. Each of the three Phase II dust samples was split into three size fractions, designated a, b, and c, for which leaching and other data were obtained. The total weighting factor for all three splits of a Phase II sample is, therefore, three. The weighted occurrences for all samples totaled 97.

Table 3. Summary of Mineral Occurrences in the 16 Assemblages in Table 2

Mineral	Formula	Occurrences
Anhydrite	$CaSO_4$	5
Calcite	$CaCO_3$	16
Nitrocalcite	$Ca(NO_3)_2{\cdot}4H_2O$	1
Fluorite	CaF_2	10
Halite	NaCl	16
KBr	KBr	16
Niter	KNO_3	16
Sepiolite	$Mg_4Si_6O_{15}(OH)_2{\cdot}6H_2O$	16
SiO_2(am)	SiO_2(am)	8
Soda Niter	$NaNO_3$	4
Glauberite	$Na_2Ca(SO_4)_2$	10
Syngenite	$K_2Ca(SO_4)_2{\cdot}H_2O$	3
Thenardite	Na_2SO_4	8
Darapskite	$Na_3NO_3SO_4{\cdot}H_2O$	5
Arcanite	K_2SO_4	4
Pirssonite	$Na_2Ca(CO_3)_2{\cdot}2H_2O$	4
Huntite	$CaMg_3(CO_3)_4$	6
Sellaite	MgF_2	8
Sylvite	KCl	1
Pentasalt	$K_2Ca_5(SO_4)_6{\cdot}H_2O$	3

Source: BSC 2003a, Section 6.7.2.10, Table 37.

A clearer picture is obtained by noting only those minerals that are the most deliquescent. Anhydrite, calcite, fluorite, sepiolite, amorphous silica (SiO_2(am)), huntite [$CaMg_3(CO_3)_4$], and sellaite (MgF_2) (7 of the 20 minerals) are not ordinarily considered deliquescent. Arcanite (K_2SO_4), thenardite (Na_2SO_4), and all of the double salts except darapskite ($Na_3SO_4NO_3{\cdot}H_2O$) are only moderately deliquescent. That focuses attention on nitrocalcite [$Ca(NO_3)_2{\cdot}4H_2O$], niter (KNO_3), soda niter($NaNO_3$), halite (NaCl), sylvite (KCl), potassium bromide (KBr), and darapskite.

Consideration of the most deliquescent minerals combined with occurrence in the 16 unique mineral assemblages indicates the key subassemblages (hereafter referred to as key assemblages) shown in Table 4. The two principal key assemblages are "A," NaCl-$NaNO_3$-KNO_3-KBr, and "B," NaCl-KNO_3-KBr. Key assemblage A is composed of soda niter (i.e.,$NaNO_3$) plus the salts of key assemblage B; therefore, B is a subassemblage of A. Assemblages A and B account for 95.9% of the total occurrence in the 51 dust samples. Key assemblage "C" is characterized by the presence of nitrocalcite [$Ca(NO_3)_2{\cdot}4H_2O$], a highly deliquescent salt. Key assemblage C is composed of nitrocalcite plus the salts of key assemblage A. Nitrocalcite appears in the calculated mineral assemblages of only two of the 51 dust samples (one of which has a unit weighting factor, the other, a weighting factor of 3, a weighted frequency of occurrence of 4.1%).

Table 4. Key Subassemblages of Reconstituted Salt Minerals in Dust Samples

Case	Key Salts	Unique Mineral Assemblages Represented	Total Occurrence Percentage
A	NaCl-$NaNO_3$-KNO_3-KBr	P14, P22, S82c	27.8
B	NaCl-KNO_3-KBr	P10, P12, P18, P24, P27, P30, S80a, S90b, S91a, S91b, S92a, S92b	68.1
C	$Ca(NO_3)_3$-NaCl-$NaNO_3$-KNO_3-KBr	P07	4.1

Source: BSC 2003a, Section 6.7.2.10, Table 38.

NOTE: The percentage occurrence values for unique phase assemblages (BSC 2003a, Table 36) sum to 99.9%. Here, the value for key assemblage B has been calculated so that the sum for the three key assemblages sums to 100%.

The definition of the mineral assemblages above is confirmed by the deliquescence relative humidity for the eutectic solution compositions in the EQ3/6 calculations for the dust leachate solutions closely cluster around three mean values. Also, these mean values should be close to calculated deliquescence relative humidity values for the corresponding pure key salt assemblages. This is confirmed by the results shown in Table 5.

Table 5. Calculated Deliquescence Relative Humidity Values for Key Assemblages at 25°C

Case	Key Salts	Deliquescence Relative Humidity for Pure Key System (%)	Deliquescence Relative Humidity for Actual Associated Sample Cases (%)
A	NaCl-$NaNO_3$-KNO_3-KBr	54.91	54.80 ±0.02
B	NaCl-KNO_3-KBr	62.97	60.44 ±0.61
C	$Ca(NO_3)_3$-NaCl-$NaNO_3$-KNO_3-KBr	38.98	38.93 ±0.00

Source: BSC 2003a, Section 6.7.2.10, Table 39.

Potassium bromide (KBr) is a highly deliquescent salt that appears in the dust leachate evaporation calculations and in the three abstracted key salt mineral assemblages. Its presence in the evaporation calculations can be traced back to the bromide concentrations in the dust leachate solutions. These levels of bromide are high in comparison to chloride (e.g., for the Phase I samples, mean bromide is 28.7 ppm, mean chloride is 181 ppm) when considered in the context of natural waters. However, as discussed below, bromide-containing waters have been used throughout the facility for various purposes. This enhances the bromide content relative to chloride over that typically present.

Lithium bromide (LiBr) was used as an additive in the water used for construction and fire suppression. The target concentration for the water is 20 ±10 ppm (CRWMS M&O 1993, p. 8). The absence of soluble lithium is due to its strong ion-exchange into mineral phases, probably exchanging for sodium and potassium.

DTN: LAJF831222AQ98.003 confirms this usage of lithium bromide in construction and fire-suppression water, and Mitchell (1998) estimated the loss of construction water during tunnel construction.

Lithium bromide (LiBr), sodium bromide (NaBr), potassium bromide (KBr), and calcium bromide ($CaBr_2$) were also used for performing hydrologic tracer tests in the rock mass surrounding the tunnels (Mitchell 1999a, p. 1; Mitchell 1999b, p. 1; Mitchell 1999c, pp. 1 to 2; Mitchell 2000, p. 1). The reported amounts of individual bromide salts used in these tests ranged from a few tens of grams to more than 150 kg. In general, there has been an effort to recover this tracer material by methods such as mineback tunneling of the rock masses involved in the tests.

Therefore, it is likely that the level of bromide measured in the dust samples taken from the tunnels is an artifact of the use of bromide in tunnel construction and hydrologic testing. Given this, it is appropriate to remove the bromide component from the key mineral assemblages.

Removing potassium bromide (KBr) from the key salt mineral assemblages results in key mineral assemblages that are less deliquescent. This is illustrated in Table 6, which compares the results of EQ3/6 calculations at 25°C for the cases with and without the presence of potassium bromide. The changes are fairly substantial for the three key assemblages. The effect of eliminating the KBr on the deliquescence relative humidity is significantly diminished at higher temperature because KNO_3 (and $NaNO_3$, in case A) becomes much more deliquescent at higher temperature, while KBr becomes only moderately more deliquescent (BSC 2003a, Section 6.7.2.10). This effect would also hold for the minor case C.

Table 6. Calculated Deliquescence Relative Humidity Values for Key Assemblages at 25°C, with and without KBr

Case	Key Salts	Deliquescence Relative Humidity Including KBr (%)	Deliquescence Relative Humidity Excluding KBr (%)
A	$NaCl$-$NaNO_3$-KNO_3-KBr	55	66
B	$NaCl$-KNO_3-KBr	63	70
C	$Ca(NO_3)_3$-$NaCl$-$NaNO_3$-KNO_3-KBr	39	49

Source: BSC 2003a, Section 6.7.2.10, Table 40.

4.3.3.2 Atmospheric (Outside) Dusts

An important issue is the relevance of the tunnel dusts to those dusts that will eventually be deposited on the waste packages. It is possible that atmospheric dust will be a significant portion of the deposited dust. Hence, a comparison of soluble chemistry of atmospheric dust with tunnel dust is appropriate. The two dust data packages (DTNs: MO0207EBSDUSTS.020; MO0209EBSDUST2.030) indicate total salt content of the tunnel dusts is typically less than 0.5 wt %. Most of the dust material appears to consist of silicates. The low percentage of soluble salts in the tunnel dusts seems to be more consistent with their origination from rock dust.

Information on the percentage of soluble salts in local and regional atmospheric dusts appears to be sparse. However, Blank et al. (1999, Table 2, p. 370) report that playa dusts in Nevada may contain about 44% soluble salts. Some data from other parts of the world (e.g., Orlovsky and Orlovsky 2001) indicate that such a high (or indeed higher) percentage is not unreasonable. Reheis (1997) reported total soluble salt contents of 8% to 30% (Reheis 1997, Figure 3B) in dusts originating from the Owens Dry Lake in California. However, regional values were

reported in the range of 9% to 16% (Reheis 1997, Figure 3B). Thus, the tunnel dusts have a much smaller soluble fraction in the expected outside dust. However, while the absolute amounts of soluble salts in outside dusts may be much larger than those in tunnel dusts, the deliquescence analysis based on the tunnel dusts will still apply if the compositions of the soluble fractions are similar.

As stated previously, the dust from the tunnels is a mixture of rock dust generated during tunneling and other operations with dust brought in from the outside air during ventilation. This mixture is likely to be highly dominated by rock dust, as suggested by the widespread presence of bromide in the samples analyzed to date. (As noted above there is widespread use of LiBr tracer in waters at Yucca Mountain.) In terms of key salt mineralogy, however, the tunnel may not be very different from outside dusts (apart from bromide contamination in the tunnel dusts). The general ubiquity of halite and nitrate minerals in desert terrains (and the usual nondriver salt minerals, including gypsum, anhydrite, calcite, glauberite, pirssonite, and thenardite) indicates that the scenario of deliquescence drawn from the tunnel dusts is likely to be consistent with one based on a similar study of local, regional, or global atmospheric dusts.

Atmospheric dusts have local, regional, and global origins (e.g., Arimoto 2001; Blank et al. 1999; Reheis and Kihl 1995; Reheis et al. 2002; Orlovsky and Orlovsky 2001; Levy, D.B. et al. 1999). Marine aerosols comprise one component of salt in atmospheric dust. In the western United States, the marine component becomes more significant closer to the Pacific coast. Some salts are also created (or modified) by atmospheric processes (e.g., creation of nitrate by electrical discharges). Salts are also included in dusts stirred up by wind from dry lake beds. Based on trace element geochemistry, Reheis et al. (2002) concluded that dust in the southwestern United States appears to come from four sources: alluvial sediments, playas, the Owens Valley Dry Lake area (a human-induced playa), and anthropogenic and/or volcanic emissions.

Levy, D.B. et al. (1999, pp. 53 to 55) point out that Owens Valley Dry Lake is the source of the largest measured values of particulate air pollution in North America. Levy, D.B. et al. (1999, pp. 59 to 60) identified the minerals in the surface and shallow sediments of the dry lake. The most important quantitatively were quartz (SiO_2) and feldspar ($Ca_xNa_{1-x}Al_{1+x}Si_{3-x}O_8$), which are not salt minerals. The salt minerals included halite (NaCl), thenardite (Na_2SO_4), pirssonite ($Na_2Ca(CO_3)_2{\cdot}2H_2O$), nesquehonite ($MgCO_3{\cdot}3H_2O$) and trona [$Na_3H(CO_3)_2{\cdot}2H_2O$], which tend to be concentrated at the surface.

Blank et al. (1999) report on dust collected from desert playa regions in Nevada. This study is notable in that it provides clear data (Blank et al. 1999, Table 2, p. 370) on the soluble salt fraction of eolian dusts: 44.20% ±2.20% in playa samples, 0.46% ±0.10% in beach samples, and 0.15% ±0.02% in dune samples. These values are higher than, but reflective of, the soluble salt fraction in corresponding soil samples (9.36% ±1.05% in playa samples, 0.15% ±0.08% in beach samples, and 0.01% ±0.004% in dune samples). These differences were attributed (Blank et al. 1999, p. 377) to recent changes in playa hydrology associated with climatic change and human activities. This report also notes the existence of pulses of nitrate-rich dust synchronous with the arrival of spring.

Bohlke et al. (1997) studied stable isotope evidence for the origin of desert nitrate deposits and concluded that atmospheric deposition was the major mechanism for their creation. Oxidation of organic nitrogen in desert soils is another likely mechanism but quantitatively much less important. The nitrate minerals in the samples studied by these authors were identified primarily as soda niter ($NaNO_3$) and darapskite ($Na_3SO_4NO_3 \cdot H_2O$).

Various nitrate minerals may be created by atmospheric reactions involving $HNO_3(g)$ created by electrochemical or photochemical reactions.

For example, soda niter may form from halite (NaCl) derived from sea salt aerosol, according to:

$$HNO_3(g) + NaC1 = NaNO_3 + HC1(g) \quad \text{(Eq. 1)}$$

Calcium nitrate (e.g., nitrocalcite $Ca(NO_3)_2 \cdot 4H_2O$) may also be created from preexisting calcium carbonate by an atmospheric reaction, such as (Arimoto 2001, p. 37, but note that Arimoto omits the water of hydration shown here):

$$2HNO_3(g) + CaCO_3 + 3H_2O(g) = Ca(NO_3)_2 \cdot 4H_2O + CO_2(g) \quad \text{(Eq. 2)}$$

There is no evidence for the presence of calcium chloride minerals in dust or atmospheric aerosols. The stable form of calcium chloride at low temperature is antarcticite ($CaCl_2 \cdot 6H_2O$), as deduced from the type of locality (a very shallow pond in Antarctica) by Torii and Ossaka (1965). It was surmised that very low temperatures were, in part, responsible for the occurrence of this mineral. A second occurrence of antarcticite was reported from Bristol Dry Lake, California, by Dunning and Cooper (1969), who found it in the near-subsurface in the course of examining trenches and pits.

Data supporting the tunnel dust soluble fractions (excluding high bromide) as representative of tunnel dusts are presented in Table 7. The soluble fraction ionic ratios of three representative tunnel dusts (DTN: MO0207EBSDUSTS.020) are compared with 2002 annual solute data for precipitation (rainfall) at three Nevada stations (National Atmospheric Deposition Program/National Trends Network 2004a, 2004b, 2004c) and three composite compositions of Asian dust samples (Topping et al. 2004). The Nevada precipitation results should correlate with the soluble fractions of local atmospheric dusts. The Asian dust results (Topping et al. 2004) are composite data for dusts originating in northern China and Mongolia (and sampled in Korea). Asian dusts are indirectly relevant because they experience similar effects and processes that determine the compositions of atmospheric dust generated in any desert or playa environment. They are also directly relevant because they can be transported by the wind to Nevada. The results given in Table 7 are very similar for these different dusts. Thus, it appears that the soluble fraction of the tunnel dusts (excluding the high bromide) is representative, compositionally, of the expected outside (atmospheric) dust. A possible explanation for the soluble fraction of the tunnel dusts (excluding the high bromide) is that these dusts are about 98% rock flour and about 2% outside dust.

Table 7. Ionic Ratios for the Soluble Fraction of Three Representative Tunnel Dusts, Three Nevada Precipitation (Rainfall) Stations Surrounding Yucca Mountain, and Three Composite Results for Asian Dust

Ionic Ratios (mol/mol)	Tunnel Dust Samples - Three Representative Cases			Nevada Precipitation Stations Mean Values for Year 2002			Asian Dust, ACE Campaign Results		
	P07	P14	P10	CA95	NV00	NV05	Whole Campaign Total	Chinese Course Total	Korean Course Total
Na/Cl	2.699	4.069	2.894	2.070	1.127	1.828	2.169	1.309	2.222
K/Cl	1.221	1.528	1.237	0.158	0.139	0.207	0.513	0.387	0.515
NH_4/Cl	N/A	N/A	N/A	2.605	5.514	4.633	4.670	2.245	4.041
Mg/Cl	0.072	0.305	0.175	0.336	0.555	0.417	0.220	0.210	0.219
Ca/Cl	8.472	6.389	2.348	3.101	2.973	2.907	0.664	0.874	0.649
NO_3/Cl	4.002	1.671	0.776	2.969	5.146	3.839	1.754	1.440	1.719
SO_4/Cl	3.123	3.293	1.458	1.009	1.384	1.555	2.473	1.679	2.006
CO_3/Cl	4.839	4.737	2.057	2.860	2.461	2.683	0.711	0.155	0.892

Source: BSC 2003a, Section 6.7.2.10, Table 43; DTN: MO0207EBSDUSTS.020 (tunnel dust samples); National Atmospheric Deposition Program/National Trend Network 2004a, 2004b, 2004c (Nevada precipitation stations); Topping et al. 2004 (Asian dust).

NOTE: The tunnel dust leachates were not analyzed for NH_4.; CO_3 here was estimated from charge balance.

4.3.3.3 Implications for Corrosion

For corrosion purposes, it is important to note that the first-formed solutions resulting from deliquescence will contain more nitrate than chloride, owing to the generally higher solubilities in the deliquescing solutions of the expected nitrate minerals (potassium, sodium, and calcium nitrates) versus those of the expected chlorides of sodium and potassium. As the solutions continue to deliquesce and the original salt mineral assemblage is changed by complete dissolution of one salt mineral after another, the solutions will become even more nitrate rich if nitrate abundance in the dust exceeds the chloride abundance; otherwise, they will become chloride rich. Regardless, any solution obtained after complete dissolution of nitrate and chloride must have (at least, in the absence of acid gas volatility and phase separation) a nitrate to chloride ratio that matches that in the soluble fraction of the original dust.

The soluble ratios of species in the original dust, therefore, limit the attainable compositions in the solution. The mean NO_3/Cl ratio in the soluble fraction of the Phase I dust samples is about 1.3 ±0.8 (1σ), with minimum and maximum values of about 0.3 and 4.0, respectively (BSC 2003a, Section 6.7.2.10, Table 41). The minimum ratio guarantees that the NO_3/Cl ratio in any solution deliquescing in contact with these dust samples will have at least this value.

The mean NO_3/Cl ratio in the soluble fraction of the Phase II dust samples is about 1.4 ±0.8 (1σ), with minimum and maximum values of about 0.4 and 3.4, respectively (BSC 2003a, Section 6.7.2.10, Table 42). These values are roughly comparable to those obtained for the Phase I samples. The minimum ratio, again, guarantees that the NO_3/Cl ratio in any solution deliquescing in contact with these dust samples will have at least this value. The precision of the numbers here is slightly overstated as the numbers are accurate to, at most, three significant figures.

Also, it can be shown that, although the apparent dust salt mineral assemblages are generally highly deliquescent, at least at elevated temperature, these assemblages tend to have high NO_3/Cl ratios at the relatively low relative humidity values at which deliquescence first occurs. Lower NO_3/Cl ratios (of, for example, 0.2 to 1.0) are only achievable at significantly higher relative humidity values (much closer to the deliquescence relative humidity for pure halite).

This fact is illustrated by the results for NaCl-$NaNO_3$-KNO_3 given in Figure 16. In addition to the usual deliquescence relative humidity curve, this figure gives as a function of temperature the minimum relative humidity required to obtain NO_3/Cl ratios of 0.2 and 1.0. As can be seen from Figure 16, the minimum relative humidity curves are not very sensitive to temperature, reflecting the fact that the deliquescence relative humidity for single salt NaCl is fairly constant (74% to 76%) across the temperature range of interest. Therefore, it can be concluded that relatively chloride-rich solutions are possible only under conditions of moderate-to-high relative humidity, with the onset close to the deliquescence relative humidity for the single-salt NaCl, and then only for cases in which the NO_3/Cl ratio in the original dry salt assemblage is relatively low.

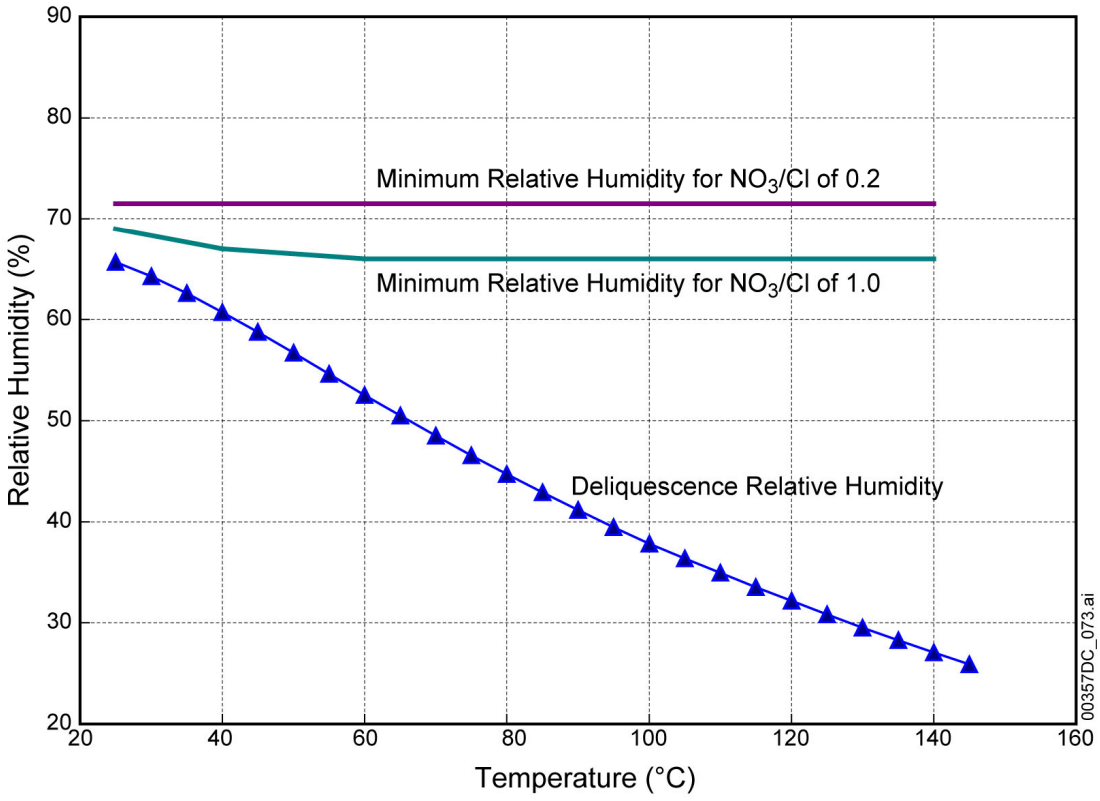

Source: BSC 2003a, Section 6.7.2.10, Figure 32.

Figure 16. Relative Humidity and Minimum Relative Humidity Values to Achieve NO_3/Cl Ratios of 1.0 and 0.2 as a Function of Temperature for the Assemblage Halite-Niter-Soda Niter (NaCl-KNO_3-$NaNO_3$)

4.3.4 Projected Deliquescence Relative Humidity for Key Salt Assemblages in Expected Dusts

The final key salt assemblage analysis of the tunnel dust leachate data is summarized in Table 8, along with percentage frequency of occurrence of each assemblage in the 51 samples used in the analysis.

Table 8. Final Key Subassemblages and Occurrence Percentages for Tunnel Dust Leachates

Case	Key Salts	Total Occurrence Percentage
A	$NaCl$-$NaNO_3$-KNO_3	27.8
B	$NaCl$-KNO_3	68.1
C	$Ca(NO_3)_3$-$NaCl$-$NaNO_3$-KNO_3	4.1

Source: BSC 2003a, Section 6.7.2.13, Table 45.

The deliquescence relative humidities for these assemblages as a function of temperature are shown in Figure 17. The deliquescence relative humidity for each assemblage decreases strongly with increasing temperature, primarily due to the deliquescence relative humidity behavior of the single-salt nitrates. The curves, as shown, extend to somewhat higher temperatures than are consistent with an expected maximum pressure of 90 kPa (0.90 bar). For Case A ($NaCl$-KNO_3-$NaNO_3$), the temperature of initial deliquescence would be about 136°C; for Case B ($NaCl$-KNO_3), it would be about 126°C; and for Case C ($NaCl$-KNO_3-$NaNO_3$-$Ca(NO_3)_2$), it would be approximately 150°C. The estimate for Case C is more uncertain because the EQ3/6 calculations were not convergent for this system above 60°C. A temperature of 160°C was originally assumed for saturated $Ca(NO_3)_2$-$NaCl$-$NaNO_3$-KNO_3, somewhat higher than the experimental value of 151°C for pure $Ca(NO_3)_2$ at standard atmospheric pressure (Kracek 1928, p. 368). The corresponding relative humidity is then about 16% (i.e., 760 torr/4,636 torr = 0.16). The 4,636 torr value is the vapor pressure of pure water at 160°C. The temperature of initial deliquescence would be lower for lower pressure, countering the influence of the presence of other highly deliquescent salts ($NaNO_3$ and KNO_3). These results are the current best estimates of when initial deliquescence would occur.

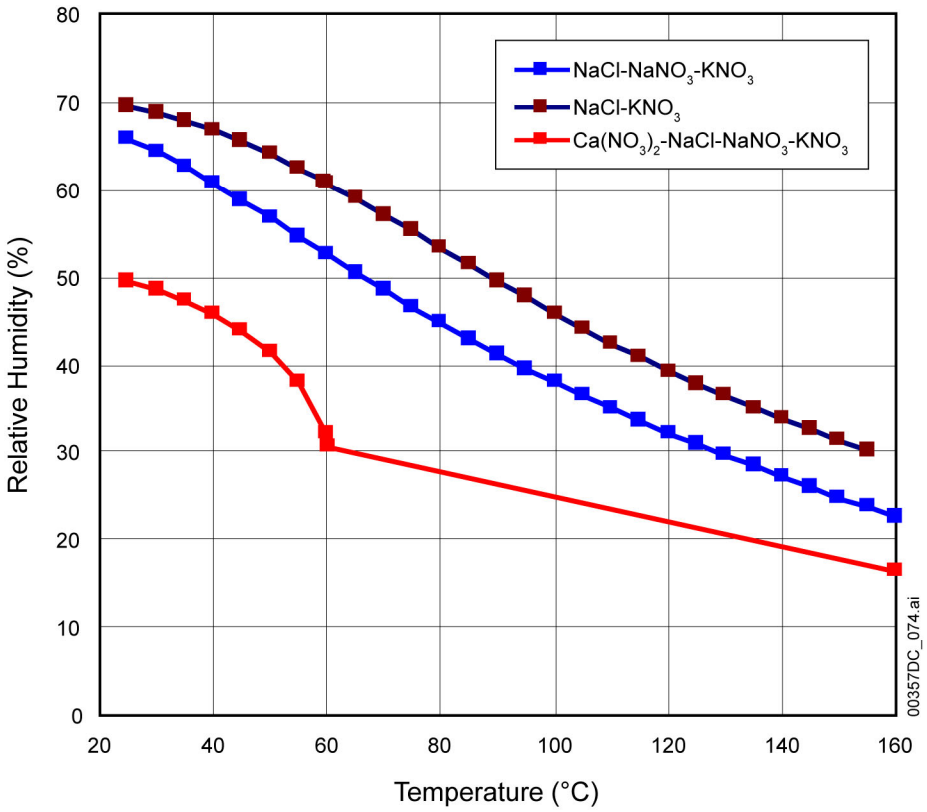

Source: BSC 2003a, Section 6.7.2.13, Figure 33.

Figure 17. Deliquescence Relative Humidity as a Function of Temperature for the Three No-Dripping (Deliquescence) Cases

4.3.5 Coupled Chemical Evolution of Dust Salt Assemblages as a Function of Temperature and Relative Humidity (Total System Performance Assessment Model)

The aqueous chemistry resulting from the response of dust to elevated temperature and decreased relative humidity is evaluated in the TSPA using the in-drift precipitates and salts model, as described below (BSC 2004d). Chemical compositions are reported for six dust bins, for discrete ranges of temperature, relative humidity, and pCO_2, suitable for use directly in the TSPA. The model is also used to determine whether the relative humidity conditions are too dry for liquid water to exist in a particular dust system (i.e., too dry for deliquescence of the salt mineral assemblage in the dust). The six bins represent the range of compositions from the same tunnel dust samples discussed previously (DTNs: MO0207EBSDUSTS.020, MO0209EBSDUST2.030).

The deliquescence response of dust is represented in the physical and chemical environment model using a binning methodology similar to that used to analyze the evolution of the seepage water chemistry (Section 4.4; see also BSC 2004d). The binning is based on the aqueous compositions of the dust leachates after evaporation (using EQ3/6 calculations) to a condition of 65% relative humidity at 25°C. This relative humidity is generally well above the deliquescence relative humidity values of the three key salt assemblages noted in Section 4.3.3. The solute

compositions in the more dilute solution for which this binning was done are strongly affected by the dissolution of the less soluble, less deliquescent minerals in the corresponding eutectic (dryout) assemblages. Consequently, the binning process leads to a larger number of groups (six bins) than was obtained in the analysis of key salt assemblages controlling initial deliquescence (three bins). A single dust leachate sample was chosen to represent the solute chemistry of each bin. The chosen samples are listed in Table 9, along with the percentages of all dust leachates in the tunnel dust sets. The sample identification in short form is given by the first four letters (the first three letters if the fourth character is an underscore) of the "Median Water File Name." For example, the file "s80c25b.6o" refers to dust sample s80c, whereas "p25_25b.6o" refers to dust sample p25.

Table 9. Median Leachates and Percentage of Leachates in Each Bin

Bin	Median Water File Name	Number of Waters In the Bin	Percent of Evaporated Waters Represented by the Bin
1	s80c25b.6o	3	5.77
2	s90b25b.6o	4	7.69
3	s86a25b.6o	9	17.31
4	p25_25b.6o	12	23.08
5	p26_25b.6o	23	44.23
6	s92a25b.6o	1	1.92
Total		52	100.00

Source: DTN: MO0310SPADLBU4.001; BSC 2004d, Section 6.10.5, Table 6.10-6.

Bin 4 water is a Case A water ($NaCl$-$NaNO_3$-KNO_3 is the key salt assemblage), while bin 1 water is a Case C water ($NaCl$-$NaNO_3$-KNO_3-$Ca(NO_3)_2$ is the key salt assemblage). Bins 2, 3, 5, and 6 waters are all Case B waters ($NaCl$-KNO_3 is the key salt assemblage). However, the binning is not perfectly consistent with the key salt assemblage grouping. For example, Table 4 shows that the frequency of occurrence of Case A water is 27.8%, whereas bin 4 water has a frequency of occurrence of 23.08%. Similarly, Case C water has a frequency of occurrence of 4.1%, whereas bin 1 water has frequency of occurrence of 5.77%.

These differences between the binning and key assemblage grouping are primarily due to the application of different criteria for binning (solution composition at 65% relative humidity) and for key assemblage grouping (the eutectic relative humidity). However, there are some additional factors that should be noted. The binning process used data for 52 leachate samples while the key assemblage grouping used only 51 samples because the evaporation calculation for one leachate sample encountered convergence problems before achieving the eutectic relative humidity state and, therefore, could not be used in the key assemblage grouping. The evaporation calculation for the same leachate, however, succeeded in reaching 65% relative humidity and was used in the binning. A more important difference between the binning and the key salt grouping is that bromide was excluded from the final key salt analysis as justified in Section 4.3.3.1, but bromide was not excluded in the binning analysis. The binning results are, therefore, more conservative in the sense that deliquescence will occur at lower relative humidity.

The advantage of the binning approach is that it provides more complete solution compositions in the range of higher relative humidity, for example, by including sulfate and carbonates. Figure 18 shows the variation of Cl/NO_3 ratio as relative humidity increases from low values (at the right) to high values (on the left) for binned waters. This analysis is consistent with the simple key assemblage system $NaCl\text{-}NaNO_3$: the solutions become increasingly chloride rich as the relative humidity rises to near the deliquescence relative humidity for the single-salt NaCl.

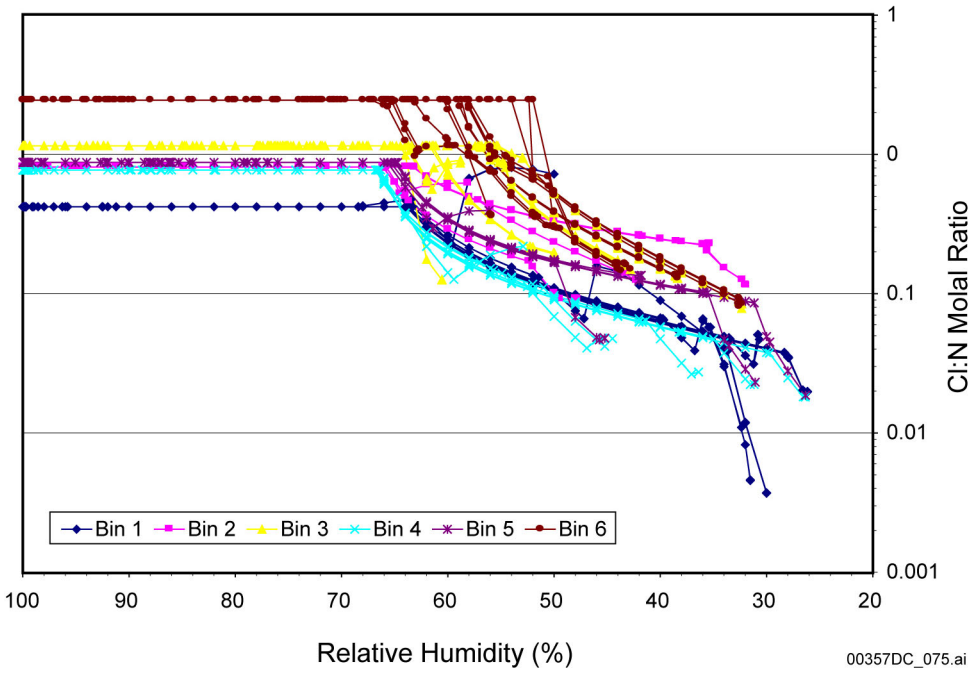

Source: BSC 2004d, Figure 6.13-38.

NOTE: Evaporation of the waters is modeled at each possible combination of four temperatures (40°C, 70°C, 100°C, and 120°C) and three pCO_2 values (10^{-2}, 10^{-3}, and 10^{-4} bar).

Figure 18. Variation of Cl/NO_3 with Relative Humidity for the Six Dust Leachate Bins

4.3.6 Expected Deliquescence Behavior for a Representative Predicted Repository Temperature and Relative Humidity

The previous analysis of deliquescence behavior can be used to predict the evolution of the chemical environment in the repository when coupled with calculated thermal-hydrologic predictions for the drifts. The deliquescence analysis is summarized for the $NaCl\text{-}KNO_3$ case (or Bins 2, 3, 5, and 6) in Figure 19. The inaccessible region corresponds to water vapor pressures that would exceed the expected maximum pressure in the drifts and to a dry state regardless of other considerations. The curve for initial deliquescence for $NaCl\text{-}KNO_3$ extends from the left (starting at 30°C and 69% relative humidity) to where it intersects the curve for the inaccessible region (at about 127°C and 37% relative humidity). As long as both of the key salts are present, the deliquescence relative humidity curve for $NaCl\text{-}KNO_3$ governs the start of deliquescence during the decay of the thermal pulse (e.g., the system is dry below this curve). If there is more Cl than NO_3 in the original dry salt assemblage, at some point the NO_3 will become completely dissolved and the system may move to a point above the two-salt deliquescence relative humidity

curve. Below about 69% relative humidity the NO_3/Cl ratio is guaranteed by the governing thermodynamic relations to exceed a value of 0.5. However, above this relative humidity it may achieve lower values and ultimately become limited by the NO_3/Cl ratio in the original dry salt assemblage. Above 80% relative humidity the governing thermodynamic relations indicate that the SO_4/Cl ratio can have values of 1.0 or greater (provided there is sufficient SO_4 in the dry salt assemblage).

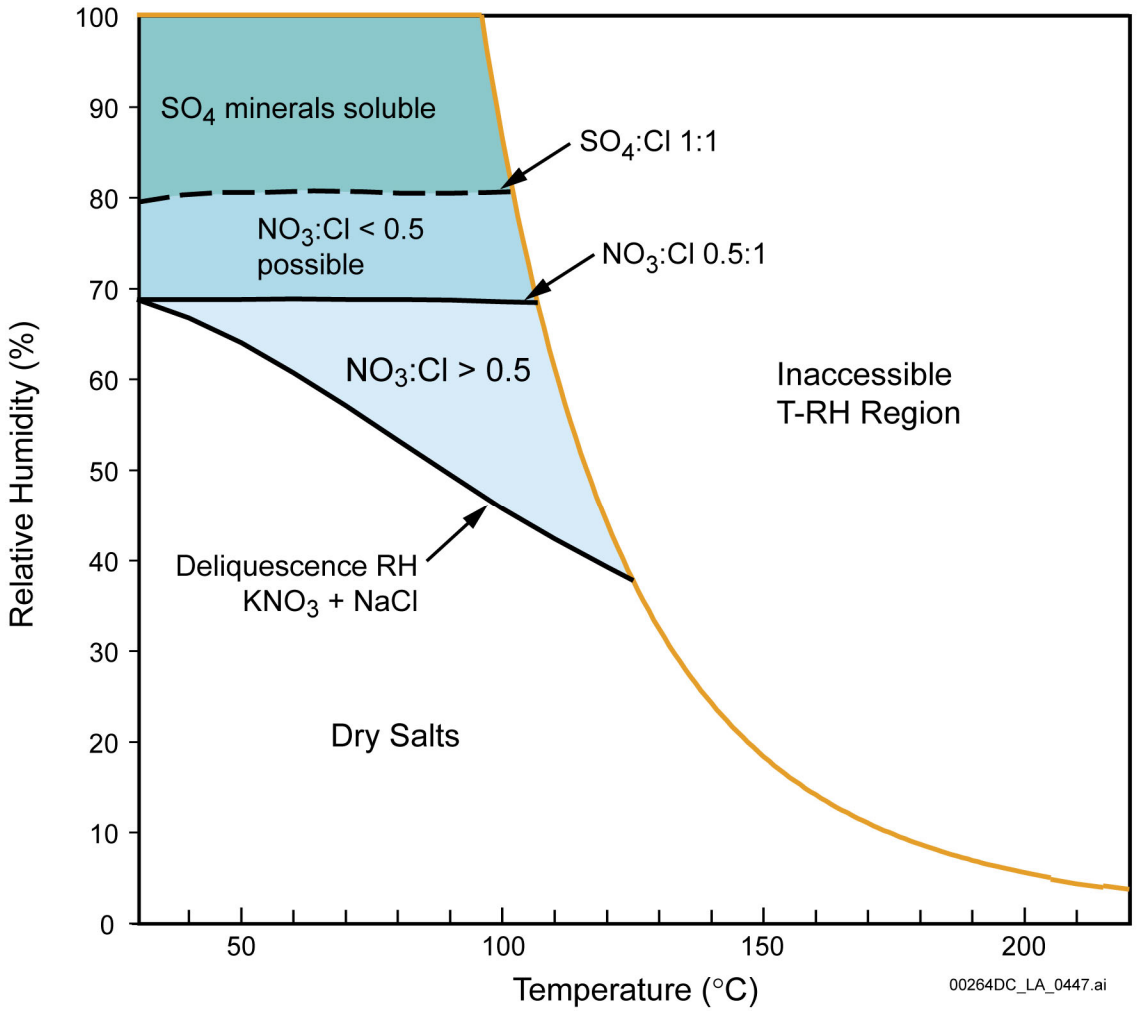

Source: Steefel 2004a, p. 46.

Figure 19. Summary Relative Humidity Versus Temperature Plot Illustrating Overall Deliquescence Behavior for the NaCl-KNO_3 (or Bins 2, 3, 5, and 6) Case

Figure 20 shows the same summary but with the superposition of three repository cooldown curves for the outer surface of the waste package derived from thermal-hydrologic calculations. Initial deliquescence occurs between about 110°C and 120°C, somewhat lower than the value imposed by the expected maximum pressure. In interpreting these results, it should be kept in mind that all waste packages are likely to have some dust on them, but only a modest fraction of these are likely to come into contact with seepage water. Thus, deliquescence of dust will continue to be a factor in the below-boiling period as well.

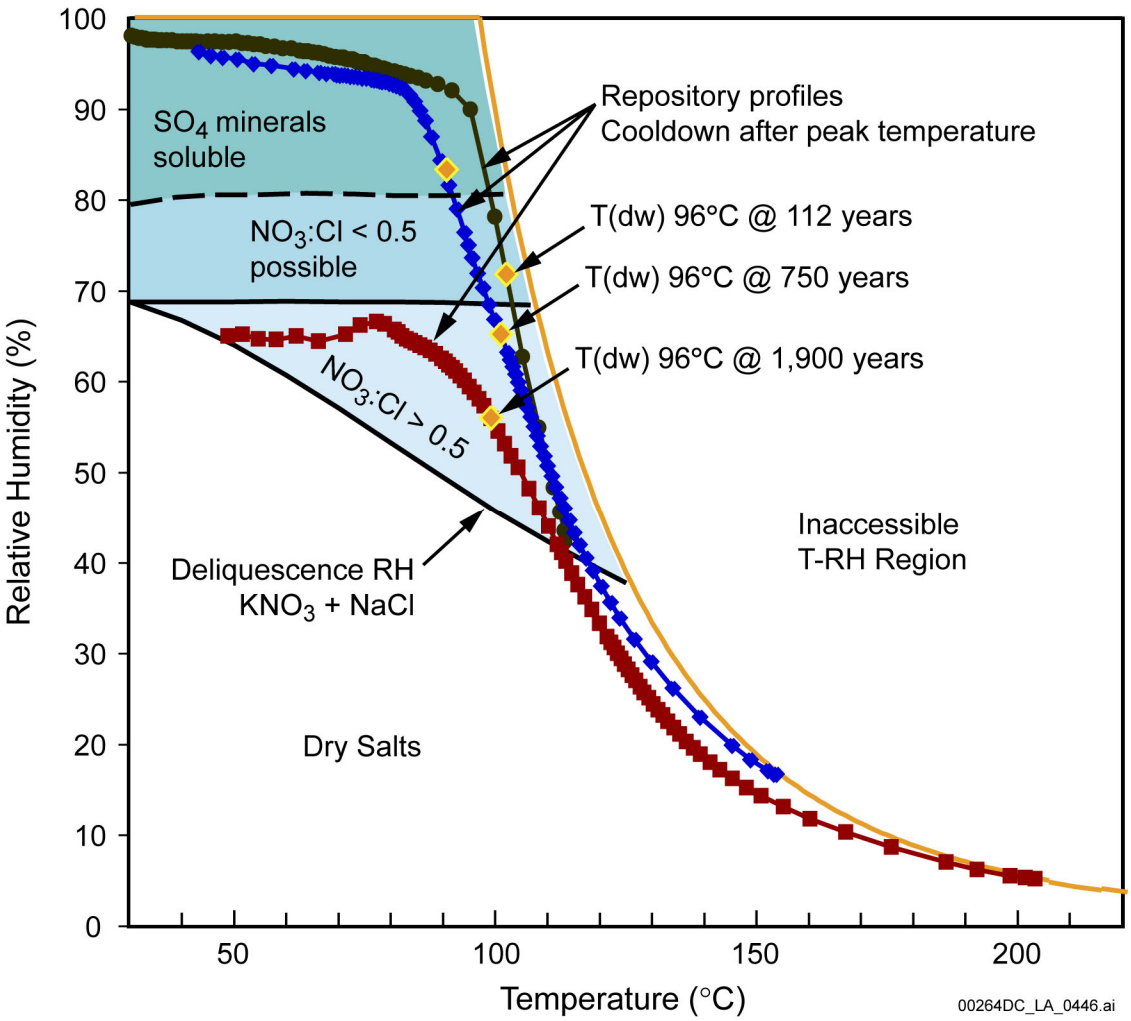

Source: Steefel 2004b, p. 37.

NOTE: Representative thermal-hydrologic curves are for a hot waste package (low thermal conductivity, low percolation flux: squares), a cool waste package (high thermal conductivity, high percolation flux: circles), and a median waste package (median thermal conductivity, median percolation flux: diamonds).

Figure 20. Summary Relative Humidity Versus Temperature Plot Illustrating Overall Deliquescence Behavior for the NaCl-KNO_3 (or Bins 2, 3, 5, and 6) Case, with Three Calculated Repository Cooldown Curves Superimposed

4.4 In-Drift Chemical Environment below Boiling Conditions at Drift Wall

When temperatures at the drift wall fall below boiling, water will begin to seep into the drift and contact the waste packages. Seepage water contacting waste package and drip shield surfaces will evaporate and will form concentrated brines, deposited salts, or both. In addition, as temperature falls and relative humidity increases, salts that accumulate on the surfaces of waste packages and drip shields will deliquesce, forming brines. The following sections describe the coupled and integrated thermal-hydrologic-chemical processes in the drift and the surrounding rock mass at temperatures below boiling.

4.4.1 Introduction to Processes Affecting Waste Package Chemical Environment below Boiling Conditions

The chemical evolution of waters, gases, and minerals in the near field and in the drift is coupled to the thermal-hydrologic processes of evaporation, condensation, and liquid and vapor mass transport. Figure 21 schematically shows the coupled relationships between geochemical processes, such as mineral dissolution and precipitation; thermal-hydrologic processes in the zones of vaporization; condensation; and drainage in the rock mass surrounding the emplacement drifts. These coupled processes, in turn, affect seepage and gas-phase compositions within the drift.

The effects of thermal-hydrologic processes on water chemistry depend on the intrinsic characteristics of the dissolved species and the types of chemical reactions in which they are involved. Conservative species (i.e., nonreactive and nonvolatile), such as Cl^-, become concentrated in waters undergoing vaporization but are essentially absent from the vapor condensing in the fractures. Therefore, the concentrations of conservative species in condensate waters are determined by the extent of mixing with background fracture waters and matrix pore waters. In addition, concentrations of aqueous species, such as calcium (Ca^{2+}), are also affected by mineral dissolution or precipitation reactions and by exchange or alteration reactions involving zeolites, clays, or feldspars.

Retrograde calcite solubility (less soluble at higher temperature) and prograde solubilities of other minerals, such as the forms of silica (more soluble at higher temperatures), cause differences between the distributions of calcite and siliceous phases (Figure 21). Precipitation of amorphous silica or a similar phase tends to be confined to a narrower zone where evaporative concentration exceeds the solubility. Calcite tends to precipitate at elevated temperature where CO_2 has exsolved (i.e., degassed) and tends to dissolve where there is lower pH. Alteration of feldspars to clays and zeolites tends to be most rapid in the zone of vaporization because of increased feldspar solubility (as well as higher dissolution and precipitation rates) at higher temperatures (Lasaga 1998, p. 66).

Exchange of CO_2 between aqueous and gas phases as temperature changes is particularly important to predicting the chemical evolution of matrix and fracture water in the rock surrounding the repository. CO_2 exsolution causes a local increase in pH. Where vapor enriched in CO_2 is transported and condenses, there is a decrease in pH. The extent to which the pH is shifted depends on the rates of mineral–water reactions that can buffer the change.

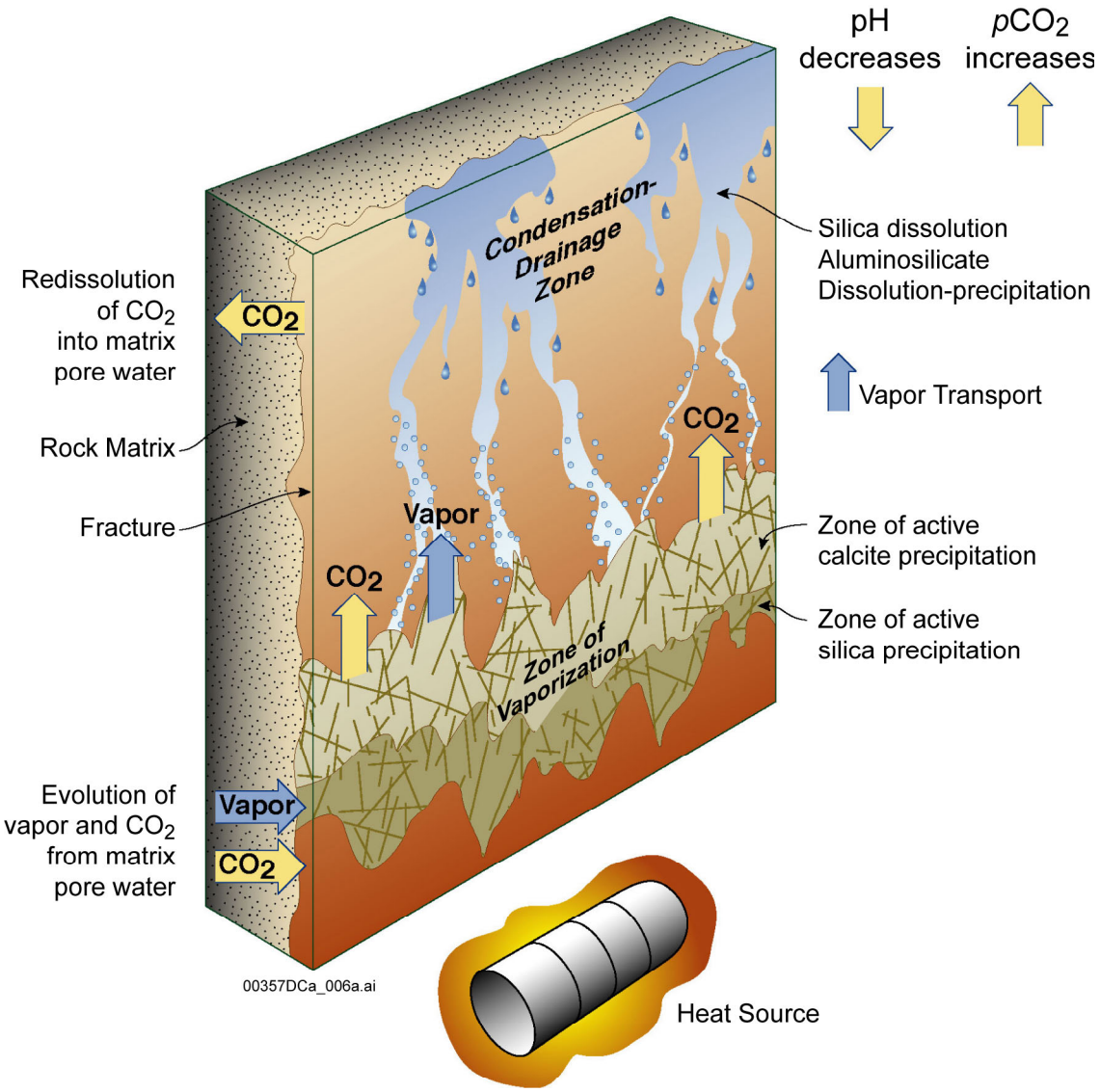

Figure 21. Schematic Diagram of Fracture–Matrix Interface, Showing the Relation between Thermal-Hydrologic Processes and Geochemical Processes

When chemical species are transported in fracture waters at rates greater than the rate of equilibration with the rock matrix, the result is disequilibrium between waters in fractures and matrix. The disequilibrium can change the prevailing mineral assemblage and lead to differences in reaction rates.

Early in the thermal evolution of the repository, the chemistry of the host rock around the emplacement drifts will be strongly influenced by the chemistry of ambient fracture and matrix pore water and affected by evaporation, condensation, and mineral–water–gas reactions. Once the peak rock temperatures have subsided, natural percolation flux will mix with the condensate above the drifts and eventually rewet the dryout zone. The composition of the percolating waters (before mixing) could be similar to that presently found in the host rock as matrix pore water, or it could be more dilute, reflecting wetter climate conditions. Future changes in the percolation

flux also affect the extent of mineral precipitation and dissolution because of dilution effects and changes in the fluxes of dissolved species to the near-field.

Mineral precipitation and dissolution in the fractures and matrix have the potential to modify the porosity, permeability, and unsaturated hydrologic properties of the host rock. Because the molar volumes of minerals created by hydrolysis reactions (e.g., feldspars reacting with water to form zeolites or clays) are commonly greater than the molar volumes of the reactant minerals, the reactions lead to porosity reduction. The extent of mineral–water reaction is controlled by the surface areas of the mineral phases in contact with water, which is sensitive to heterogeneity in the distribution of minerals in the fractures. Therefore, changes in porosity and permeability may also be heterogeneously distributed. Other factors that could lead to heterogeneity in property changes are the distribution of liquid saturation in fractures and the proportion of fractures having actively flowing water.

As seepage waters make their way into the drift, their chemical composition can significantly change by evaporation and mineral precipitation. Evaporation causes the concentrations of aqueous species to increase, minerals to precipitate, and the most soluble components to become concentrated in the brine.

When minerals (salts) precipitate, the relative concentrations of dissolved components change. This effect is a result of chemical divides that are encountered whenever minerals precipitate. The concept of chemical divides is summarized as follows by Drever (1988, p. 235):

> Whenever a binary salt is precipitated during evaporation, and the effective ratio of the two ions in the salt is different from the ratio of these ions in solution, further evaporation will result in an increase in the concentration of the ion present in greater relative concentration in solution and a decrease in the concentration of the ion present in lower relative concentration.

There are six common geochemical divides for natural lakes (Drever 1988) (see Figure 22) that largely control the types of waters that can develop in these lakes. Analogous evaporite minerals are commonly found on desert playa lakes in Nevada as the result of evaporative concentration of relatively dilute and low-solute-content rainwater and snowmelt (see Papke 1976, Table 1).

Evaporite minerals are usually deliquescent to some degree. There are generally two types of deliquescent minerals, those that incorporate water within their mineral lattice structure (e.g., sodium silicate gel desiccants) and soluble salts (e.g., sodium chloride and other minerals bound by ionic forces). The first type of mineral is stable and transfers water from air or liquid to the mineral phase without significant disruption of the solid lattice structure. The second type of mineral is unstable above a mineral-specific threshold relative humidity and can dissolve from a solid salt into a liquid brine.

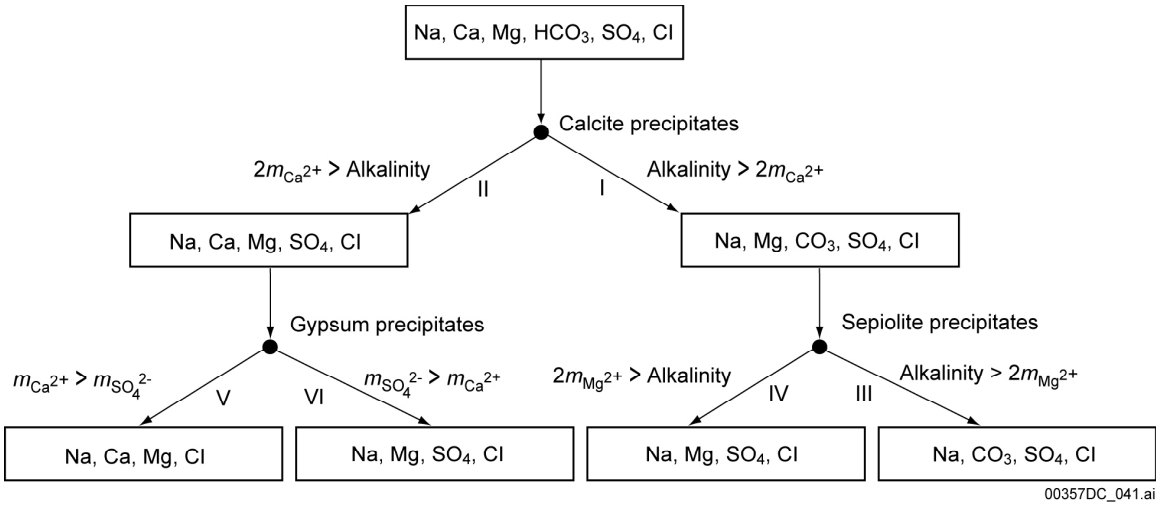

Source: Drever 1988, p. 236.

Figure 22. Simplified Chemical Divides Diagram Based on Evaporative Concentration of Dilute Starting Waters to Form a Suite of Naturally-Occurring Lake Waters

Deliquescent minerals in the drift are of consequence because of their ability to change the microscale liquid environment as they absorb water vapor from the air. Campbell and Smith (1951, p. 237) state: "It is clear that if the pressure of the aqueous vapor in the atmosphere is greater than that of the saturated solution of a salt, that salt will, on being placed in the air, form a solution: it will deliquesce." Deliquescence of highly deliquescent salts, such as NaC1 and $NaNO_3$, is expected to be rapid and complete.

4.4.2 Coupling of Models in Total System Performance Assessment

The coupling of the below-boiling processes of evaporation, condensation, deliquescence, liquid and vapor mass transport, mineral precipitation and dissolution, chemical divides, porosity changes, and other processes described in the previous section are accomplished in the TSPA by integrating thermal-hydrologic modeling, thermal-hydrologic-chemical water seepage modeling, and in-drift chemistry modeling. The thermal-hydrologic modeling is developed and documented in *Multiscale Thermohydrologic Model* (BSC 2004b). It provides temperature and relative humidity relationships and time predictions for various locations around the repository. The thermal-hydrologic-chemical seepage modeling, documented in *Drift-Scale Coupled Processes (DST and THC Seepage) Models* (BSC 2003c) uses an integrated approach to predict changes in the chemical composition and quantity of water in the fractures and matrix surrounding the drifts over time. The third component, in-drift chemistry modeling, uses the water and gas compositions from the thermal-hydrologic-chemical seepage model to predict the chemistry of seepage and deliquescence water within the drift as a function of temperature, relative humidity, and pCO_2. The in-drift chemistry modeling is documented in *In-Drift Precipitates/Salts Model* (BSC 2004e) and in *Engineered Barrier System: Physical and Chemical Environment Model* (BSC 2004d). The thermal-hydrologic-chemical seepage and in-drift chemistry models are explained in more detail in the following sections.

4.4.2.1 Thermal-Hydrologic-Chemical Model

The thermal-hydrologic-chemical seepage model is a forward numerical model used by the TSPA to predict the effects of thermal-hydrologic-chemical processes around the drift. This model, documented in *Drift-Scale Coupled Processes (DST and THC Seepage) Models* (BSC 2003c), uses a two-dimensional dual-permeability grid to represent a vertical cross section through the drift.

Simulations of thermal-hydrologic-chemical processes include coupling between heat, water, and vapor flow; aqueous and gaseous species transport; kinetic and equilibrium mineral–water reactions; and includes feedback of mineral precipitation and dissolution on porosity, permeability, and capillary pressure (BSC 2003c). Aqueous species included in the model are H^+, Ca^{2+}, Na^+, K^+, $SiO_2(aq)$, Mg^{2+}, Al^{3+}, Fe^{3+}, SO_4^{2-}, HCO_3^-, Cl^-, and F^-, and NO_3^-. Minerals considered include silica phases (cristobalite, quartz, tridymite, amorphous silica, and opal-CT), calcite, feldspars, smectites, illite, kaolinite, sepiolite, zeolites, fluorite, hematite, gypsum, and various salt phases. Treatment of CO_2 includes gas–water equilibration, diffusion, and advection. Simulations were performed using TOUGHREACT V3.0 (LBNL 2002).

The thermal-hydrologic-chemical seepage model requires a starting composition for pore water surrounding the drift. The initial composition for matrix pore water could be selected from pore water chemistry in the unsaturated zone at or above the repository horizon, from perched water, or from the saturated zone. Perched waters are generally more dilute than unsaturated zone pore waters. Isotopic compositions ($^{36}Cl/Cl$, $^{18}O/^{16}O$, δD, ^3H, ^{14}C as percent modern carbon) and chloride concentrations of the perched waters indicate that they have a large proportion of late Pleistocene/early Holocene water (Levy, S.S. et al. 1997, p. 906; Sonnenthal and Bodvarsson 1999, pp. 107 to 108). The saturated zone waters are also more dilute than the unsaturated zone pore waters, and neither saturated zone waters nor perched waters reflect calculated CO_2 partial pressures consistent with CO_2 concentrations in gas measured in the unsaturated zone in repository units. The saturated zone and perched-water compositions are, therefore, deemed poor candidates as initial input water compositions. Preference is given instead to actual pore waters from unsaturated rocks within or above the repository units.

During the initial stages of thermal-hydrologic-chemical model development, a few pore water samples were ultracentrifuged from core samples that originated in the middle nonlithophysal unit (Tptpmn) near the Drift Scale Test. Nearly complete chemical analyses were obtained for three samples (HD-PERM-1, HD-PERM-2, and HD-PERM-3) using core from one general location, yielding similar water compositions. Two of these analyses were combined to develop an input water composition for the model. More recently, additional pore water samples from the repository host-rock units have been obtained from core collected in the ECRB Cross-Drift and in boreholes USW SD-9 and USW NRG-7/7a. These water compositions are discussed in detail below.

Measured compositions for the more recent series of matrix pore waters are depicted on a Piper diagram in Figure 23, along with the HD-PERM samples, perched waters, pore water from similar depths (base of the nonlithophysal Tptpln unit) in borehole USW UZ-14, and groundwater from well J-13. Thus, this figure summarizes the characteristics of waters from the site and indicates a wide range of potential initial water compositions. The HD-PERM samples

represent one endpoint of the range (calcium-sulfate-chloride type waters), and groundwater from well J-13 defines another endpoint (sodium-bicarbonate type). Figure 23 also shows that samples from deeper units tend to exhibit higher sodium (plus potassium) concentrations relative to calcium (plus magnesium), and a higher proportion of aqueous carbonate (relative to chloride and sulfate) compared to shallower waters (see also Yang et al. 1996, p. 13). These trends are probably caused by the hydrolysis of volcanic glass and feldspars and exchange reactions with zeolites below the host-rock units (e.g., BSC 2002; Vaniman et al. 2001).

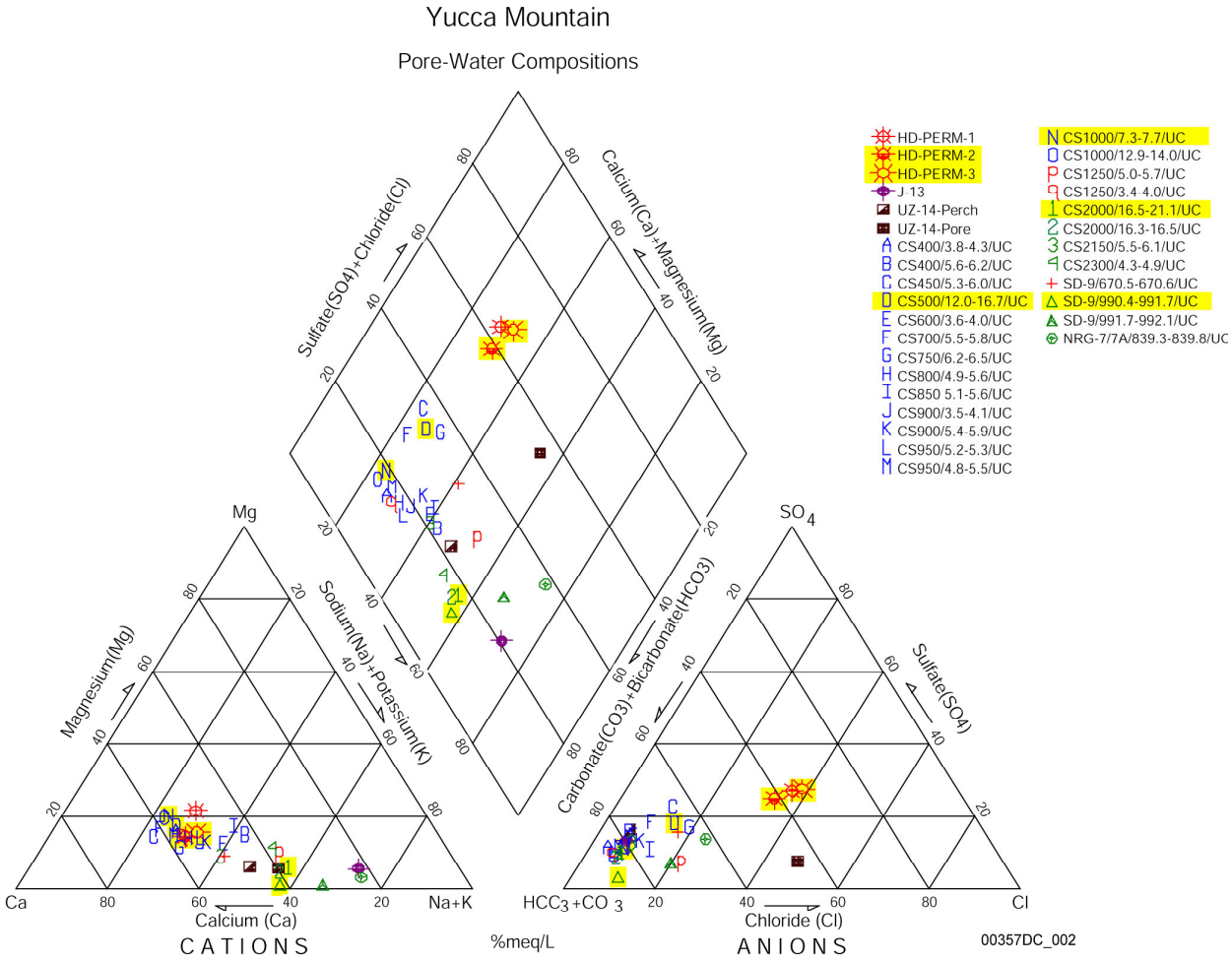

Source: BSC 2003c, Figure 6.2-4.

NOTE: Samples labeled HD-PERM are pore waters from the Tptpmn unit in Alcove 5 of the Exploratory Studies Facility. Sample IDs starting with CS represent pore waters from the ECRB Cross-Drift and are listed in order of increasing distance (feet) into the drift (down stratigraphy), with labels reflecting lithostratigraphic units as follows: Tptpul (uppercase A to O), Tptpmn (lowercase p to q), and Tptpll (numbers 1 to 4). Sample IDs starting with SD-9 and NRG-7 represent pore waters from boreholes with the same names and show the sampling interval in feet from the ground surface. The first SD-9 sample at 670 ft is from the base of the Tptpul, and the others are from the Tptpll. The NRG-7 sample is from the Tptpmn. Highlighted samples were chosen for this study (see text).

Figure 23. Piper Plot of Water Compositions from Repository Units

Differences in the proportions of the various cations and anions (i.e., ratios, not concentrations) have an important influence on the types of evaporated solutions or brines that could develop as a result of evaporation or boiling (BSC 2004e, Section 6). Should these waters seep onto the surface of a hot waste package or drip shield, the composition of the resulting brine can affect corrosion rates (BSC 2004d). Therefore, the selection of input water compositions for thermal-hydrologic-chemical modeling takes into account the end-brine compositions of these waters and the natural variability of pore water compositions in the host-rock units (Figure 23). The pore waters highlighted in yellow in Figure 23 were chosen to represent the range of initial waters considered for thermal-hydrologic-chemical analyses at Yucca Mountain. To propagate this variability to TSPA, each of these waters was used in a separate thermal-hydrologic-chemical model simulation as the initial starting water. The starting waters were assigned arbitrary identifiers (W0, W4, W5, W6, and W7). W0 is a composite of the HD-PERM-2 and HD-PERM-3 samples.

4.4.2.2 In-Drift Precipitates and Salts Model

The *In-Drift Precipitates/Salts Model* (BSC 2004e) is the primary analytical tool used for in-drift chemistry modeling and is used to generate the in-drift chemical response surfaces documented in *Engineered Barrier System: Physical and Chemical Environment Model* (BSC 2004d). This model, which uses the geochemical modeling code EQ3/6 (BSC 2003b) for calculations, determines the effects of temperature and relative humidity on the chemical evolution of aqueous solutions and the deliquescence of salts in the drift (BSC 2004d). In order to predict the behavior of aqueous systems at high salinity conditions, a database including Pitzer thermodynamic parameters extending to elevated temperature was developed to calculate the in-drift precipitates and salts model.

The in-drift precipitates and salts model integrates processes of evaporation, condensation, deliquescence, mineral precipitation, mineral dissolution, chemical divides, aqueous speciation, and carbon dioxide exchange with the atmosphere. Calculations using this model are performed for all combinations of temperature and relative humidity profiles predicted by the thermal-hydrologic model and for potential ranges of carbon dioxide fugacity and seepage water compositions predicted by the thermal-hydrologic-chemical water seepage model. These calculations result in multidimensional response surfaces used by the TSPA to determine the values of key output parameters important to corrosion and transport modeling, such as pH, ionic strength, and concentrations of chloride and nitrate. These response surfaces also indicate whether the waste package surfaces are predicted to be dry or wet.

To generate this set of response surfaces, the large set of water compositions from the thermal-hydrologic-chemical model is reduced to a manageable number of water types that effectively represent the range of potential seepage water chemistries. The different water types are distinguished by grouping similar waters from the thermal-hydrologic-chemical water seepage model results according to their chemical compositions upon evaporation. Application of this classification process generated 11 groups of water types, operationally called bins. A median water was selected from each group (or bin) to represent the seepage water type, and response surfaces were generated for each representative seepage water. To couple the thermal-hydrologic-chemical model results with the generated in-drift chemistry response surfaces, the response surfaces were mapped back to the time histories of the predicted thermal-hydrologic-

chemical seepage model water compositions according to the determined water type for each time interval. This integration technique is explained in more detail in Section 4.4.4.

4.4.3 Evolution of Water Composition in Rock

The thermal-hydrologic-chemical model represents the effects of waste package heating over time, changes in heat load caused by preclosure ventilation, the effective heat transfer within the drift, and thermal-hydrologic-chemical processes in the unsaturated zone around waste emplacement drifts. Thermal-hydrology is represented using the same conceptual basis, and similar formation properties, initial and boundary conditions, and representations of in-drift thermal-hydrologic processes. Model results predict the chemistry of matrix and fracture water in the host rock next to the drift wall at various locations around the drift, the times of rewetting around the drifts, and the net gas flux through the drift wall for a simulation period of 100,000 years. As discussed in Section 4.4.4.1, the composition of water that could potentially seep into the drift is selected from the predicted chemistry in model gridblocks at the margin of the dryout zone around the opening, or nearest the opening after the rock cools below the boiling temperature.

Several simulations were performed to characterize the effects of natural variability and uncertainty on the thermal-hydrologic-chemical seepage model predictions. These sensitivity analyses address the following major issues and variables:

- Different repository host-rock geologic units (Tptpmn and Tptpll)
- Alternative geochemical systems (base case and extended case, which adds more mineral species and chemical components)
- Alternative thermodynamic data sets (different equilibrium constants for key minerals)
- Different treatments of mineral–water reactions (different kinetic rate constants and reactive surface areas; equilibrium versus kinetic reactions)
- Spatial heterogeneity in fracture permeability
- Different infiltration rates and effects of climate change
- Alternative water vapor pressure models
- Alternative initial water compositions
- Different effective CO_2 diffusivities
- Alternative drift-wall conceptualizations (open versus closed to liquid flow).

These thermal-hydrologic-chemical model simulations cover a wide range of the most important uncertainties from the standpoint of model validation, bounding analyses, conservatism, impact on model results, and propagation of uncertainty between different component models. Based on the natural variability in input water composition and the resulting spread in simulation results, the uncertainties in predicted concentrations of aqueous species and of CO_2 gas are estimated to be up to about one order of magnitude (BSC 2003c).

4.4.4 Evolution of In-Drift Water Composition

The water and gas compositions used as input to the in-drift chemistry modeling originate from thermal-hydrologic-chemical seepage model predictions of seepage water chemistry and gas-phase composition in the host rock (near-field environment) adjacent to the drift wall (Section 4.4.3). These results are abstracted using a methodology designed to identify and track waters according to the water types they produce upon evaporation. The in-drift water composition predictions from the in-drift precipitates and salt model are then compiled in a set of lookup tables that represent the in-drift chemistry response surfaces used in TSPA.

4.4.4.1 Thermal-Hydrologic-Chemical Seepage Model Abstraction

The primary purpose of the thermal-hydrologic-chemical seepage model abstraction is to integrate and propagate the results of the thermal-hydrologic-chemical model into the in-drift precipitates and salt model simulations that predict water composition evolution in the drift. Full details of this abstraction are documented in *Engineered Barrier System: Physical and Chemical Environment Model* (BSC 2004d, Section 6.6).

Five complete sets of thermal-hydrologic-chemical model results, corresponding to the five initial starting waters identified in Section 4.4.2, were selected to represent the spread of potential seepage water compositions. Each of the five thermal-hydrologic-chemical model runs produce time histories of changing water compositions for a large number of locations around the drift. The time history is documented at approximately 50 discrete points distributed in time over the 100,000-year modeling period. In total, there are approximately 3,600 discrete water chemistries for each of the thermal-hydrologic-chemical outputs so that the inputs contain approximately 18,000 water chemistries.

An abstraction methodology is used to reduce the number of lookup tables required to adequately represent the effects of evaporation within the drift for any given time period. This methodology involves grouping (or binning) each input water composition at each point in time according to how it evaporatively evolves and then selecting a water composition within each group (or bin) to represent all waters in the bin.

Abstracting the thermal-hydrologic-chemical model results using the binning methodology requires five steps:

- **Step 1**—Selection of a subset of thermal-hydrologic-chemical model grid nodes to provide the representative seepage water composition.

- **Step 2**—The general evaporative evolution pathway for each water composition is determined using the in-drift precipitates and salts model to evaporate the waters selected in Step 1 to a common relative humidity.

- **Step 3**—The evaporated waters are sorted into groups (bins) containing similar evaporated water types. This step makes use of the concept of chemical divides to develop these groups.

- **Step 4**—A representative water composition is chosen from the various waters in each bin to represent all of the waters in the bin. The water determined to be nearest to the statistical median values for each of the reported chemical parameters is selected as the representative water for the bin.

- **Step 5**—The thermal-hydrologic-chemical water seepage model results are mapped back to the bins so that the predictions in time provided by the thermal-hydrologic-chemical model can be represented by a time series of representative water compositions.

Step 1 reduces the 18,000 input waters to 368. Steps 2 and 3 reduce the 368 input waters to 11 groups of similar water types. In Step 3, the 368 waters evaporated using the in-drift precipitates and salts model are sorted based on yes/no answers to the following questions:

- Is total aqueous calcium molality greater than 0.01 mol/kg?
- Is total aqueous carbonate molality greater than 0.1 mol/kg?
- Is total aqueous calcium molality less than total aqueous sodium molality?
- Is total aqueous calcium molality greater than total aqueous potassium molality?
- Is total aqueous sodium molality greater than total aqueous carbonate molality?
- Is total aqueous fluorine molality less than 0.1 mol/kg?
- Is total aqueous fluorine molality less than 0.03 mol/kg?
- Is total aqueous sulfate molality greater than 1 mol/kg?

These questions were developed based on relationships important to chemical divides and (or) on the ability of each question to establish water types among the 368 waters identified in Step 1. In this case, these questions identify and resolve 11 water types. Evaporated waters having the same set of answers to these questions are placed in the same bin. From each of these groups, one median water is selected to represent all waters in the group (Step 4).

In Step 5, the water types were mapped back to the thermal-hydrologic-chemical seepage model results by noting which group each of the 368 waters from Step 3 is sorted into. These maps, shown in Figure 24, provide time histories of water types (bins 1 through 11) for each thermal-hydrologic-chemical seepage model starting water (W0, W4, W5, W6, or W7) for two locations at the crown and the invert. There are exactly 368 cells in Figure 24, corresponding to the 368 waters determined in Step 1.

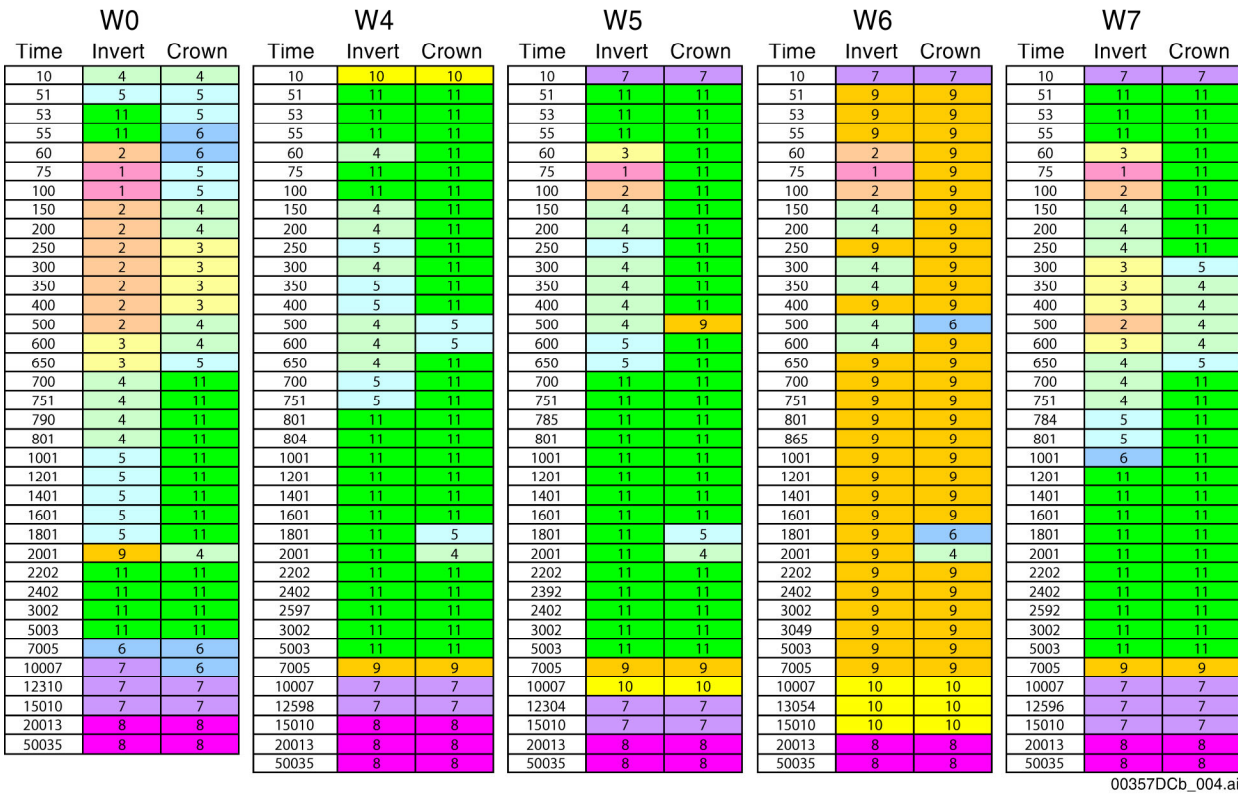

W0

Time	Invert	Crown
10	4	4
51	5	5
53	11	5
55	11	6
60	2	6
75	1	5
100	1	5
150	2	4
200	2	4
250	2	3
300	2	3
350	2	3
400	2	3
500	2	4
600	3	4
650	3	5
700	4	11
751	4	11
790	4	11
801	4	11
1001	5	11
1201	5	11
1401	5	11
1601	5	11
1801	5	11
2001	9	4
2202	11	11
2402	11	11
3002	11	11
5003	11	11
7005	6	6
10007	7	6
12310	7	7
15010	7	7
20013	8	8
50035	8	8

W4

Time	Invert	Crown
10	10	10
51	11	11
53	11	11
55	11	11
60	4	11
75	11	11
100	11	11
150	4	11
200	4	11
250	5	11
300	4	11
350	5	11
400	5	11
500	4	5
600	4	5
650	4	11
700	5	11
751	5	11
801	11	11
804	11	11
1001	11	11
1201	11	11
1401	11	11
1601	11	11
1801	11	5
2001	11	4
2202	11	11
2402	11	11
2597	11	11
3002	11	11
5003	11	11
7005	9	9
10007	7	7
12598	7	7
15010	8	8
20013	8	8
50035	8	8

W5

Time	Invert	Crown
10	7	7
51	11	11
53	11	11
55	11	11
60	3	11
75	1	11
100	2	11
150	4	11
200	4	11
250	5	11
300	4	11
350	4	11
400	4	11
500	4	9
600	5	11
650	5	11
700	11	11
751	11	11
785	11	11
801	11	11
1001	11	11
1201	11	11
1401	11	11
1601	11	11
1801	11	5
2001	11	4
2202	11	11
2392	11	11
2402	11	11
3002	11	11
5003	11	11
7005	9	9
10007	10	10
12304	7	7
15010	7	7
20013	8	8
50035	8	8

W6

Time	Invert	Crown
10	7	7
51	9	9
53	9	9
55	9	9
60	2	9
75	1	9
100	2	9
150	4	9
200	4	9
250	9	9
300	4	9
350	4	9
400	9	9
500	4	6
600	4	9
650	9	9
700	9	9
751	9	9
801	9	9
865	9	9
1001	9	9
1201	9	9
1401	9	9
1601	9	9
1801	9	6
2001	9	4
2202	9	9
2402	9	9
3002	9	9
3049	9	9
5003	9	9
7005	9	9
10007	10	10
13054	10	10
15010	10	10
20013	8	8
50035	8	8

W7

Time	Invert	Crown
10	7	7
51	11	11
53	11	11
55	11	11
60	3	11
75	1	11
100	2	11
150	4	11
200	4	11
250	4	11
300	3	5
350	3	4
400	3	4
500	2	4
600	3	4
650	4	5
700	4	11
751	4	11
784	5	11
801	5	11
1001	6	11
1201	11	11
1401	11	11
1601	11	11
1801	11	11
2001	11	11
2202	11	11
2402	11	11
2592	11	11
3002	11	11
5003	11	11
7005	9	9
10007	7	7
12596	7	7
15010	7	7
20013	8	8
50035	8	8

00357DCb_004.ai

Source: BSC 2004d, Figure 6.13-1, DTN: MO0312SPAPCESA.002.

Figure 24. Color-Coded Bin History Maps Showing Bin Occurrence for Crown Seepage and Invert Wicking Locations

4.4.4.2 Coupling of the Thermal-Hydrologic-Chemical Water Seepage Model with In-Drift Chemistry

The 11 representative water compositions determined in Step 4 of the thermal-hydrologic-chemical seepage abstraction are used as inputs to the in-drift precipitates and salts model to generate lookup tables for the TSPA. These waters are evaporated over a range of temperatures (100°C, 70°C, and 40°C) and pCO_2 values (10^{-2}, 10^{-3}, and 10^{-4} bar CO_2) to produce 99 lookup tables (11 representative waters × three temperatures × three pCO_2 values) that represent temperature and relative humidity and pCO_2 effects on the 11 water types. The calculated values of pH, ionic strength, and chemical species are listed in the lookup tables as a function of relative humidity so that the evaporative concentration of each of the 11 representative waters can be determined at any relative humidity. Figure 25 displays the values in one of the lookup tables for one of the water types (Bin 7). This figure describes the predicted effects of relative humidity on pH and water composition at 70°C and 10^{-3} bar pCO_2.

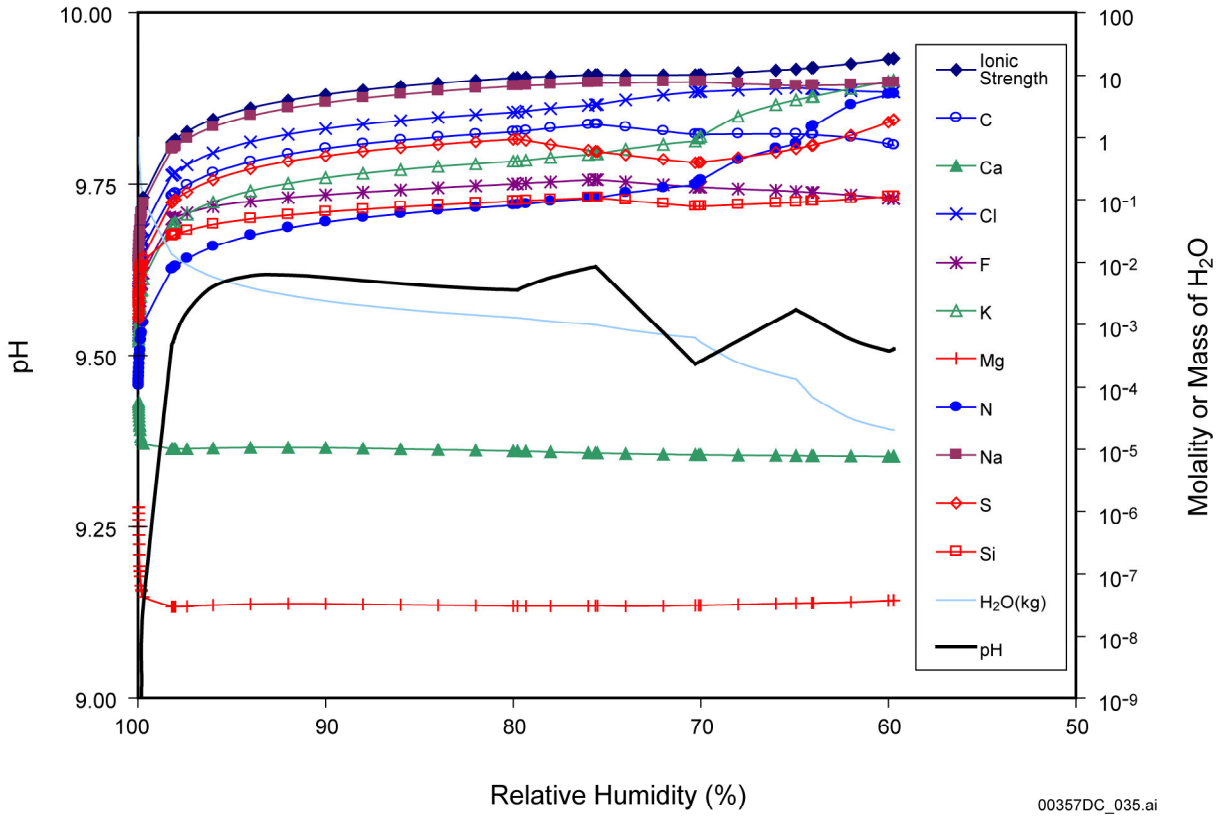

Source: DTN: MO0304SPACSALT.000, 07C3T7E.XLS.XLS; BSC 2004d.

Figure 25. Bin 7 Aqueous Composition Evaporation Predictions Versus Relative Humidity at 70°C and CO_2 Fugacity of 10^{-3} bar

Because condensation of water vapor into the liquid phase is the reverse of evaporation, these lookup tables indicate the effects of both condensation and evaporation. Evaporation occurs as relative humidity falls, and condensation occurs as relative humidity rises. An additional 99 lookup tables were generated by the in-drift precipitates and salts model by condensing water vapor into the 11 representative water compositions (i.e., by diluting the 11 representative water compositions with pure water). These additional lookup tables ensure that the highest potential relative humidity values in the drift (about 100%) are included in the response surface for each water type.

The lookup tables, as a whole, composes the suite of in-drift chemistry response surfaces. These surfaces incorporate and propagate the effects of the coupled processes of the thermal-hydrologic-chemical model into the coupled processes of the in-drift precipitates and salts model. The variations in pore water compositions (Section 4.4.2) are passed to the in-drift precipitates and salts model simulations from the thermal-hydrologic-chemical seepage model by way of the 11 bin seepage abstraction (above). Each of these water types is subjected to wide ranges of temperature, relative humidity, and pCO_2 in the in-drift precipitates and salts model simulations to generate lookup tables to accommodate all potential temperature and relative humidity and pCO_2 profiles predicted by the thermal-hydrologic and thermal-hydrologic-chemical models.

In effect, the in-drift chemistry response surfaces serve to integrate thermal-hydrologic, thermal-hydrologic-chemical seepage, and in-drift chemistry processes for the TSPA. The integration and coupling occurs as the TSPA uses the following inputs to interpolate in-drift water chemistry from the lookup tables:

- The temperature and relative humidity profiles from the thermal-hydrologic model
- The water-type profiles (bin maps) from the thermal-hydrologic-chemical model abstraction (Figure 24)
- The pCO_2 profiles from the thermal-hydrologic-chemical model (BSC 2004d, Section 6.7).

Details of the TSPA implementation of the in-drift chemistry response surfaces are provided in *Engineered Barrier System: Physical and Chemical Environment Model* (BSC 2004d, Section 6.14).

Although all potential temperature and relative humidity and pCO_2 profiles are in the range of the in-drift chemistry response surfaces, large portions of the surfaces are never used in the TSPA because of the limited combinations of temperature, relative humidity, and CO_2 over time (Section 4.4.5). The lookup tables do, however, provide the range of possible chemical compositions that result from all simulated combinations of temperature (40°C, 70°C, and 100°C), pCO_2 (10^{-4}, 10^{-3}, and 10^{-2} bar CO_2), and relative humidity (nominally every 2% down to dryout but including smaller intervals where solution conditions change because of mineral precipitation).

An example of the ranges of outputs in the in-drift chemistry response surfaces is shown in Figure 26. This graph shows the range of $Cl:NO_3$ ratios calculated for Bins 3 to 11. The $Cl:NO_3$ ratio is an important output parameter of the in-drift chemistry response surfaces because chloride facilitates corrosion while nitrate inhibits it. Bins 1 and 2 are not included in this figure because seepage from the crown is never predicted to have a water type similar to those in Bins 1 and 2 (Figure 24).

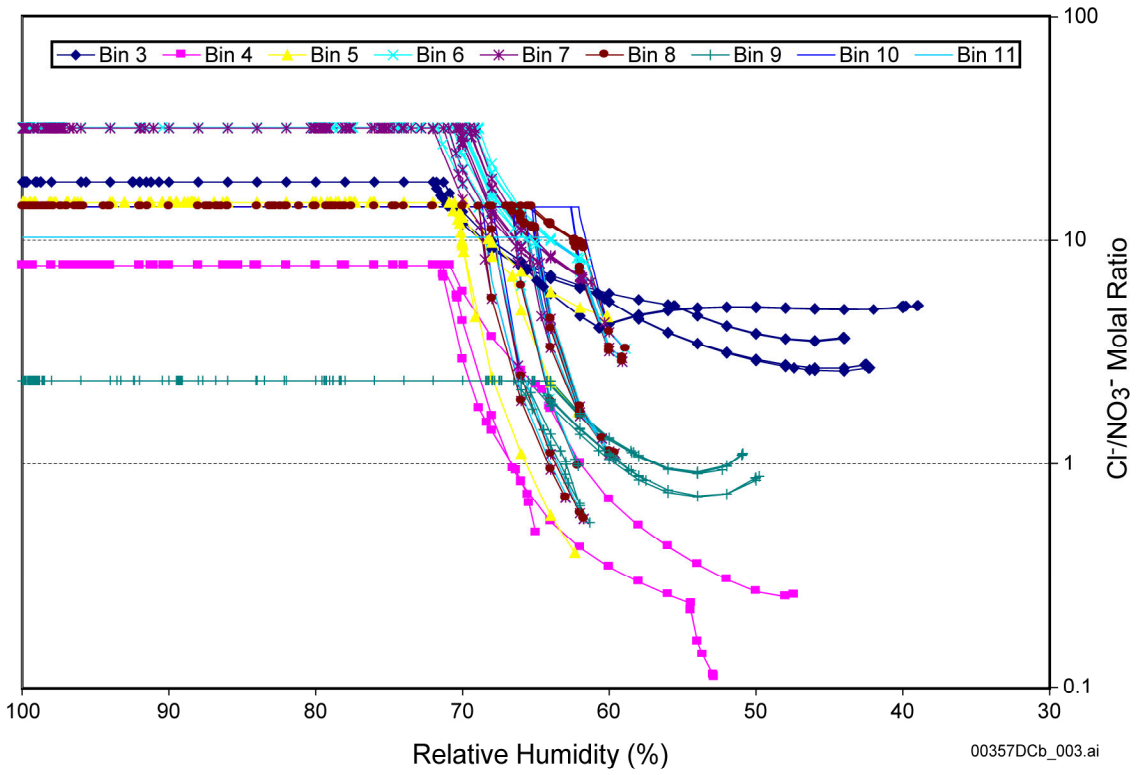

Source: BSC 2004d, Figure 6.13-29; DTN: MO0312SPAPCESA.002.

Figure 26. Range of Cl to NO_3 Molal Ratios for the Seepage Evaporation Lookup Tables Representing Bins 3 to 11

4.4.4.3 Consolidation of the 11 Bin Water Types into Brine Types

As noted above, the 11 bin water types represent the range of in-drift aqueous solution chemistries. The in-drift solution chemistries for the 11 bins will evolve as a function of temperature, relative humidity, and carbon dioxide partial pressure, and a variety of solution chemistries are possible. However, for the purposes of materials degradation studies, it is useful to consolidate the 11 bin water types into brine types sharing common characteristics. To this end, it is known from the geochemistry literature that natural water evolve into 3 brine types: calcium chloride, carbonate, and sulfate.

The calcium chloride brine has near neutral pH and no significant bicarbonate-carbonate, fluoride, or sulfate content. These brines may contain other cations, such as Na^+, K^+, and Mg^{2+}, and other anions, such as NO_3^-. The endpoint of the evaporative concentration of this type of brine would contain Ca-Cl/NO_3 or a mixture of Ca/Mg-Cl/NO_3. The quantity of Mg^{2+} and Ca^{2+} in this type of brine would be limited due to the precipitation of calcium carbonates and sulfates and magnesium silicates. Bins 1, 2, and 3 evolve into calcium chloride type brine.

The carbonate brine is alkaline and does not contain significant calcium or magnesium. In the early stages of the evaporative concentration, calcium precipitates predominately as carbonate minerals (calcite or aragonite). Magnesium precipitates as a minor component in the calcium carbonate species and as magnesium silicate. In the repository, it is expected that magnesium

will be removed efficiently, and potassium may be significant in some of these brines. Bins 6 through 11 evolve into carbonate type brine.

The sulfate brine has near-neutral pH and no significant carbonate or calcium content. Calcium precipitates as carbonates and possibly sulfates. In addition, brines typically have only a small amount of magnesium, though some surface brines have been observed to have high magnesium (Drever 1988, Table 15-1, p. 333, brines 1 through 3). The dominant cation is typically Na^+. In the repository brines, K^+ may be more significant than Na^+, and Mg^{2+} is expected to be insignificant due to Mg-silicate precipitation. Bins 4 and 5 evolve into sulfate type brine.

4.4.5 Evolution of Water Composition Evolution for a Representative Temperature and Relative Humidity Profile

When the temperature at the drift wall falls below boiling and seepage begins to enter the drift, the TSPA determines the effects of in-drift seepage evaporation on concentrations of key chemical constituents, such as Cl and NO_3, by coupling the seepage evaporation response surfaces with the appropriate temperature and relative humidity profiles. As shown in Figure 4, relative humidity is strongly dependent on temperature and the coupled processes in the thermal-hydrologic model.

The temperature and relative humidity profiles for the cool, average, and hot waste packages in Figure 4 are compared to several chemical characteristics in Figure 20. Stable aqueous (wet) conditions cannot be maintained until the temperature falls below the boiling point of the brine. For the seepage waters identified in Section 4.4.4, the shaded areas of Figure 20 represent conditions that are conducive to stable NaCl-KNO_3 aqueous solutions that could evolve from either carbonate or sulfate type brines. Thus, dry conditions exist for the temperature and relative humidity profiles until the in-drift temperature falls below about 120°C and the relative humidity rises to about 40% for the illustrated NaCl-KNO_3 system.

4.5 Significance of Other Processes Excluded from Coupling

The above discussion illustrates the principal couplings included in the models used to evaluate the temporal and spatial evolution of the waste package and drip shield chemical conditions and the uncertainty in these conditions. In particular, the thermal-hydrologic-chemical coupled processes are used to abstract the projected brine compositions in either the dusts or the aqueous environments present on the drip shield and waste package surfaces. This discussion focused on the technical basis for the different salt and aqueous bins abstracted for use in the TSPA model.

As noted in the KTI agreement, other coupled processes could potentially affect the chemical conditions. These other potential coupled processes are addressed in the following sections and also addressed in feature, event, and process screening arguments described in *Engineered Barrier System Features, Events, and Processes* (BSC 2004f).

4.5.1 Effect of Gamma Radiation on Waste Package Chemical Environment

Effect of Coupled Gamma Radiation on Aqueous Chemical Environment–Gamma radiation could affect aqueous environments by creating oxidizing conditions due to the formation of species such as hydrogen peroxide (H_2O_2). Two primary consequences of radiation on the

environment are the elevation of the open circuit potential of metallic materials and the production of nitric acid. These potential coupled processes are discussed below.

Under bulk aqueous solution conditions, anodic shifts in the open circuit potential of stainless steel in gamma irradiated solutions have been experimentally observed. Glass et al. (1986) found a corrosion potential shift in the anodic direction by approximately 200 mV on Stainless Steel Type 316L in 0.018 mol/L NaCl solution during exposure to 3.5 Mrad/hr gamma radiation. Kim (1988) also found an increased corrosion potential of about 100 mV for stainless steel in 1.5 mol/L NaCl (approximately pH 2) solution exposed to 0.14 Mrad/hr gamma radiation.

In addition to affecting the redox potential of metals, gamma radiation could have an effect on the chemical composition of aqueous solutions. Changes in the redox potential of the aqueous solution are not expected to change the nature and composition of either the major cationic species or the major anionic species, with the exception of the nitrogen-containing species. The major cationic species are calcium, magnesium, sodium, and potassium. The unaffected anionic species are the halide species (fluoride, chloride, and bromide), sulfate, and carbonate–bicarbonate. Gaseous nitrogen (N_2) can be oxidized to nitric acid (HNO_3) under certain combinations of gamma radiation and relative humidity conditions.

The waste packages that are emitting high gamma radiation are expected to have elevated temperatures. The high gamma radiation fields are limited to those times when no seepage is expected because the elevated temperatures and decreased relative humidity cause a vaporization barrier effect in addition to the capillary diversion of potential seepage. When the host-rock temperature is at or above boiling, the relative humidity in the drift environment is predicted to be low (BSC 2004b, Section 6.3.3), particularly during the first few hundred years after emplacement, when gamma radiation outside the waste package is potentially significant.

Hence, gamma radiation effects are limited to aqueous solutions that result from very deliquescent dust salt minerals that are deposited on the waste packages. Solutions of interest are those predicted to form from deliquescence of salts contained in deposited dust at elevated temperature and low relative humidity. The salt mineral assemblages that control the deliquescence behavior of dust salt have been determined (BSC 2003a, Section 6.7.2.10). They are:

- $Ca(NO_3)_2 + KNO_3 + NaNO_3 + NaCl$
- $KNO_3 + NaNO_3 + NaCl$
- $KNO_3 + NaCl$.

The addition of nitric acid to these solutions would lower the solution pH to the point where volatilization of HCl would occur, removing chloride from the solution. There is expected to be a strong temperature and solution composition dependence on HCl volatility (BSC 2003a). At some point, the aqueous solutions would reach a pH level that is consistent with a sustainable partial pressure of nitric acid in the drift. The partial pressure of nitric acid and, hence, the sustainable pH, will be limited by the radiolysis yield and by transport and reaction of the acid vapor with the host rock.

The overall effect of gamma radiation–induced nitric acid formation on solution chemistry is to lower solution pH, remove chloride from solution, and add nitrate to the solution. The endpoint pH is a function of solution composition, temperature, and the partial pressures of the in-drift acid gases. Given the beneficial effect of nitrate in solution, these changes are not significant from a corrosion-performance perspective.

4.5.2 Potential Effects of Coupled Microbial Processes

Microbial processes can alter aqueous solution chemistry and influence its redox potential on metal surfaces. Aqueous solution chemistry can be altered by processes such as denitrification (i.e., the reduction of aqueous nitrate (NO_3)) and microbes can alter the redox potential of a metal by depositing redox-influencing materials on the metal's surface.

Denitrification is a process by which microbes reduce nitrate into various other nitrogen containing species, such as nitrite (NO_2^-), nitrogen (N_2), ammonia (NH_3), and nitrous oxide (N_2O). Two primary pathways exist for denitrification: heterotrophic and autotrophic.

Heterotrophic denitrification requires an available reduced organic carbon source as an electron donor. The carbon source needs to be more abundant than the nitrate. It is known in groundwater systems that the lack of available carbon is commonly found to limit the extent of nitrate reduction; this is probably the situation presently at Yucca Mountain. The denitrification process is an anaerobic process. The microbes use nitrate as a terminal electron acceptor; however, if oxygen is available, microbes will preferentially use oxygen. There is some indication that some microbes are nitrate specific. The redox conditions in the unsaturated zone at Yucca Mountain are oxidizing because the highly fractured rock allows communication between the inside of the mountain and the outside air.

Autotrophic denitrification requires an inorganic reduced electron source and can access carbon dioxide (CO_2) from the air as a carbon source; that is, there is no requirement for organic carbon by these microbes. The extent to which this process takes place in the environment is known. However, the mineralogy at Yucca Mountain shows the presence of metals in oxidized state; that is, inorganic reduced electron sources, such as ferrous sulphide (FeS_2), are not present in significant quantities. Autotrophic denitrification is not expected to occur in the ambient rock due to the lack of electron donors.

4.5.3 Potential Coupled Effect of Electric Fields Caused by Compton Electron Scattering

As noted by Green et al. (1987), the possibility exists for the generation of electron fields around the waste packages caused by Compton electron scattering. Assuming a completely degraded canister with no shielding effect by cladding or canister wall, Green et al. (1987) calculated that the electric field at 10 cm would be much greater in air (10^2 V/cm) than in rock ($10^{-8.5}$ V/cm) at 300 years. However, since photon energies are severely degraded by materials with high Z (the sum of element's neutron and protons), the waste package wall (which consists of 5 cm of Stainless Steel Type 316 and 2 cm Alloy 22) would degrade the electric field in air outside the waste package to a value similar to that calculated for solid rock at 10 cm, approximately $10^{-8.5}$ V/cm at 300 years. The magnitude of the resulting electric current is not significant to the

geochemical processes occurring on the waste package surface. Furthermore, the electric field decreases significantly with distance and age of the waste package.

Another way to describe the potential effects from electric fields due to Compton scattering is by calculating the current density. Green et al. (1987, Figure 6) examined the variation of the current density in air with the radial distance from the waste package. Again, using the example of 10 cm distance for 1.55 MeV gamma rays, the current density would be less than 10^{-25} A/cm^2. Extrapolated for 1,000 years for the surface of a 1.7-m diameter cylinder, the resulting accumulation associated with this is an insignificant increase of less than 1 picomole (10^{-12} mole).

4.5.4 Physical Separation of Salts

When no transport of the seepage is involved, equilibrium with the local temperature and relative humidity is approached, and minerals accumulate in contact with the aqueous system. These minerals in contact with the aqueous system do not significantly affect the relevant evolution of the aqueous system because the rate of change in conditions is quite slow when compared to the dissolution rates for performance-affecting salts of chloride and nitrate (BSC 2004d). However, for the case when transport occurs with significant evaporation, then a distribution of minerals may precipitate along the transport pathway. This leads to the potential for spatial separation of components, both in the aqueous and solid phases, with more soluble components being transported farther than those that are less soluble and precipitate. When temperatures decrease and relative humidity increases, the less soluble precipitates will deliquesce or dissolve and change the local aqueous chemical environment. Of particular interest in regard to this salt separation is halite (NaCl), which may in the future lead to increases in chloride concentrations by deliquescence.

For slow flow rates, diffusion will dominate, and a fully mixed condition with no salt separation may occur. For high flow rates, possibly associated with splashing, salt separation is feasible. The degree of physical salt separation is a function of the relative advective flow of water (i.e., the seepage or drip rate) versus the diffusion of dissolved constituents.

In cases where the relative humidity at the waste package surface is low enough and halite reaches saturation, it is possible that sufficient fluid will remain to allow advective flow to exceed mass transport by diffusion.

The possibility of salt separation has been addressed in the TSPA. Although it is expected that the degree of salt separation depends on the magnitude of the seepage flux and the angle inclination to the vertical of the waste package surface contacted by the seepage water, the residence time of fast flowing water would be insufficient to permit significant salt separation. To be conservative, the treatment in the TSPA assumes that salts in any aqueous brine that contacts the waste package surface will separate if the relative humidity is low enough at the time the water contacts the surface to preferentially precipitate halite (NaC1). Although some time would elapse from the time when the salt is precipitated (at low relative humidity) and the time when that precipitated salt would deliquesce (at higher relative humidity), on the order of hundreds of years, the corrosive effects of the deliquescent NaC1 brine are implemented beginning at the time of seepage.

4.5.5 Electrochemical Processes

Electrochemical processes occurring on the surfaces of the waste packages and drip shield will alter the chemistry of the aqueous solutions. The aqueous solution pH is lowered in regions of actively corroding metal, that is, at anodic sites, such as crevices and pits. The pH lowering is due to the alloy metal ion hydrolysis. The aqueous solution pH is raised in regions where oxygen reduction to hydroxyl is occurring, that is, at cathodic sites. The separation of the cathodic and anodic regions can be on the order of micrometers.

The lowering of the pH at anodic sites can lead to environmental conditions where acid gas volatility can occur. The loss of the acid gas component (e.g., HCl) will elevate the solution pH at these sites and could lead to precipitation of metal oxides and hydroxide, some of which are stable under moderately acidic conditions.

The raising of the pH at cathodic sites can lead to environmental conditions where precipitation of alkaline earth (Ca and Mg) and alkali (K and Na) metals can occur as hydroxides ($Mg(OH)_2$ and $Ca(OH)_2$), hydroxy-chlorides (MgOHCl and CaOHCl) and carbonates ($MgCO_3$, $CaCO_3$, Na_2CO_3, $NaHCO_3$, and $KHCO_3$). These minerals are less soluble than the corresponding chloride minerals (salts).

While the electrochemical processes would tend to inhibit other corrosive processes, neither the lowering of aqueous solution pH at anodic sites with subsequent acid gas volatility nor the raising of aqueous solution pH at cathodic sites with subsequent mineral precipitation are implemented in TSPA. Corrosion is modeled as being dependent on the initial aqueous solution that comes into contact with the waste package or drip shield. No credit is taken for the aqueous solution chemical transformations that could occur as a result of the electrochemical processes that are occurring on the surfaces of the waste package and drip shield.

5 REFERENCES

5.1 Documents Cited

Ansari, A.S. and Pandis, S.N. 1999. "Prediction of Multicomponent Inorganic Atmospheric Aerosol Behavior." *Atmospheric Environment, 33,* (5), 745–757. New York, New York: Pergamon. TIC: 254406.

Arimoto, R. 2001. "Eolian Dust and Climate: Relationships to Sources, Tropospheric Chemistry, Transport and Deposition." *Earth-Science Reviews, 54,* (1–3), 29–42. New York, New York: Elsevier. TIC: 254407.

Blank, R.R.; Young, J.A.; and Allen, F.L. 1999. "Aeolian Dust in a Saline Playa Environment, Nevada, U.S.A." *Journal of Arid Environments*, *41*, (4), 365–381. New York, New York: Academic Press. TIC: 254405.

Böhlke, J.K.; Ericksen, G.E.; and Revesz, K. 1997. "Stable Isotope Evidence for an Atmospheric Origin of Desert Nitrate Deposits in Northern Chile and Southern California, U.S.A.." *Chemical Geology, 136,* (1–2), 135–152. New York, New York: Elsevier. TIC: 254348.

BSC (Bechtel SAIC Company) 2002. *Analysis of Geochemical Data for the Unsaturated Zone.* ANL-NBS-HS-000017 REV 00 ICN 02. Las Vegas, Nevada: Bechtel SAIC Company. ACC: MOL.20020314.0051.

BSC 2003a. *Environment on the Surfaces of the Drip Shield and Waste Package Outer Barrier.* ANL-EBS-MD-000001 REV 01D. Las Vegas, Nevada: Bechtel SAIC Company. ACC: MOL.20030825.0151.

BSC 2003b. *Software Code: EQ3/6.* V8.0. PC Windows 95/98/2000/NT 4.0. 10813-8.0-00.

BSC 2003c. *Drift-Scale Coupled Processes (DST and THC Seepage) Models.* MDL-NBS-HS-000001 REV 02. Las Vegas, Nevada: Bechtel SAIC Company. ACC: DOC.20030804.0004.

BSC 2004a. *Multiscale Thermohydrologic Model.* ANL-EBS-MD-000049 REV 02A. Las Vegas, Nevada: Bechtel SAIC Company. ACC: MOL.20040630.0537.

BSC 2004b. *Multiscale Thermohydrologic Model.* ANL-EBS-MD-000049 REV 01. Las Vegas, Nevada: Bechtel SAIC Company. ACC: DOC.20040301.0004.

BSC 2004c. *Ventilation Model and Analysis Report.* ANL-EBS-MD-000030 REV 03 ICN 03, with errata. Las Vegas, Nevada: Bechtel SAIC Company. ACC: DOC.20031216.0002; DOC.20040202.0004; DOC.20040325.0003.

BSC 2004d. *Engineered Barrier System: Physical and Chemical Environment Model.* ANL-EBS-MD-000033 REV 02, with errata. Las Vegas, Nevada: Bechtel SAIC Company. ACC: DOC.20040212.0004; DOC.20040426.0003.

BSC 2004e. *In-Drift Precipitates/Salts Model.* ANL-EBS-MD-000045 REV 01 ICN 01. Las Vegas, Nevada: Bechtel SAIC Company. ACC: DOC.20040202.0001.

BSC 2004f. *Engineered Barrier System Features, Events, and Processes.* ANL-WIS-PA-000002 REV 02. Las Vegas, Nevada: Bechtel SAIC Company. ACC: DOC.20040505.0003.

Campbell, A.N. and Smith, N.O. 1951. *The Phase Rule and its Applications.* 9th Edition. New York, New York: Dover Publications. TIC: 254360.

Creahan, J. 1991. "Controlling Relative Humidity with Saturated Calcium Nitrate Solutions." *WAAC Newsletter, 13,* (1), 17–18. Los Angeles, California: Western Association for Art Conservation. TIC: 254503.

CRWMS M&O (Civilian Radioactive Waste Management System Management and Operating Contractor) 1993. *Chemical Tracer Injection System Analysis for Construction Process and Firewater Usage.* BABFAE000-01717-0200-00030 REV 01. Las Vegas, Nevada: CRWMS M&O. ACC: MOL.19951019.0473.

Drever, J.I. 1988. *The Geochemistry of Natural Waters.* 2nd Edition. Englewood Cliffs, New Jersey: Prentice-Hall. TIC: 242836.

Dunning, G.E. and Cooper, J.F., Jr. 1969. "A Second Occurrence of Antarcticite, from Bristol Dry Lake, California." *American Mineralogist, 54,* (7–8), 1018–1025. Washington, D.C.: Mineralogical Society of America. TIC: 254451.

Farmer, J.; McCright, D.; Gdowski, G.; Wang, F.; Summers, T.; Bedrossian, P.; Horn, J.; Lian, T.; Estill, J.; Lingenfelter, A.; and Halsey, W. 2000. "General and Localized Corrosion of Outer Barrier of High-Level Waste Container in Yucca Mountain." *Transportation, Storage, and Disposal of Radioactive Materials, 2000, Presented at the 2000 ASME Pressure Vessels and Piping Conference, Seattle, Washington, July 23–27, 2000.* Hafner, R.S., ed. PVP-Vol. 408. 53–69. New York, New York: American Society of Mechanical Engineers. TIC: 251259.

Ge, Z.; Wexler, A.S.; and Johnston, M.V. 1998. "Deliquescence Behavior of Multicomponent Aerosols." *Journal of Physical Chemistry A, 102,* (1), 173–180. Washington, D.C.: American Chemical Society. TIC: 254410.

Glass, R.S.; Overturf, G.E.; Van Konynenburg, R.A.; and McCright, R.D. 1986. "Gamma Radiation Effects on Corrosion—I. Electrochemical Mechanisms for the Aqueous Corrosion Processes of Austenitic Stainless Steels Relevant to Nuclear Waste Disposal in Tuff." *Corrosion Science*, *26*, (8), 577–590. Oxford, Great Britain: Pergamon. TIC: 226179.

Green, R.T.; Fillippone, W.L.; and Evans, D.D. 1987. "Effect of Electric Fields on Vapor Transport Near a High-Level Waste Canister." *Coupled Processes Associated with Nuclear Waste Repositories.* C.-F. Tsang. 421–432. Orlando, Florida: Academic Press. TIC: 200325.

Greenspan, L. 1977. "Humidity Fixed Points of Binary Saturated Aqueous Solutions." *Journal of Research of the National Bureau of Standards, 81A,* (1), 89–96. Washington, D.C.: U.S. Department of Commerce. TIC: 241138.

Hill, C. and Forti, P. 1997. *Cave Minerals of the World.* 2nd Edition. Huntsville, Alabama: National Speleological Society. TIC: 254549.

Kim, Y.-K. 988. "Electrochemical Mechanisms for Radiation Corrosion Processes of 316 Austenitic Stainless Steel in Chloride Environment." *Journal of the Corrosion Science Society of Korea, 17*, (1), 20–26. Seoul, Korea: Korean Corrosion Science Society. TIC: 246622.

Kracek, F.C. 1928. "P-T-X Relations for Systems of Two or More Components and Containing Two or More Phases (L-V, L_I-L_{II}-V and S-L-V Systems)." *International Critical Tables of Numerical Data, Physics, Chemistry and Technology.* Washburn, E.W., ed. Volume III. 1st Edition. New York, New York: McGraw-Hill. TIC: 243268.

Lasaga, A.C. 1998. *Kinetic Theory in the Earth Sciences.* Princeton, New Jersey: Princeton University Press. TIC: 246279.

LBNL (Lawrence Berkeley National Laboratory) 2002. *Software Code: TOUGHREACT.* V3.0. DEC ALPHA/OSF1 V5.1, DEC ALPHA/OSF1 V5.0, Sun UltraSparc/Sun OS 5.5.1, PC/Linux Redhat 7.2. 10396-3.0-00.

Levy, D.B.; Schramke, J.A.; Esposito, K.J.; Erickson, T.A.; and Moore, J.C. 1999. "The Shallow Ground Water Chemistry of Arsenic, Fluorine, and Major Elements: Eastern Owens Lake, California." *Applied Geochemistry, 14,* (1), 53–65. New York, New York: Pergamon. TIC: 254418.

Levy, S.S.; Fabryka-Martin, J.T.; Dixon, P.R.; Liu, B.; Turin, H.J.; and Wolfsberg, A.V. 1997. "Chlorine-36 Investigations of Groundwater Infiltration in the Exploratory Studies Facility at Yucca Mountain, Nevada." *Scientific Basis for Nuclear Waste Management XX, Symposium held December 2-6, 1996, Boston, Massachusetts.* Gray, W.J. and Triay, I.R., eds. *465,* 901–908. Pittsburgh, Pennsylvania: Materials Research Society. TIC: 238884.

Mitchell, A. 1998. "Water Data." E-mail from A. Mitchell (LANL) to R. Wemheuer (CRWMS M&O), February 23, 1998. ACC: MOL.19990305.0201.

Mitchell, A.J. 1999a. "Tracers, Fluids, and Materials Evaluation for Gases and Aqueous Tracers for the Systematic Hydrological Investigation of the Fracture Flow and Transport in the East-West Cross Drift." Interoffice correspondence from A.J. Mitchell (CRWMS M&O) to D. Gwyn, December 14, 1999, LV.NEPO.TEST.AJM.12/99-410, with enclosures.
ACC: MOL.20000204.0132.

Mitchell, A.J. 1999b. "Request for Additional Water for Phase II of Infiltration and Percolation Study Being Conducted in Upper Tiva Canyon Alcove – Alcove 1 in Support of Field Work Package FWP-ESF-96-004." Interoffice correspondence from A.J. Mitchell (CRWMS M&O) to D. Gwyn, October 25, 1999, LV.NEPO.TEST.AJM.10/99-374, with enclosure.
ACC: MOL.20000204.0133.

Mitchell, A.J. 1999c. "Tracers, Fluids, and Materials Evaluation for Tracers to be Conducted in Alcove 8 in Association with Infiltration Testing in Support of Field Work Package FWP-ESF-96-004." Interoffice correspondence from A.J. Mitchell (CRWMS M&O) to D. Gwyn, March 10, 1999, LV.NEPO.TEST.AJM.03/99-259. ACC: MOL.19990329.0083.

Mitchell, A.J. 2000. "Request for Additional Water for the Infiltration and Percolation Study Being Conducted in Upper Tiva Canyon Alcove – Alcove 1, in Support of Field Work Package FWP-ESF-96-004, Moisture Studies in the ESF." Interoffice correspondence from A.J. Mitchell (CRWMS M&O) to D. Gwyn, January 7, 2000, LV.NEPO.TEST.AJM.01/00-105, with enclosure. ACC: MOL.20000204.0134.

National Atmospheric Deposition Program/National Trends Network 2004a. 2002 Annual & Seasonal Data Summary for Site NV00. Champaign, Illinois: NADP Program Office, Illinois State Water Survey. TIC: 256214.
http://nadp.sws.uiuc.edu/ads/2002/NV00.pdf

National Atmospheric Deposition Program/National Trends Network 2004b. 2002 Annual & Seasonal Data Summary for Site NV05. Champaign, Illinois: NADP Program Office, Illinois State Water Survey. TIC: 256215.
http://nadp.sws.uiuc.edu/ads/2002/NV05.pdf

National Atmospheric Deposition Program/National Trends Network 2004c. 2002 Annual & Seasonal Data Summary for Site CA95. Champaign, Illinois: NADP Program Office, Illinois State Water Survey. TIC: 256216.
http://nadp.sws.uiuc.edu/ads/2002/CA95.pdf

Orlovsky, N. and Orlovsky, L. 2001. "White Sandstorms in Central Asia." Chapter 8 of *Global Alarm: Dust and Sandstorms from the World's Drylands.* Youlin, Y.; Squires, V.; and Qi, L., eds. Beijing, China: United Nations Convention to Combat Desertification. TIC: 254449.

Papke, K.G. 1976. *Evaporites and Brines in Nevada Playas.* Nevada Bureau of Mines and Geology Bulletin 87. Reno, Nevada: University of Nevada, Reno, Mackay School of Mines. TIC: 211869.

Pilinis, C. 1999. "Modeling Atmospheric Aerosols Using Thermodynamic Arguments—A Review." *Global Nest: the International Journal, 1,* (1), 5–13. Athens, Greece: Global Nest. TIC: 254346.

Pitzer, K.S. 1991. "Ion Interaction Approach: Theory and Data Correlation." Chapter 3 of *Activity Coefficients in Electrolyte Solutions.* 2nd Edition. Pitzer, K.S., ed. Boca Raton, Florida: CRC Press. TIC: 251799.

Reamer, C.W. 2001. "U.S. Nuclear Regulatory Commission/U.S. Department of Energy Technical Exchange and Management Meeting on Evolution of the Near-Field Environment (January 9–12, 2001)." Letter from C.W. Reamer (NRC) to S. Brocoum (DOE/YMSCO), January 26, 2001, with enclosure. ACC: MOL.20010810.0033.

Reheis, M.C. 1997. "Dust Deposition Downwind of Owens (Dry) Lake, 1991-1994: Preliminary Findings." *Journal of Geophysical Research*, *102*, (D22), 25999–26008. Washington, D.C.: American Geophysical Union. TIC: 255971.

Reheis, M.C.; Budahn, J.R.; and Lamothe, P.J. 2002. "Geochemical Evidence for Diversity of Dust Sources in the Southwestern United States." *Geochimica et Cosmochimica Acta*, *66*, (9), 1569–1587. New York, New York: Pergamon. TIC: 254213.

Reheis, M.C. and Kihl, R. 1995. "Dust Deposition in Southern Nevada and California, 1984–1989: Relations to Climate, Source Area, and Source Lithology." *Journal of Geophysical Research, 100,* (D5), 8893–8918. Washington, D.C.: American Geophysical Union. TIC: 234886.

Schlueter, J. 2003. "Pre-Licensing Evaluation of Evolution of the Near-Field Environment (ENFE) Key Technical Issue (KTI) Agreements 2.07 and 2.08." Letter from J.R. Schlueter (NRC) to J.D. Ziegler (DOE). October 21, 2003. ACC: MOL.20031219.0056.

SNL (Sandia National Laboratories) 2003. *Software User's Manual, EQ3/6, Version 8.0.* SDN: 10813-UM-8.0-00. Albuquerque, New Mexico: Sandia National Laboratories. ACC: MOL.20030312.0084.

Sonnenthal, E.L. and Bodvarsson, G.S. 1999. "Constraints on the Hydrology of the Unsaturated Zone at Yucca Mountain, NV from Three-Dimensional Models of Chloride and Strontium Geochemistry." *Journal of Contaminant Hydrology, 38,* (1–3), 107–156. New York, New York: Elsevier. TIC: 244160.

Steefel, C.I. 2004a. "The In-Drift Chemical Environment During the Above-Boiling Period." Presentation to the Nuclear Waste Technical Review Board on May 19, 2004, Washington, D.C. Las Vegas, Nevada: Bechtel SAIC Company. ACC: MOL.20040629.0419.

Steefel, C.I. 2004b. "The In-Drift Chemical Environment During the Below-Boiling Period" Presentation to the Nuclear Waste Technical Review Board on May 19, 2004, Washington, D.C. Las Vegas, Nevada: Bechtel SAIC Company. ACC: MOL.20040629.0420.

Tang, I.N. and Munkelwitz, H.R. 1993. "Composition and Temperature Dependence of the Deliquescence Properties of Hygroscopic Aerosols." *Atmospheric Environment, 27A,* (4), 467–473. New York, New York: Pergamon. TIC: 254415.

Tang, I.N. and Munkelwitz, H.R. 1994. "Aerosol Phase Transformation and Growth in the Atmosphere." *Journal of Applied Meteorology, 33,* (7), 791–796. Boston, Massachusetts: American Meteorological Society. TIC: 254414.

Topping, D.; Coe, H.; McFiggans, G.; Burgess, R.; Allan, J.; Alfarra, M.R.; Bower, K.; Choularton, T.W.; Decesari, S.; and Facchini, M.C. 2004. "Aerosol Chemical Characteristics from Sampling Conducted on the Island of Jeju, Korea during ACE Asia." *Atmospheric Environment, 38*, (14), 2111–2123. Oxford, England: Pergamon-Elsevier Science, LTD. TIC: 256037.

Torii, T. and Ossaka, J. 1965. "Antarcticite: A New Mineral, Calcium Chloride Hexahydrate, Discovered in Antarctica." *Science, 149,* (3687), 975–977. Washington, D.C.: American Association for the Advancement of Science. TIC: 254426.

Vaniman, D.T.; Chipera, S.J.; Bish, D.L.; Carey, J.W.; and Levy, S.S. 2001. "Quantification of Unsaturated-Zone Alteration and Cation Exchange in Zeolitized Tuffs at Yucca Mountain, Nevada, USA." *Geochimica et Cosmochimica Acta, 65,* (20), 3409–3433. New York, New York: Elsevier. TIC: 251574.

Weast, R.C. and Astle, M.J., eds. 1981. *CRC Handbook of Chemistry and Physics.* 62nd Edition. Boca Raton, Florida: CRC Press. TIC: 240722.

Wolery, T.J. 1979. *Calculation of Chemical Equilibrium Between Aqueous Solution and Minerals: The EQ3/6 Software Package.* UCRL-52658. Livermore, California: Lawrence Livermore Laboratory. ACC: HQS.19880517.2586.

Yang, I.C.; Rattray, G.W.; and Yu, P. 1996. *Interpretation of Chemical and Isotopic Data from Boreholes in the Unsaturated Zone at Yucca Mountain, Nevada.* Water-Resources Investigations Report 96-4058. Denver, Colorado: U.S. Geological Survey. ACC: MOL.19980528.0216.

Ziegler, J.D. 2002. "Transmittal of Reports Addressing Key Technical Issue (KTI) Agreement Unsaturated And Saturated Flow Under Isothermal Conditions (USFIC) 5.09." Letter from J.D. Ziegler (DOE/YMSCO) to J.R. Schlueter (NRC), September 26, 2002, 0926024420, OL&RC:TCG-1813, with enclosures. ACC: MOL.20021111.0022; MOL.20030816.0263; MOL.20000825.0122. TIC: 253754.

5.2 Data, Listed by Data Tracking Number

LAJF831222AQ98.003. Chloride, Bromide, Sulfate, and Chlorine-36 Analysis of Construction Water. Submittal date: 09/09/1998.

LL030409012251.048. EQ3/6 and Excel Calculations of Salt Mineral Deliquescence. Submittal date: 05/24/2003.

LL030500712251.060. Vapor Pressure of Water as a Function of Temperature and Water Activity; Range of Accessible Relative Humidity (RH) at Standard Atmospheric Pressure and at Repository Ambient Pressure. Submittal date: 05/24/2003.

LL030905931032.001. Sensitivity Studies for Evaluating the Impact of Thermal Conductivity and Percolation Rate on LA Multi-Scale Analyses. Lower Percolation Case, Low Thermal Conductivity in Host Rock. Submittal date: 10/23/2003.

LL030906131032.002. Output from the Multi-Scale AMR for the Lower Percolation Mean Thermal Conductivity Case including Drift Wall Temperatures. Submittal date: 9/16/2003.

LL030906331032.004. Sensitivity Studies for Evaluating the Impact of Thermal Conductivity and Percolation Rate on LA Multi-Scale Analyses. Upper Percolation Case, High Thermal Conductivity in Host Rock. Submittal date: 10/23/2003.

LL030906531032.005. Output from the Multi-Scale AMR for the Upper Percolation Mean Thermal Conductivity Case including Drift Wall Temperatures. Submittal date: 9/16/2003.

LL031206723122.041. WAPDEG Output from the Multi-Scale AMR for the Mean Percolation Mean Thermal Conductivity Case including Drift Wall Temperatures. Submittal date: 12/22/2003.

MO0207EBSDUSTS.020. Geochemical Composition of Dust Samples. Submittal date: 07/11/2002.

MO0209EBSDUST2.030. Geochemical Composition of Dust Samples (Phase II). Submittal date: 09/30/2002.

MO0304SPACSALT.000. EBS P&CE Model THC Seepage Analysis Spreadsheets. Submittal date: 12/10/2003.

MO0310SPADLBU4.001. Dust Leachate Binning and Uncertainty Analysis Spreadsheets. Submittal date: 10/08/2003.

MO0312SPAPCESA.002. EBS P&CE Model THC Seepage Analysis Spreadsheets. Submittal date: 12/10/2003.

SN0302T0510102.002. Pitzer Thermodynamic Database (data0.ypf, Revision 1). Submittal date: 02/06/2003.

INTENTIONALLY LEFT BLANK